The role of CBFβ in ovarian cancer

Anne Lewis Carlton
Andover, Massachusetts

B.S., Bates College, 2010
M.S., University of Virginia, 2016

A Dissertation presented to the Graduate Faculty
of the University of Virginia in Candidacy for the Degree of Doctor of Philosophy

Department of Biochemistry and Molecular Genetics

University of Virginia
August, 2018

_____

_____

_____

_____

_____

Abstract

Ovarian cancer is the second most common and the deadliest gynecologic malignancy. Approximately 60% of women with ovarian cancer present with metastatic disease and the 5-year survival for these women is 30%. Standard treatments for ovarian cancer have not been modified in the last few decades, therefore novel treatment strategies and molecular targets are urgently needed for this disease. The RUNX family of transcription factors includes RUNX1, RUNX2 and RUNX3, which bind to DNA, and their shared binding partner CBFβ. These proteins are overexpressed in epithelial ovarian cancers. Prior studies have shown that genetic inhibition of RUNX1, RUNX2, RUNX3 and CBFβ in ovarian cancer cell lines reduces proliferation and decreases anchorage-independent growth in soft agar; however, the mechanisms underlying these effects remain elusive, and genetic inhibition is not an applicable strategy for patient care. Recently, inhibitors of the CBFβ/RUNX protein-protein interaction have been developed. These compounds bind to CBFβ and block its ability to bind RUNX proteins. In this dissertation, we used these novel tool compounds and genetic reduction of CBFβ to study both the effects of CBFβ inhibition in ovarian cancer and the downstream mechanisms underlying these effects. CBFβ inhibitor treatment reduces the proliferation of ovarian cancer cell lines and causes an S-phase delay. CBFβ inhibitor treatment also impairs wound healing and anchorage-independent growth. These phenotypes are driven by a small set of gene expression changes, including decreases in INBHA and MMP1. Reduction of INHBA or MMP1 recapitulates the effects of CBFβ inhibitor treatment. Knockdown of CBFβ results in a large number of gene expression changes. Additionally, CRISPR, but not siRNA-mediated, reduction of CBFβ reduces ovarian cancer cell proliferation and migration, and

alters the expression of some genes reduced by inhibitor treatment. Lastly, cells lacking CBFβ retain their sensitivity to CBFβ inhibitors. In sum, this dissertation establishes that CBFβ functions as an oncogene in ovarian cancer by altering a gene expression network and that CBFβ/RUNX inhibition represents a viable treatment strategy worthy of additional study.

Acknowledgements

First, I would like to thank my mentors Dr. John Bushweller and Dr. David Wotton for all of their guidance during my PhD. Your mentorship, scientific wisdom, and creativity helped me grow as a scientist and will enhance my future endeavors.

Second, I would like to thank my thesis committee, Dr. Charles Landen, Dr. Patrick Grant, and Dr. Michael Guertin, for their assistance during my PhD. Your thoughtful questions and feedback strengthened the scientific rigor of my work and helped me develop strong critical thinking skills.

I would also like to thank the Landen lab for their assistance. The materials and scientific guidance you provided me with enabled me to design better experiments and broaden the conclusions of my work. I would especially like to thank Danielle Llaneza for her assistance in conducting animal experiments. Your patience in helping me learn to work with animals again and your expertise with regards to xenografts were indispensible.

I would also like to thank everyone in both the Bushweller and Wotton labs. In the Bushweller lab, I would especially like to thank Dr. Anurahda Illendula for synthesizing all of the inhibitors used in this dissertation; without these compounds, none of this would have been possible. I would also like to thank Yan Gao, who assisted with cell culture and Adam Boulton, who assisted with RNA-seq data analysis. I would also like to thank Bushweller lab members, past and present, for their guidance and support during my PhD. I am also very grateful for members of the Wotton lab. I would like to thank

Tiffany Melhuish-Baxter for her help in troubleshooting and designing experiments. Your lab ninja skills have helped me improve many of my experiments and strengthened my technical skills greatly. I would also like to thank Anant Shah and Dr. Anoush Anderson for being such supportive friends and entertaining lab mates. It would have been very painful to spend so much time in lab if I did not have you both to be there with. I would also like to thank other past Wotton lab members for their assistance and company across my PhD.

Lastly, I would like to thank my friends and family. To my friends, thank you for supporting me during my PhD. You have been patient when things have been crazy and always willing to go on a hike, cook dinner, or just hang out the rest of the time. I am also grateful to the many older MSTP students who provided me with great wisdom about navigating life as an MSTP student at UVA. I would also like to thank my family, near and far, for their support during this time. To David and Julie, thank you for being my Virginia home base. Your welcoming spirit has made my time in Charlottesville very special. To my parents, thank your for your unwavering support and belief that I can succeed in anything I put my mind to.

Table of Contents

List of Figures

List of Tables

List of Abbreviations

ALL	acute lymphoblastic leukemia
AML	acute myelogenous leukemia
B-ALL	precursor b-cell acute lymphoblastic leukemia
CBFβ	core binding factor subunit beta
CDK	cyclin dependent kinase
COL7A1	collagen Alpha-1(VII)
ddPCR	digital droplet PCR
DEG	differentially expressed gene
DMSO	dimethyl sulfoxide
EGFR	epidermal growth factor receptor
EMT	epithelial to mesenchymal transition
EOC	epithelial ovarian cancer
FBS	fetal bovine serum
FDP/AML	familial platelet disorder with a predisposition to develop AML
FGF	fibroblast growth factor
FRET	fluorescence resonance energy transfer
GSEA	gene set enrichment analysis
HGSOC	high-grade serous ovarian cancer
i.p.	intraperitoneally
INHBA	inhibin beta a subunit
KD	knockdown
MDS	myelodysplastic syndrome
MEF	mouse embryonic fibroblast
MMP1	matrix metalloprotease 1
OPN	osteopontin
PBS	phosphate buffered saline
PDAC	pancreatic ductal adenocarcinoma
PDGF	platelet derived growth factor
PEI	polyethylenimine
PFA	paraformaldehyde
pHH3	phospho-histone H3 (ser10)
PPI	protein-protein interactions
PROTAC	proteolysis targeting chimera
RHD	runt homology domain
rrSO	risk-reducing salpingo-oophorectomy
RUNX1	runt related transcription factor 1
RUNX2	runt related transcription factor 2
RUNX3	runt related transcription factor 3
SD	standard deviation

STIC	serous tubal intraepithelial carcinoma
TF	transcription factor
TGFβ	transforming growth factor beta
VEGF	vascular endothelial growth factor

Chapter 1. Introduction

1.1 Ovarian cancer

1.1.1 Ovarian cancer epidemiology

Ovarian cancer is the 2nd most common and deadliest gynecologic malignancy amongst women in the United States. It is estimated that 22,440 women in the United States were diagnosed with ovarian cancer in 2016, and an estimated 14,080 women will die of this disease. Underscoring this cancer's aggressiveness, ovarian cancer is the 5th leading cause of cancer-related death in women despite accounting for only 1% of new cancer diagnoses (Siegel et al., 2017). Total 5-year survival for women with ovarian cancer is 46%. However, 60% of women present with metastatic disease at diagnosis, and the 5-year survival for those women is only 29% (Siegel et al., 2017). Unlike other female-specific cancers, the survival rate for ovarian cancer has not improved substantially over the past 40 years (Bowtell et al., 2015).

1.1.2 Ovarian cancer subtypes

There are several subtypes of ovarian cancer; however, epithelial ovarian cancer (EOC) accounts for 90% of diagnosed cases. The remaining 10% of ovarian cancers are derived from the germ cells or sex chord stromal cells (Kumar, 2013). Molecularly, EOC tumors have been characterized into two categories: type I and type II. Type I tumors consist of low-grade serous tumors, as well as low grade endometrioid, clear cell, and mucinous tumors. Type I tumors are generally slower growing and more likely to be confined to the ovary at diagnosis (Kurman and Shih, 2010). Overall, type I tumors account for 30% of ovarian tumors. The genetics of type I tumors are characterized by recurrent point

mutations in traditional cancer-associated genes. Over 60% of Type I serous tumors have a point mutation in *KRAS*, *BRAF* or *ERBB2*, while mutations in *TP53* are rare (Nakayama et al., 2006; Singer et al., 2003, 2005). Recurrent point mutations in *ARID1A*, *CTNNB1*, *PTEN* and *PIK3CA* are common in the other subtypes of type I tumors (Kuo et al., 2009; Nakayama et al., 2006; Wiegand et al., 2010). The prognosis for type I tumors is more favorable, with higher overall survival rates (Prahm et al., 2015).

Type II tumors are comprised primarily of high-grade serous tumors, but also include a small number of other tumor types, including high-grade endometrioid tumors and poorly differentiated tumors. The most common type II tumor is high-grade serous, accounting for 78% of type II tumors (Bowtell, 2010; Prahm et al., 2015). Type II tumors are fast growing and highly aggressive. Underscoring this aggressive phenotype, 75% of women with high-grade serous ovarian cancer (HGSOC) are diagnosed with Stage III or Stage IV disease.

HGSOC has a unique genetic landscape that differentiates itself from other epithelial cancers. *TP53* mutations are seen in almost 100% of patients and there are few other recurrent point mutations. The next most common mutations are germline or somatic mutations of *BRCA1* or *BRCA2*, which are seen in approximately 20% of patients (Cancer Genome Atlas Research Network, 2011). In lieu of recurrent point mutations in individual genes, the shared feature between HGSOC tumors is wide scale copy number alterations and chromosomal instability causing recurrent amplifications and deletions. Focal amplifications of oncogenes are common; *MYC* amplification occurs in over 20% of tumors, and *KRAS* is amplification occurs in at least 10% of tumors. Recurrent focal

deletions of tumor suppressors are also common and include deletions of *RB* (8%), *PTEN* (7%), and *NF1* (12%) (Cancer Genome Atlas Research Network, 2011).

While there is not much overlap in genetic alterations between tumors, these genetic changes taken together target recurrent pathways. Fifty percent of patient tumors have some defect in homologous DNA repair. The Rb pathway is altered in 67% of tumors, suggesting its importance in the control of proliferation in this context. Lastly, the PI3K/AKT pathway is upregulated in 45% of tumors (Cancer Genome Atlas Research Network, 2011). The lack of shared genetic mutations in HGSOC has made the application of targeted therapies, which often target a single protein, difficult.

1.1.3 High-grade serous ovarian cancer is derived from the fallopian tube

High-grade serous ovarian cancer is currently believed to originate from dysplastic lesions in the fimbriated end of the distal fallopian tube. Prior to the past decade, it was believed that ovarian cancer originated from the ovarian surface epithelium cells. However, precancerous lesions were not identified in the ovaries of women with ovarian cancer, and attempts to transform ovarian surface epithelial cells in cellular or mouse models were largely unsuccessful at replicating the human disease (Kurman and Shih, 2016; Shan and Liu, 2009).

In the past 10 years, there has been a paradigm shift to the thought that most HGSOC originates in the fallopian tube, rather than the ovary itself. Several lines of evidence lend credence to this hypothesis. First, histological examination of the fallopian tubes of women with germline *BRCA* mutations undergoing risk-reducing salpingo-oophorectomies (rrSO) revealed precancerous lesions in the distal end of the fallopian

tube, closest to the ovary (Carcangiu et al., 2006). These lesions, termed serous tubal intraepithelial carcinomas (STICs), harbored *TP53* mutations. In instances where material from a STIC lesion and an ovarian tumor were available, the *TP53* mutation was identical in both samples, indicating a likely clonal relationship (Lee et al., 2007). After identifying these lesions by chance in a high-risk population, studies were conducted to proactively look for STIC lesions in women with ovarian cancer who did not harbor a germline *BRCA1* or *BRCA2* mutation. These studies identified a STIC lesion in 50-60% of women with *BRCA* wild-type HGSOC, supporting the hypothesis that STIC lesions are a precursor to HGSOC in a majority of cases of ovarian cancer (Ducie et al., 2017; Przybycin et al., 2010). Similarly to women with germline *BRCA* mutation, studies have demonstrated a shared *TP53* mutation between STIC lesions and metastatic lesions in women where both are present, supporting the idea that the metastatic tumor arose from the STIC lesion itself (Kuhn et al., 2012).

In tandem, several animal models supported the concept of a fallopian origin for ovarian cancer. Three independent groups, using three unrelated methods, generated STIC lesions and subsequent HGSOC using the fallopian tube secretory epithelial cell as the cancer cell of origin. Lineage-specific inactivation of *Tp53*, *Brca1/2*, and *Pten* in the fallopian tube secretory epithelial cells under control of the *Pax8* promoter lead to the development of both STIC lesions and invasive HGSOC in mice, recapitulating the human disease (Perets et al., 2013). An independent group inserted the SV40 T-antigen under the control of *Ovgp1a*, which also resulted in the development of both STIC lesions and HGSOC (Sherman-Baust et al., 2014). Lastly, a third group showed that inactivation of *Pten* and *Dicer*, under the control of *Amhr2* led to the same phenotype (Kim et al., 2012).

Together these observations support the idea that STICs are likely the precursor lesion to most high-grade serous ovarian tumors; however, the mechanism by which these cancerous cells invade the ovary and spread to the peritoneum remains elusive. The current hypothesis for the formation of tumors is as follows: a *TP53* mutation in a secretory cell at the distal fallopian tube initiates the formation of a STIC lesion. At some point, this lesion invades the basement membrane, becoming a frank carcinoma, and implants on the ovary through a currently undefined process. From there, metastatic disease disseminates from both the ovary and fallopian tube throughout the peritoneal cavity (Figure 1.1) (Bowtell et al., 2015).

A

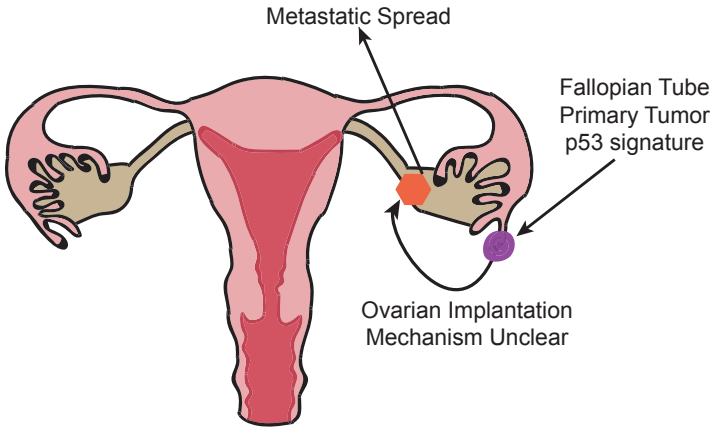
Metastatic Spread
Fallopian Tube
Primary Tumor
p53 signature
Ovarian Implantation
Mechanism Unclear

B

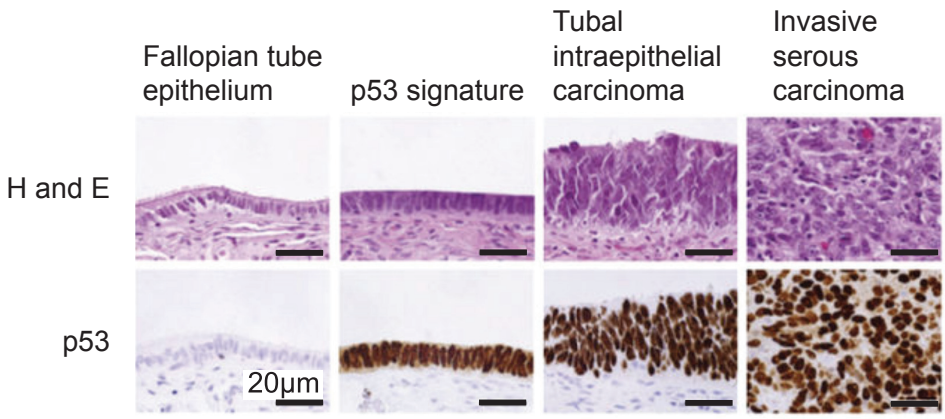
Fallopian tube epithelium
p53 signature
Tubal intraepithelial carcinoma
Invasive serous carcinoma
H and E
p53
20μm

Figure 1.1 Model of high-grade serous ovarian cancer development

A. Schematic depicting the progression of a fallopian tube pre-cancerous lesion to a metastatic tumor. B. Histological images of fallopian tube oncogenic transformation. Tissue sections are stained with hematoxylin and eosin and anti-p53 antibodies and demonstrate the transition from normal tissue to a carcinoma. Image was modified from doi:10.1038/nrc4019.

1.1.4 Ovarian cancer risk factors

There are several established risk factors for the development of EOC. As with most cancers, the risk of developing ovarian cancer increases with age. The median age of diagnosis is 63. The risk of developing ovarian cancer increases 2% per year up to age 50. Above age 50, the risk of developing ovarian cancer increases by 11% annually (Siegel et al., 2017).

Several hormonal and reproductive factors can influence ovarian cancer risk. Ovulation has been associated with an increased risk of ovarian cancer. Stemming from this, women who undergo late menopause (after age 52) have an increased risk of ovarian cancer (Gates et al., 2010). Conversely, women taking oral contraceptives that prevent ovulation have a reduced risk of developing ovarian cancer (Beral et al., 2008; Gates et al., 2010). Use of oral contraceptive for 5 years reduces the risk of developing ovarian cancer by 30%, and the benefit of oral contraceptives in reducing ovarian cancer risk persists for at least 30 years (Beral et al., 2008). Additionally increased parity (number of pregnancies carried to at least 24 weeks), hysterectomy, and salpingo-oophorectomy decrease ovarian cancer risk (Bodelon et al., 2013; Falconer et al., 2015).

In addition to the hormonal factors that influence ovarian cancer risk, several genetic syndromes greatly impact a woman's risk of developing ovarian cancer. *BRCA1* and *BRCA2* participate in repairing double-stranded DNA breaks by homologous recombination (Farmer et al., 2005). Women with germline *BRCA* mutations have an increased risk of developing ovarian cancer. Compared with all women, who have a 1.4% lifetime risk of developing ovarian cancer, the lifetime risk of developing ovarian cancer is 35 – 46% for *BRCA1* carriers and 13-23% for *BRCA2* carriers (Chen and Parmigiani,

2007). The average age at diagnosis is 52 for *BRCA1* and 57 for *BRCA2*, significantly younger than women who do not carry these mutations (Brose, 2002; Risch et al., 2001). It is recommended that women with *BRCA1* and *BRCA2* mutations undergo rrSO procedures, which reduces the risk of developing ovarian cancer by approximately 80% (Rebbeck et al., 2009).

Women with Lynch Syndrome also have an increased risk of developing ovarian cancer. Lynch Syndrome is caused by mutations in genes involved with mismatch DNA repair; the three most commonly mutated genes are *MLH1* (42%), *MSH2* (37%) and *MSH6* (13%) (Moreira et al., 2012). Women with Lynch Syndrome have an approximately 9% lifetime risk of developing ovarian cancer, higher than the general population, but lower than women with *BRCA* mutations (Vasen et al., 2013). Additionally, the mean age at diagnosis for women with Lynch Syndrome is 43 - 50, compared with 63 for women without germline DNA repair mutations (Crijnen et al., 2005; Watson et al., 2001). Overall, women with germline mutations in DNA repair genes have an increased risk of developing ovarian cancer and benefit from increased surveillance and risk-reducing surgical procedures.

1.1.5 Treatment of high-grade serous ovarian cancer

Treatment of stage III or IV HGSOC, which accounts for 75% of ovarian cancers, consists of primary surgery to remove as much tumor from the ovaries and peritoneum as possible, followed by adjuvant chemotherapy with platinum-containing drugs and a taxane; carboplatin plus paclitaxel is the most frequently used combination. This chemotherapy can be administered intravenously or intraperitoneally (Kyrgiou et al., 2006; Vergote et al., 2010). Despite many women seeing an initial response to this

chemotherapy combination, 80-85% of women with stage III or IV ovarian cancer will experience recurrent disease (Salani et al., 2011).

As our understanding of the molecular underpinnings of ovarian cancer has improved, it has been a goal to use rationally designed and targeted therapies to improve treatment outcomes in this disease. Several available targeted therapies have been investigated, with mixed results. Studies revealed that ovarian cancer tumors express high levels of vascular endothelial growth factor (VEGF), and increased VEGF was associated with a poor prognosis (Shen et al., 2000). Consequently, there was great interest in elucidating if anti-angiogenic therapies would be of benefit to patients with ovarian cancer. Multiple studies, including several Phase III double-blind clinical trials, have failed to demonstrate an increase in overall survival using any anti-angiogenic agent. Multiple studies have investigated the potential benefit of bevacizumab, a monoclonal antibody against the VEGF receptor. When used alone or in combination, in the treatment of first-line, maintenance, or recurrent disease, addition of bevacizumab failed to increase overall survival in any trial. Bevacizumab did increase progression-free survival and overall response rate in the setting of multiply relapsed disease (Cannistra et al., 2007; Perren et al., 2011; Pujade-Lauraine et al., 2014). Other anti-angiogenesis inhibitors have been evaluated for efficacy in ovarian cancer. Similar to bevacizumab, trials of aflibercept (antibody that binds VEGF ligands), pazopanib (small molecule inhibitor of VEGF1/2/3, c-KIT, and platelet derived growth factor (PDFG)), or nintedanib (small molecule inhibitor of VEGF, PDGF, and fibroblast growth factor (FGF)), failed to increase overall survival (du Bois et al., 2014, 2016; Friedlander et al., 2010; Ledermann et al., 2011; Tew et al., 2014).

Recent biochemical studies have determined that inhibition of PARP in combination with a loss of BRCA function leads to catastrophic DNA damage and resultant cell death (Bryant et al., 2005). This finding generated great interest in the ability of PARP inhibitors to provide benefit to women with *BRCA* mutations – 20% of all women with ovarian cancer. Three PARP inhibitors are currently FDA approved. Olaparib and rucaparib are FDA approved for women with germline *BRCA* mutations and relapsed ovarian cancer. Niraparib is FDA approved for any woman with relapsed ovarian cancer, regardless of *BRCA* mutation status. All three drugs have been shown to increase progression-free survival, with an average progression-free survival of 18.9 months in women with germline *BRCA* mutations treated with inhibitors vs. an average progression-free survival of 5.45 months in women with germline *BRCA* mutations treated with placebo. Progression-free survival was extended by an average of 8 months for women treated with inhibitors who did not have germline *BRCA* mutations. Data on the impact of these inhibitors on overall survival is still being collected (Coleman et al., 2017; Mirza et al., 2016; Pujade-Lauraine et al., 2017). As approximately 50% of women with HGSOC have a defect in homologous DNA repair by some mechanism, there is great interest expanding the use of PARP inhibitors in women with these tumoral defects. It has been difficult so far to determine which patients should be offered therapy with PARP inhibitors. Not all women with *BRCA* mutations respond to PARP inhibitor therapy, and, conversely women without *BRCA* mutations or defects in homologous DNA repair still had significantly increased progression-free survival in studies of rucaparib and niraparib (Coleman et al., 2017; Mirza et al., 2016). Further studies are needed to best understand

which patients would benefit most from this treatment and to identify screening biomarkers to assist with patient selection.

Many other targeted agents have been evaluated for efficacy in ovarian cancer, but none have stood out as promising new avenues for treatment. The RAS/PI3K pathway is upregulated in 40% of HGSOC tumors; therefore the efficacy of PI3K/mTOR pathway inhibitors was investigated. Neither temsirolimus (small molecule mTOR inhibitor), nor MC2206 (small molecule AKT inhibitor), showed any benefits (Behbakht et al., 2011; Yap et al., 2014). The epidermal growth factor receptor (EGFR) and its cognate pathway are upregulated in some ovarian cancers, and can be inhibited by several targeted therapies. No studies targeting the EGFR pathway showed benefit in ovarian cancer (Cortez et al., 2018; Vetter and Hays). Other targeted strategies that have been investigated without success include antibody targeting of folate receptor α, which is expressed on approximately 70% of ovarian cancer tumors (Kalli et al., 2008). Several clinical trials are currently recruiting, including trials evaluating the potential efficacy of checkpoint inhibitors and other immunomodulatory therapies (Cortez et al., 2018; Vetter and Hays). In sum, despite an enhanced understanding of the molecular pathology of ovarian cancer, the application of targeted therapies has been slow. Novel targets and treatment strategies are needed to help improve outcomes in this disease.

1.2 RUNX and CBFβ proteins

1.2.1 RUNX and CBFβ transcription factor complex

Core Binding Factor Beta (CBFβ) and its cognate DNA-binding partner RUNX form a heterodimeric transcription factor complex that is essential for proper tissue development

and differentiation (Ito et al., 2015). The RUNX family includes three Runt-Domain containing proteins: Runt Related Transcription Factor 1 (RUNX1), Runt Related Transcription Factor 2 (RUNX2), and Runt Related Transcription Factor 3 (RUNX3). All three proteins use CBFβ as their binding partner. RUNX proteins have several highly conserved domains that influence their function. DNA binding is mediated through the highly conserved Runt Homology Domain (RHD), a 128 amino acid region that binds to a shared consensus sequence of 5'-TGTGGTT-3' (Kamachi et al., 1990). There is greater than 90% homology between the Runt domains of RUNX1, RUNX2, and RUNX3, yielding this shared consensus DNA binding sequence (Tahirov et al., 2001). The CBFβ interaction with RUNX proteins is mediated by the RHD (Figure 1.2) (Zhang et al., 2003). Additionally, all three RUNX proteins share a common promoter structure with both a distal P1 and a proximal P2 promoter, leading to alternate splicing patterns and variable C-terminal domains (Bangsow et al., 2001; Ghozi et al., 1996; Xiao et al., 1998). Unbound RUNX proteins are in an auto-inhibitory conformation which yields low affinity for DNA (Gu et al., 2000). Upon CBFβ binding, RUNX proteins undergo a conformation shift and exhibit a 6 – 10 fold increased affinity for DNA, making the CBFβ/RUNX complex the functional transcriptional unit (Gu et al., 2000; Tang et al., 2000).

RUNX:

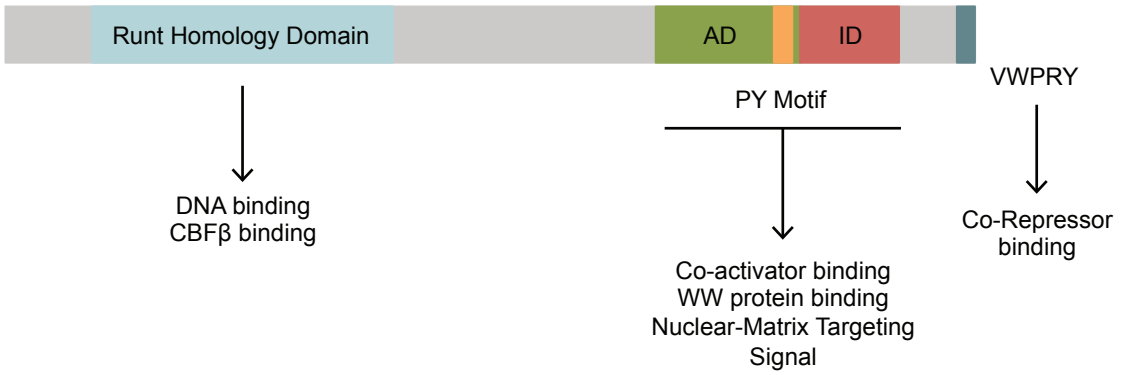
Runt Homology Domain
AD
ID
VWPRY
PY Motif
DNA binding
CBFβ binding
Co-activator binding
WW protein binding
Nuclear-Matrix Targeting
Signal
Co-Repressor
binding

CBFβ:

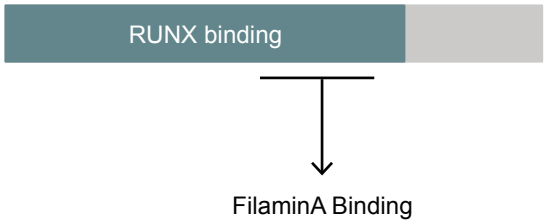
RUNX binding
FilaminA Binding

Figure 1.2 Schematic of RUNX and CBFβ proteins

Diagram depicting a generalized RUNX protein and CBFβ. Major functional and interacting domains and motifs are noted. This image was modified from doi:10.1002/ijc.27964.

In addition to the RHD, RUNX proteins have several other conserved functional motifs. All three RUNX proteins share two C-terminal domains: a nuclear matrix attachment signal and a VWRPY motif (Zeng et al., 1997). The VWRPY motif mediates the binding of transcriptional repressors (Aronson et al., 1997). RUNX proteins also have conserved, but more variable, transactivation, inhibitory, and PY domains. These domains bind a wide variety of transcriptional activators and repressors, including SMAD3, P300, p53, YAP1, FOXP3, and HES1(Chuang et al., 2013). Structural variation in the transactivation and inhibitory domains cause variations in co-factor binding, leading to diverse effects of RUNX complexes. Additionally, the availability of associated transcriptional proteins in a given nuclear environment likely mediates the effects of RUNX proteins in a given context. Lastly, the function of RUNX proteins can also be modified by post-translational modifications, adding another layer of regulatory complexity (Ito et al., 2015).

Less is known about the structure and interaction network of CBFβ. CBFβ is found in both the cytoplasm and the nucleus. CBFβ lacks a nuclear localization signal and is dependent on binding to the RUNX1 runt domain for nuclear entry (Tanaka et al., 1998). As the Runt domains of all RUNX proteins are highly similar, it is likely that RUNX2 and RUNX3 can import CBFβ into the nucleus, though their ability to do so has not been explicitly tested. In addition to RUNX binding, CBFβ binds to MYOD in the nucleus, and this interaction promotes proliferation and blocks differentiation in myoblasts (Philipot et al., 2010). In the cytoplasm, CBFβ has been shown to bind to a small number of cytoplasmic proteins, many of which are structural. CBFβ colocalizes with the cellular cytoskeleton, and has been shown to be localized with VINCULIN and F-ACTIN fibers.

CBFβ also binds to FilaminA, and this binding enforces a cytoplasmic localization of CBFβ (Tanaka et al., 1997; Yoshida et al., 2005). Additionally, CBFβ is present at the midbody during cytokinesis, and siRNA-targeting of CBFβ alters this structure (Lopez-Camacho et al., 2014a). The function of CBFβ at this location remains unclear. CBFβ also binds to nucleolar organizing regions during mitosis and inhibits ribosomal gene synthesis (Lopez-Camacho et al., 2014b). Studies to rigorously characterize the binding partners of CBFβ have not been conducted; therefore, CBFβ may interact with yet-to-be identified proteins in both in the nucleus and the cytoplasm.

1.2.2 RUNX and CBFβ in embryonic development

RUNX proteins and CBFβ have essential roles in embryonic development. Whole animal *Runx1* $^{-/-}$ mice have an embryonic lethal phenotype. Mice die between E11.5 and E12.5 due to central nervous system hemorrhage and a lack of definitive erythropoiesis in the fetal liver (Wang et al., 1996a). Myeloid differentiation is also absent in the fetal liver of *Runx1*$^{-/-}$ embryos. This dramatic phenotype strongly supports the essential role of RUNX1 in hematopoiesis.

Whole animal *Runx2*$^{-/-}$ deletion leads to death shortly after birth due to failed lung expansion. The failed lung expansion is secondary to a lack of skeletal ossification, which is caused by a deficit in osteoblast differentiation. Additionally, *Runx2*$^{-/-}$ mice weigh 20% less than control littermates and have shorter legs (Komori et al., 1997). This phenotype highlights the essential role of RUNX2 is osteoblast lineage differentiation. *Runx3* $^{-/-}$ mice are able to survive postnatally; however, they have a high rate of postnatal death, and they exhibit neurological and gastric alterations. *Runx3* $^{-/-}$ mice are smaller

than wild-type littermate controls and have severe limb ataxia. Additionally, marked alterations in the dorsal root ganglion were observed, likely explaining the severe peripheral ataxia observed (Levanon et al., 2002). Long-term surviving mice show continued ataxia, as well as eosinophilic airway inflammation, inflammatory colitis and gastric mucosal hypertrophy (Brenner et al., 2004). This phenotype demonstrates the roles of RUNX3 in immune and neurologic development.

Cbfb$^{-/-}$ mice display embryonic lethality at day E11.5 due to hemorrhage and lack of hematopoietic differentiation similar to *Runx1*$^{-/-}$ animals (Wang et al., 1996b). These murine phenotypes together provide important insight into the functional roles of CBFβ and the RUNX proteins. First, the embryonic lethality of the *Cbfb*$^{-/-}$ mouse is consistent with the idea that while RUNX proteins can bind to DNA in the absence of CBFβ, the *in vivo* function of RUNX proteins requires the presence of CBFβ. Second, each RUNX knockout mouse displays a unique phenotype, demonstrating that while all 3 RUNX proteins bind to the same target DNA sequence, they cannot functionally substitute for one another *in vivo*.

1.2.3 Contributions of RUNX1 to human disease

RUNX1 has a pathologic role in multiple diseases. Classically, dysregulation of RUNX1 is a feature of hematopoietic diseases, consistent with the role of RUNX1 in embryonic hematopoietic development. Germline mutations in *RUNX1* cause familial platelet disorder with a predisposition to develop AML (FDP/AML), an autosomal dominant disorder that causes low platelet counts and a predisposition to develop myelodysplastic syndrome (MDS) and acute myelogenous leukemia (AML). The lifetime risk of

developing either MDS or AML is at least 40%. Most people with FDP/AML have mutations in the RHD of *RUNX1*, and the increased risk of developing malignancy appears to be due to haploinsufficiency (Balduini and Savoia, 2012).

Additionally, acquired alterations in *RUNX1* are a common feature of many leukemias. Translocations involving *RUNX1* are common in both acute lymphoblastic leukemia (ALL) and AML. Fifteen to twenty five percent of children with precursor B-cell acute lymphoblastic leukemia (B-ALL) have an *ETV6/RUNX1* t(12;21) chromosomal translocation (Jamil et al., 2000; Moorman et al., 2010). Children with *ETV6/RUNX1* fusions have a favorable prognosis relative to other ALL subtypes and a 5-year survival of 91 – 99% (Bhojwani et al., 2012; Moorman et al., 2010). Translocations involving *RUNX1* are also relatively common in AML. The *RUNX1/RUNX1T1* t(8;21) translocation occurs in 7% of newly diagnosed cases of adult AML and confers a more favorable prognosis (Grimwade et al., 2010). However, the 10-year survival for patients with *RUNX1/RUNX1T1* AML remains poor at 61% (Metzeler and Bloomfield, 2017). Additionally, there are several other rare translocations involving RUNX1 that are associated with leukemias (Metzeler and Bloomfield, 2017). In addition to *RUNX1* translocations, point mutations in *RUNX1* are present in 5-10% of adults with AML and 25% of adults with MDS with elevated blasts, and these point mutations are associated with unfavorable prognoses (Kihara et al., 2014; Metzeler and Bloomfield, 2017; Network, 2013; Patel et al., 2012).

RUNX1 also has an emerging role in epithelial cancers. RUNX1 is overexpressed in a wide variety of epithelial cancers (Scheitz et al., 2012). Upregulation of RUNX1 has been shown in skin cancers, and RUNX1 is required for the development and maintenance of skin squamous cell carcinomas in mice (Hoi et al., 2010). Loss of RUNX1 decreases tumor formation of oral squamous cell carcinoma (Scheitz et al., 2012). RUNX1 also has a primarily oncogenic role in breast cancer. Upregulation of RUNX1 is associated with a poor prognosis in ER-negative and triple-negative breast cancer (Ferrari et al., 2014). Additionally, knockdown of RUNX1 in a mouse breast cancer cell line reduced migration and invasion (Browne et al., 2015). However, other studies dispute this oncogenic role. RUNX1 is mutated in a small subset of breast cancer samples and the mutations are predicted to be inactivating (Banerji et al., 2012). Knockdown of RUNX1 in three-dimensional cultures of normal breast epithelial cells resulted in hyperproliferation of 3-D acini, and shRNA-mediated knockdown of RUNX1 in normal breast epithelial cells induced the expression of vimentin, indicative of epithelial-to-mesenchymal transition (Hong et al., 2017; Wang et al., 2011). RUNX1 also has a dual role in prostate cancer; RUNX1 knockdown inhibited the growth of androgen-dependent prostate cancer cell lines but enhanced the growth of androgen-independent cell lines (Takayama et al., 2014). More work will be needed to dissect the role of RUNX1 in hormonally driven cancers.

1.2.4 Contributions of RUNX2 to human disease

Germline mutations in *RUNX2* lead to the development of cleidocranial dysplasia, an autosomal dominant disorder of skeletal development (Mundlos et al., 1997). *RUNX2* mutations are generally either point mutations in the RHD leading to impaired DNA

binding or truncating mutations. The loss of function of RUNX2 causes widespread skeletal and dental abnormalities but does not increase the risk for cancer (Ito et al., 2015; Jaruga et al., 2016).

RUNX2 has a more consistent oncogenic role in cancers derived from both epithelial and mesenchymal tissues. The oncogenic role of RUNX2 is best defined in breast cancer, prostate cancer, and osteosarcoma. RUNX2 is overexpressed in breast cancer tumors and high expression is associated with an increased risk of bone metastases and poor overall survival (Brusgard et al., 2015; Chang et al., 2014; Li et al., 2016; Tandon et al., 2014). RUNX2 plays a critical role in the development of bone metastases in breast cancer. Knockdown of RUNX2 decreases the migration of breast cancer cells towards osteoblasts, decreases cellular invasion, and decreases xenograft tumor growth in mice (Chang et al., 2014; Li et al., 2015b, 2016; Pratap et al., 2009; Tan et al., 2016). The corresponding overexpression of RUNX2 increases breast cancer cell migration and adhesion (Brusgard et al., 2015). The RUNX2 targeting microRNAs miR-135 and miR-203 are decreased in breast cancer tumors and metastases. Reexpression of either micro-RNA decreases breast cancer cell proliferation, migration and xenograft tumor formation (Taipaleenmäki et al., 2015).

In prostate cancer, increased expression and nuclear localization of RUNX2 as assessed by immunohistochemistry is associated with a poor prognosis and metastatic disease (Chua et al., 2009; Yun et al., 2012). Multiple studies using cell lines have demonstrated that RUNX2 is essential for prostate cancer proliferation, migration, invasion, and

homing to bone (Baniwal et al., 2010; van der Deen et al., 2010; Ge et al., 2015; Little et al., 2014). Additionally, RUNX2 promotes tumor growth in a phosphorylation-dependent manner in xenograft animal experiments, and knockout of *Runx2* in the *Pten*$^{-/-}$ mouse model of prostate cancer lead to decreased tumor formation (Ge et al., 2015; Yang et al., 2018). RUNX2 has been associated with the androgen receptor on chromatin, and knockdown of RUNX2 decreases the production of intratumoral testosterone (Little et al., 2014; Yang et al., 2018).

Elevation of RUNX2 has also been demonstrated in osteosarcoma patient samples and is associated with a poor response to treatment (van der Deen et al., 2013; Martin et al., 2014; Sadikovic et al., 2010; Yang et al., 2013). RUNX2 knockdown in osteosarcoma cell lines decreases the expression of genes related to invasion, as well as migration and invasion of the cells themselves (van der Deen et al., 2012). The RUNX2-targeting microRNAs miR-205 and miR-32a have low expression in osteosarcoma tumors compared to adjacent normal tissue. Overexpression of these micro-RNAs leads to decreased proliferation, migration, invasion, and in the case of miR-23a, xenograft tumor growth in mice (He et al., 2014; Zhang et al., 2016). The effects of RUNX2 knockdown on proliferation in osteosarcoma cell line proliferation are inconsistent and may be mediated by the *TP53* mutation status of the line (van der Deen et al., 2013; Lucero et al., 2013).

1.2.5 Contributions of RUNX3 in human disease

Unlike *RUNX1* and *RUNX2*, there are no inherited diseases caused by germline mutations in *RUNX3*. However, RUNX3 has a complex and often contradictory role in epithelial

cancers. *RUNX3* sits on the 1p36 locus that is frequently lost in various types of cancer, which could indicate that RUNX3 functions as a tumor suppressor (Henrich et al., 2012; Schwab et al., 1996). However, the 1p36 locus contains several other putative tumor suppressors in addition to RUNX3, including *CHD5*, *CAMTA1*, *ARID1A*, *E2F2*, *KIFIB*, *TP73*, miR-34a, and *PAX7*. Therefore loss of heterozygosity at this locus may be due to tumor suppressive functions of these other genes rather than RUNX3 (Henrich et al., 2012; Mayrhofer et al., 2014). Additionally supporting the role of RUNX3 as a tumor suppressor, hypermethylation of the RUNX3 promoter has also been demonstrated in a variety of cancers including, gastric, bladder, colorectal, pancreatic, breast, hepatocellular carcinoma, leukemia, and papillary thyroid cancer (Estécio et al., 2015; Kim et al., 2004, 2005; Lau et al., 2006; Nomoto et al., 2008; Oshimo et al., 2004; Shin et al., 2018; Wang et al., 2014; Yang et al., 2014). In all cancers except for hepatocellular carcinoma, hypermethylation of the *RUNX3* promoter is correlated with either more invasive disease or a poor prognosis (Estécio et al., 2015; Jiang et al., 2008; Nomoto et al., 2008; Shin et al., 2018; Wang et al., 2014, 2016; Yan et al., 2012).

However, in certain cancers the role of RUNX3 appears to be more context dependent. In pancreatic cancer, RUNX3 was shown to be both tumor-promoting and tumor-suppressive, depending on when it was expressed, with high expression of RUNX3 driving pancreatic cancer metastasis in a mouse model (Whittle et al., 2015). Additionally, a new study revealed that low expression of RUNX3 protein levels by immunohistochemistry in pancreatic cancer led to improved outcomes, contradicting the promoter prior hypermethylation data (Rossi et al., 2017). In ovarian and squamous head

and neck cancers, RUNX3 has a more clearly defined oncogenic role (Lee et al., 2011; Tsunematsu et al., 2009). More studies will need to be conducted to understand the context-dependent role of RUNX3. As *RUNX3* promoter hypermethylation is often found in cancers derived from the foregut, it is possible that the developmental cell of origin may also contribute to the dualistic roles of RUNX3.

1.2.6 Contributions of CBFβ in human disease

While there are no diseases associated with germline mutations of *CBFB*, there is a clear role of this protein is in leukemia. *CBFB* is involved in a translocation with *MYH11* (inv(16)), yielding a fusion protein that exerts a dominant-negative function on RUNX transcription. The *CBFB/MYH11* translocation is present in approximately 5-9% of all AML and it has been associated with M4Eo FAB subtype (Grimwade et al., 2010; Kihara et al., 2014; Metzeler and Bloomfield, 2017). Similar to the *RUNX1* fusions, patients with a *CBFB/MYH11* fusion have more favorable prognoses compared with all subtypes of AML. However, AML survival is still quite poor, and 10-year overall survival for the CBFβ/MYH11 subtype of AML is 55% (Grimwade et al., 2010; Kihara et al., 2014). In contrast with CBFβ translocations, increased mRNA expression of CBFβ is associated with decreased overall survival in AML (Morita et al., 2017a).

CBFβ has a less well-studied but growing role in epithelial cancers. One study examining CBFβ across many cancers found a general upregulation of CBFβ in cancerous tissues when compared to normal tissues (Morita et al., 2017b). High-throughput sequencing approaches in many cancers have reveled recurrent mutations in *CBFB*. A recent genomic profiling of cervical adenocarcinomas revealed recurrent point mutations of

CBFB in 1% of tumors, and *CBFB* is amplified in 3% of adrenocortical carcinoma tumors, though the biological significance of these mutations is yet to be defined (Ojesina et al., 2014; Zehir et al., 2017). Recent work has shown that CBFβ is overexpressed in gastric cancer, and this overexpression is associated with decreased patient survival. In this context, the overexpression of CBFβ is driven by alterations in the expression of a lncRNA/miRNA pathway targeting CBFβ (Chen et al., 2018). Knockdown of CBFβ in gastric cancer cell lines decreased proliferation, colony formation in soft agar, and xenograft growth in mice (Chen et al., 2018). In bladder cancer, CBFβ is targeted by the tumor suppressive microRNA miR-145 (Ostenfeld et al., 2010). miR-145 expression is decreased in bladder cancers compared to normal tissue, and low expression is correlated with poor overall survival. Additionally, forced expression of miR-145 decreases bladder cancer cell line viability (Ostenfeld et al., 2010).

CBFβ has a more studied role in breast cancer. *CBFB* is mutated in approximately 4% of breast cancer patients. Twenty percent of the identified *CBFB* mutations in breast cancer are X55_splice mutations, though the functional consequence of this mutation on protein function has not yet been identified (Ciriello et al., 2015; Pereira et al., 2016; Zehir et al., 2017). Genomic profiling of metastatic breast tumors also identified *CBFB* as a significant recurrent mutation (Lefebvre et al., 2016). From a functional standpoint, CBFβ plays an important role in the invasiveness of triple-negative breast cancer; CBFβ knockdown in a triple-negative breast cancer cell line decreased invasion through matrigel (Mendoza-Villanueva et al., 2010). Additionally, knockdown of CBFβ

decreased the production of sclerostin, which contributes to the formation of osteolytic bone metastases in breast cancer (Mendoza-Villanueva et al., 2011).

1.2.7 Molecular role of CBFβ and RUNX in cancer

The CBFβ and RUNX proteins play important roles in several physiologic processes related to cancer. The contributions of these proteins to critical cellular behaviors will be briefly reviewed in the following section.

Proliferation: Increased proliferation is a key hallmark of cancer cells and contributes directly to tumor growth (Hanahan and Weinberg, 2011). CBFβ and the RUNX proteins interface with and promote proliferation in several key contexts. Ectopic expression of RUNX1 in *Tp53*$^{-/-}$ mouse embryonic fibroblasts (MEFs) increased cellular proliferation in cell culture and tumor xenografts (Wotton et al., 2004). Additionally RUNX1 was found to be oncogenic in lymphocytes after p53 inactivation (Shimizu et al., 2013). Downstream analysis of shared RUNX1, RUNX2, and RUNX3 target genes revealed that RUNX proteins control several genes essential for cell survival (Wotton et al., 2008).

Studies have also shown that RUNX1 and RUNX2 are regulated across the cell cycle (Galindo et al., 2005; San Martin et al., 2009; Wang et al., 2007). In normal cells, RUNX1 and RUNX2 are highest at G_2/M (Galindo et al., 2005; Qiao et al., 2006; Wang et al., 2007). However, this dynamic regulation of RUNX2 is lost in osteosarcoma cell lines, indicating that this pattern may contribute to uncontrolled cancer proliferation. Protein expression of RUNX1 and RUNX2 is also important in the G_1 to S transition in multiple cell culture models (Bernardin-Fried et al., 2004; Galindo et al., 2005; Hoi et al.,

2010). Adding an additional layer of complexity, RUNX1 is phosphorylated by cyclin dependent kinase (CDK) 1, 2 and 6, and this phosphorylation affects protein stability in a cell-cycle dependent manner (Biggs et al., 2006; Wang et al., 2007).

Epithelial-to-mesenchymal transition: Epithelial-to-mesenchymal transition (EMT) is a cellular reprograming event where cells with an epithelial phenotype transdifferentiate into a more mesenchymal phenotype. As EMT occurs, cells lose their junctions with each other and the basement membrane via downregulation of E-cadherin and reorganization of their cytoskeleton. Master transcriptional regulators SNAI1/2, TWIST, and ZEB1/2 coordinate this change in cell shape and function (Lamouille et al., 2014). Activation of EMT transcription factors leads to increased gene expression of mesenchymal products including mesenchymal cadherins and matrix metalloproteases. This mesenchymal phenotype is associated with increased motility, increased ability to degrade extracellular matrix, and enhanced invasive capabilities. EMT is activated by several pathways, but is canonically associated with transforming growth factor beta (TGFβ) signaling. EMT has a normal physiologic role in development and wound healing but can also contribute to the growth and metastasis of cancer. In the context of cancer, EMT is most associated with tumor invasion and metastasis (Lamouille et al., 2014).

The RUNX proteins and CBFβ contribute to EMT. RUNX2 has a well-studied role in promoting EMT by upregulating many mediators of this process. RUNX2 has been shown to upregulate SNAI2 in multiple contexts (Baniwal et al., 2010; Chimge et al., 2011; Lambertini et al., 2010; Little et al., 2014; Niu et al., 2012). RUNX2 also has been

shown to regulate several other mediators of EMT in breast, prostate and thyroid cancers including: MMP2, MMP9, MMP13, osteopontin (OPN), sclerostin, S100A4, SMAD3, and SOX9 (Baniwal et al., 2010; Chimge et al., 2011; Little et al., 2012; Mendoza-Villanueva et al., 2011; Niu et al., 2012; Pratap et al., 2005; Taipaleenmäki et al., 2015). CBFβ has been shown to regulate the expression of several genes related to the cytoskeleton, indicating that CBFβ can exert control of cellular structure (Michaud et al., 2008). Less is known about the contributions of RUNX1 to EMT; however, knockdown of RUNX1 in certain cancers decreases invasion and migration, two phenotypes associated with EMT (Keita et al., 2013). The role of RUNX3 in EMT is complex. However; it is clear that RUNX3 can exert control over the EMT process, but whether it promotes or inhibits EMT appears to be context dependent (Voon and Thiery, 2017).

1.2.8 Overall effects of CBFβ and RUNX proteins in cancer

Overall, the RUNX proteins and CBFβ contribute to the development of several classes of cancer: hematologic, epithelial, and mesenchymal. Whether or not RUNX and CBFβ are tumor-suppressive or oncogenic depends on the cell of origin of the cancer and the other associated mutations. In epithelial cancers, which are the focus of this dissertation, a preponderance of evidence indicates that RUNX and CBFβ are oncogenic. Their expression is upregulated in a variety of cancers, reduction in their levels decreases cancer-associated phenotypes, and their target gene sets are enriched for many cancer causing gene programs. The evidence that CBFβ and RUNX promote the migration and invasion of epithelial cancers is particularly strong and consistent. As migration and invasion are strong surrogate markers of metastatic ability, it follows that these proteins play a strong role in epithelial cancer metastasis.

1.2.9 Oncogenic effect of CBFβ/RUNX proteins in ovarian cancer

While the RUNX proteins and CBFβ have complex roles in cancer as a whole, RUNX1, RUNX2, RUNX3 and CBFβ all appear to be oncogenic in the context of HGSOC. RUNX1 is overexpressed by immunohistochemistry and RT-qPCR in patient samples of HGSOC, and overexpressed by western blot in ovarian cancer cell lines (Ge et al., 2014; Keita et al., 2013). shRNA-mediated knockdown of RUNX1 in ovarian cancer cell lines leads to decreased cell growth, invasion, colony formation in soft agar, and a G_1 cell cycle arrest (Keita et al., 2013). Additionally, the RUNX1-targeting microRNA miR-302b is decreased in ovarian cancer tumors. Overexpression of this micro-RNA decreases ovarian cancer cell line growth, colony formation in soft agar, and tumor formation in subcutaneous xenograft models. Expression of miR-302b also induced a G_1 cell cycle arrest, similar to shRNA-mediated knockdown of RUNX1 (Ge et al., 2014). Expression of the RUNX1-targeting microRNA miR-144 is also decreased in ovarian cancer cell lines. Reexpression of miR-144 decreased ovarian cancer cell line proliferation and migration (Han et al., 2018).

RUNX2 is overexpressed in a subset of ovarian cancer tumors as assessed by immunohistochemistry or mRNA levels (Li et al., 2017, 2012b; Wang et al., 2013). shRNA-mediated knockdown of RUNX2 leads to decreased growth, migration, invasion, and colony formation in soft agar of ovarian cancer cell lines (Wang et al., 2013). Three RUNX2 targeting micro-RNAs, miR-23b, miR-218, and miR-338-3p, are decreased in ovarian cancer tumors relative to adjacent normal tissues. Overexpression of these microRNAs in ovarian cancer cell lines leads to a decrease in RUNX2 mRNA and

protein levels, as well as decreased growth, migration, invasion, colony formation in soft agar, and xenograft tumor formation in mice (Li et al., 2017, 2014; Wen et al., 2015).

RUNX3 is overexpressed in a subset of patient tumors, as assessed by immunohistochemistry, as well as in several ovarian cancer cell lines (Lee et al., 2011; Nevadunsky et al., 2009). RUNX3 knockdown leads to reduced growth and colony formation in soft agar (Lee et al., 2011). Additionally, RUNX3 is overexpressed in a cell culture model of cisplatin resistance (Barghout et al., 2015).

CBFβ is expressed in ovarian cancer cell lines as measured by RT-qPCR (Greer et al., 2013). shRNA-mediated knockdown of CBFβ leads to decreased proliferation, decreased colony formation in soft agar, and increased autophagy of ovarian cancer cells (Davis et al., 2010; Greer et al., 2013). While a considerable body of work has characterized the phenotypes associated with RUNX and CBFβ in ovarian cancer, the molecular mechanisms underlying these effects remains unknown. Work to better understand the downstream signaling of CBFβ/RUNX complexes in ovarian cancer may bring novel understanding to the molecular pathogenesis of this disease and speed along the development of novel treatments, which are desperately needed for this terrible disease.

1.3 Small molecule targeting of transcription factors

1.3.1 Rational drug discovery and design in cancer

To date, there are approximately 1600 FDA approved drugs, which are predicted to target 900 proteins. However, the targets of these drugs are not uniformly distributed throughout the proteome (Santos et al., 2017). This skewed distribution of drug targets is

because historically, drug development has been biased towards the development of molecules that inhibit the enzymatic activity of proteins; as they have a defined drug-binding pocket, and it is relatively easy to screen for enzymatic function. Reflecting this, currently the most common drug targets are enzymes and transmembrane proteins (Imming et al., 2006; Santos et al., 2017).

Currently, cancer pharmacotherapy reflects overall patterns in drug development, with the majority of cancer pharmacotherapies consisting of non-specific agents, which target all rapidly dividing cells, both normal and cancerous. While these molecules can be efficacious, they have severe side effects due to on-target activity in normal tissues, and fail to cure a majority of cancers due to acquired tumor resistance (Chikarmane et al., 2012; Sawicka et al., 2004). As genetic and molecular profiling has exploded in recent years, the goal of targeted and personalized chemotherapies has grown. In conjunction with this characterization of tumors, it has been estimated that there are approximately 125 shared driver mutations in cancers; however, only 25 of them are in the "druggable" class of enzymes (Kandoth et al., 2013; Vogelstein et al., 2013). Improvements in cancer therapeutics will require creative strategies to target these remaining "undruggable" cancer drivers.

While the majority of cancers are treated with traditional non-targeted chemotherapies, successful therapies using small-molecule kinase inhibitors and monoclonal antibodies have been developed. For example, chronic myelogenous leukemia is driven by the BCR/ABL fusion protein, which encodes a kinase. Inhibition of this kinase activity with

imatinib reverses the course of this disease so dramatically that patients with an initial response to imatinib now have an overall death rate equivalent to that of the general population (Gambacorti-Passerini et al., 2011). Imatinib has also shown success in the treatment of gastrointestinal stromal tumors, which are driven by c-Kit (Blanke et al., 2008). A second targeted kinase inhibitor has shown short-term success in metastatic melanoma. Approximately half of disseminated melanoma tumors often harbor a V600E mutation in *BRAF* (Long et al., 2011). This mutant protein is targeted by vemurafenib, and its inhibition is associated increased overall survival of advanced melanoma patients (Chapman et al., 2011). However, despite initial success, most patients will eventually develop resistant disease, highlighting the selective pressure tumors exert against drugs targeting a specific protein. Other tyrosine kinase inhibitors have shown efficacy in specific subsets of patients, however tumor responses are generally temporary and escape mutations in alternate pathways are common (Gross et al., 2015).

Antibody-based therapies in cancer have limited applications due to the small number of proteins that can be targeted by these modalities; however, they have shown success in specific instances. One of the most successful examples of a targeted antibody therapy is the HER2-targeting antibody trastuzumab. *HER2* is amplified in a subset of aggressive breast cancers, and monoclonal antibody targeting of the HER2 receptor on the cell membrane has improved outcome dramatically for this disease (Slamon et al., 2001). Another FDA-approved antibody therapy is bevacizumab, a monoclonal antibody against VEGF. Bevacizumab increases overall survival in some cancer settings and is approved for use in recurrent breast, colon, brain, renal, and ovarian cancers. Bevacizumab has

been studied in other cancers with mixed results, and has been associated with rare, but life-threatening side effects (Kong et al., 2017). Further work to understand how to use bevacizumab for maximal patient benefit needs to be completed. Other antibody based therapies have been developed and many are FDA-approved; however, their target range is limited to soluble molecules and extracellular proteins, impeding the utility of such drugs (Wang and Jia, 2016).

Transcription factors are over-represented in oncogenic driver proteins; however, they have traditionally been considered poor drug targets, as they typically lack a deep binding pocket for drug binding to inhibit the essential protein/protein or protein/DNA interactions. Novel strategies to target these non-enzymatic proteins are necessary to target this large class of oncogenic driver proteins.

One mechanism of targeting transcription factors is target protein degradation. siRNAs and miRNAs are widely used in the laboratory setting to reduce the protein levels of targets by inducing mRNA degradation. However, translation of this approach to a human therapy has been challenging, due to the poor stability of siRNAs in the *in vivo* setting. Improvements in delivery and molecular distribution have allowed for the use of these therapies in limited trials in patients. A first-in-human report of the use of siRNAs in liposomal nanoparticles showed target protein degradation without acute toxicity (Tabernero et al., 2013). The most studied application of siRNAs in humans comes from trials of inclisiran, a nanoparticle containing siRNAs targeting PCSK9, an enzyme involved in LDL processing, to reduce cholesterol in patients with familial

hypercholesterolemia. Phase I and Phase II clinical trials of inclisiran demonstrated protein reduction of PCSK9 in patients, as well as a corresponding decrease in LDL, the normal output of this protein's function. No severe toxicity was observed, indicating that future trials using this approach may be feasible in cancer (Fitzgerald et al., 2017; Frank-Kamenetsky et al., 2008; Ray et al., 2017).

Another approach to targeted protein degradation is proteolysis targeting chimera (PROTAC) compounds. These compounds are bivalent small molecules. One portion of the molecule binds to the protein of interest, and the other binds to an E3 ubiquitin ligase. The sum effect of these compounds is recruitment of the protein of interest to the proteasome for degradation (Neklesa et al., 2017). One of the primary benefits of a PROTAC approach is that the portion of the compound that binds to the protein of interest does not need to inhibit protein function; rather it just needs to bind with high avidity and specificity. This feature is especially beneficial for targeting transcription factors whose function is often not easily inhibited by compound binding (Bondeson et al., 2015). A second benefit of PROTAC compounds is that protein degradation is a form of irreversible inhibition, and therefore the theoretical half-life of these compounds is greatly extended compared with traditional inhibitors whose half-life is determined by compound stability (Neklesa et al., 2017). A few PROTAC molecules have been described with excellent efficacy in pre-clinical models. Three independent groups described structurally similar PROTAC compounds linking JQ1, a BRD4 inhibitor, to an ubiquitin targeting ligand. These compounds cause robust degradation of BRD4 as expected, and were effective in Burkitt's lymphoma cell lines and mouse models of

leukemia (Lu et al., 2015; Winter et al., 2015; Zengerle et al., 2015). Several additional proteins have been targeted using this mechanism, and the concept is experiencing explosive growth (Jiang et al., 2018; Lai and Crews, 2017; Lu et al., 2018; Robb et al., 2017; Schiedel et al., 2018). To date, no PROTAC compounds have been used in clinical trials, and our understanding of the clinical utility of these compounds will improve as we gain this additional data.

Another approach to inhibiting the function of transcription factors is inhibition of protein-protein interactions (PPI). Transcription factors generally function in large complexes, and disruptions of these interactions often modulate their activity. However, the large contact areas between proteins and the lack of specific drug binding sites on targets have hampered the development of PPI inhibitors. Currently, novel medicinal chemical approaches to compound synthesis and screening are overcoming these challenges. Some of the first identified PPI inhibitors disrupt the interaction between MDM2 and p53, stabilizing wild-type p53 and reactivating its function (Vassilev et al., 2004). These compounds and their optimized derivatives show efficacy in several animal models of cancer. Derivative compounds have also been evaluated in Phase I clinical trials. Some trials were discontinued due to toxicity, and other are still recruiting (Burgess et al., 2016). Another group identified a peptide-based inhibitor of the PPI between ICN1, CSL and MAML1 in T-ALL. *NOTCH1* mutations are present in 50% of patients with T-ALL and lead to increased levels of ICN1 in the nucleus. Normally, ICN1, CSL, and MAML1 form a trimeric complex necessary for the transcriptional function of ICN1. The identified peptide mimics MAML1 binding and sequesters the

ICN1/CSL complex away from DNA, inhibiting its function (Moellering et al., 2009). A chemical inhibitor of this complex has also been identified. This small molecule binds to ICN1, blocking its interaction with CSL thereby preventing MAML1 binding and stabilizing the complex (Astudillo et al., 2016). Enhancements in computer assisted compound screening and *in vitro* assay development have increased compound development in this area, but further work is needed to both identify useful compounds and optimize their use for clinical application.

1.3.2 Small molecule targeting of CBFβ/RUNX

As many cancers are dependent on CBFβ/RUNX transcriptional activity, there has been considerable interest in identifying and developing inhibitors of this complex. The functional transcriptional unit is comprised of a CBFβ/RUNX complex bound to DNA, resulting in three potential sites for targeting: CBFβ, RUNX, and DNA. Small molecules acting at each of these three sites have been developed, and, in general, these molecules have shown broad anti-cancer activity, supporting the hypothesis that chemical inhibition of the CBFβ/RUNX interaction is a viable strategy for cancer treatment.

Two chemicals that target RUNX proteins have been reported. CADD522 was identified using a computational approach and is reported to bind to RUNX proteins blocking their interaction with DNA (Kim et al., 2017). MMTV-PyMT mice treated with CADD522 developed fewer breast tumors, and individual tumors were reduced in weight. Also, Mice xenografted with a triple-negative breast cancer patient derived xenograft had reduced tumor growth after treatment with CADD522 (Kim et al., 2017). A second

inhibitor, also binding to RUNX proteins, has also been reported (Oo et al., 2017). A virtual screen looked for compounds that bind to the Runt domain of RUNX proteins at the site of the CBFβ interaction to block binding and inhibition functional transcription. Lead compounds from this screen inhibit hematopoietic development in zebrafish, demonstrating physiologic inhibition of RUNX1 function. Additionally, treatment of leukemia cell lines with these compounds reduced their proliferation and colony formation, indicating these compounds have efficacy in a more relevant cancer model as well (Oo et al., 2017).

Inhibitors targeting the RUNX consensus DNA binding site have also been described. These compounds, termed PI polyamides, bind to the RUNX consensus site on DNA, and are conjugated to the alkylating agent Chb. The result of treatment with these compounds is DNA alkylation at RUNX binding sites throughout the genome and decreased transcription of genes regulated by CBFβ/RUNX binding (Morita et al., 2017b). Treatment of cell lines of various types cancer types with these compounds resulted in dramatically reduced proliferation. Additionally, treatment of leukemia xenografts in mice with PI polyamides reduced tumor growth *in vivo* (Morita et al., 2017b).

Inhibitors of CBFβ have also been identified using qualitative screening methods. A zebrafish screen looking for compounds that inhibit hematopoiesis (presumed to be driven by CBFβ/RUNX) identified Ro5-3335 (Cunningham et al., 2012). Ro5-3335 inhibits the protein-protein interaction between CBFβ and RUNX in an *in vitro* Alpha-Screen assay. Additionally, Ro5-3335 extended survival in a mouse model of leukemia

(Cunningham et al., 2012). However, other work studied Ro5-3335 in a FRET assay looking for disruption of the CBFβ/RUNX protein-protein interaction and did not observe any inhibition with this compound. Additionally, NMR studies did not indicate any binding between Ro5-3335 and either CBFβ or RUNX. Therefore, while this compound alters the output of CBFβ and RUNX function, it does not appear to inhibit either protein directly, as first reported (Illendula et al., 2016). Another CBFβ inhibitor, kartogenin, was identified using a phenotypic screen (Johnson et al., 2012). Compounds were screened for their ability to enhance the chondrogenesis of bone marrow cells. Kartogenin was identified as a potent activator of this process, and biophysical work identified this compound as an inhibitor of the CBFβ/FilaminA interaction. The enhancement of chondrogenesis is believed to be secondary to increased CBFβ in the nucleus leading to increased transcription of RUNX2 target genes (Johnson et al., 2012).

1.3.3 CBFβ inhibitors used in this dissertation

A chemical screen using the National Cancer Institute Diversity Set chemical library was performed to identify compounds that disrupt the CBFβ/RUNX protein-protein interaction. Compounds were screened in a fluorescence resonance energy transfer (FRET) assay looking for disruption of the FRET signal generated by the protein-protein interaction between the RUNX runt domain fused to cerulean, and CBFβ fused to venus (Figure 1.3A) (Illendula et al., 2015). Several compounds with intermediate potency were identified using this method, and their ability to inhibit CBFβ/RUNX binding was optimized by iterative medicinal chemistry (Illendula et al., 2016). Two lead compounds, AI-10-104 and AI-14-91 were identified as most promising, with *in vitro* FRET IC_{50} values in the low micromolar range. AI-4-88 is a compound with a similar chemical

structure that does not inhibit CBFβ /RUNX binding and is used as an inactive chemical control (Figure 1.3B). NMR and other biophysical experiments revealed that these compounds bind to CBFβ, inducing a change in its dynamics, such that it no longer binds to RUNX proteins. In the absence of CBFβ binding, RUNX binding to DNA is dramatically reduced, as well as transcription of downstream target genes (Figure 1.3C) (Illendula et al., 2015, 2016).

As a confirmation of these *in vitro* findings, the ability of active compounds to block CBFβ binding to RUNX proteins was investigated in cell culture. SEM cells were treated with compounds, and lysates were immunoprecipitated with anti-RUNX1 antibodies. The amount of CBFβ bound to RUNX1 was investigated by western blotting. AI-10-104 and AI-14-91 both dramatically reduced CBFβ/RUNX1 binding, while treatment with AI-4-88, the inactive chemical control, did not alter CBFβ/RUNX binding (Figure 1.3D). These results were replicated for RUNX3 and a similar result would be expected for RUNX2 (Choi et al., 2017). These three compounds together allow for robust investigation of the roles of CBFβ and RUNX proteins in multiple contexts.

A

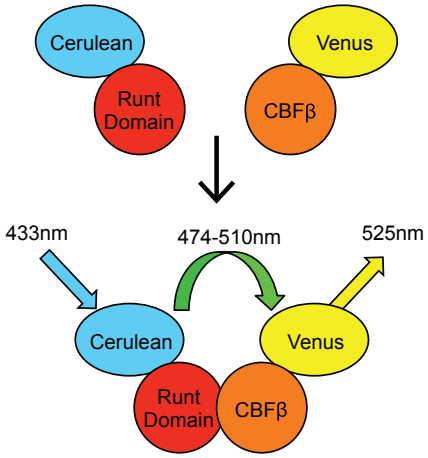

B

Compound	FRET IC_{50}(μM)	Structure
AI-4-88	> 240	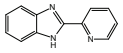
AI-10-104	1.25	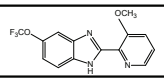
AI-14-91	3.0	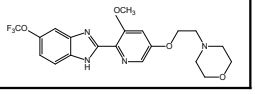

C

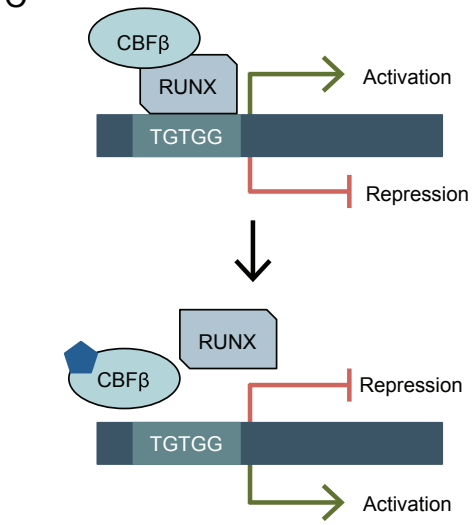

D

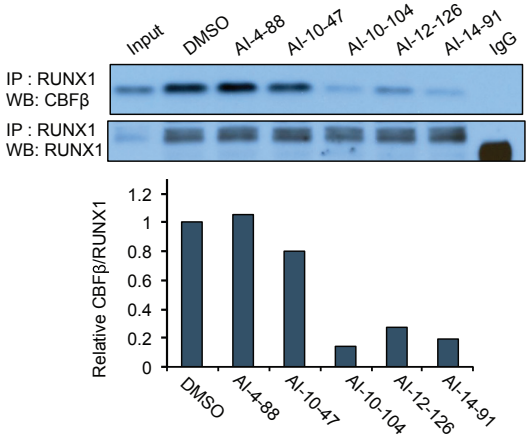

Figure 1.3 Discovery and validation of CBFβ/RUNX protein-protein inhibitors

A. Schematic depicting the FRET assay used to screen for CBFβ/RUNX inhibitors. Compounds were screened for their ability to disrupt the FRET signal between RHD-cerulean and CBFβ-venus. B. Table containing the structure and *in vitro* FRET IC_{50} values for lead compounds. C. Schematic depicting the mechanism of action of CBFβ/RUNX inhibitors. The inhibitors bind to CBFβ (blue hexagon) and inhibit RUNX binding, therefore decreasing CBFβ/RUNX-mediated gene transcription. D. SEM cells were treated with indicated inhibitor for 6 hours. Lysates were immunoprecipitated with anti-RUNX1 antibodies and the levels of bound CBFβ was analyzed by western blot. The graph is a quantification of the above western blot. Image modified from doi:10.1016/j.ebiom.2016.04.032.

1.4. Overview of this dissertation

This section will provide a brief overview of the following chapters. In general, this dissertation investigates the role that CBFβ plays in ovarian cancer, using both chemical and genetic approaches. The hypothesis at the outset of this work was that CBFβ enhances ovarian cancer growth and metastasis by controlling a transcriptional network that regulates proliferation and cell adhesion. In Chapter 2, the effects of chemical inhibition of the CBFβ/RUNX PPI in ovarian cancer will be evaluated. In sum, chemical inhibition using AI-10-104 and AI-14-91 inhibits the proliferation and anchorage-independent growth of ovarian cancer cell lines. AI-10-104 treatment causes an S-phase delay and inhibits migration. These phenotypes are driven by a small number of gene expression changes, including a decrease in INHBA and MMP1. Knockdown of these genes recapitulates the effects of compound treatment. In Chapter 3, the effects of genetic reduction of CBFβ in ovarian cancer cells will be evaluated. The expression of a large number of genes are altered after siRNA-mediated knockdown of CBFβ. These differentially expressed genes are enriched for many TF consensus sequences, miRNA targets and KEGG pathways. GSEA identified “E2F targets” as the most enriched hallmark gene set in downregulated genes, and “Epithelial to Mesenchymal” transition in upregulated genes. siRNA-mediated knockdown of CBFβ does not alter proliferation or migration. CRISPR-mediated loss of CBFβ decreases both proliferation and migration. Cells lacking CBFβ, either by siRNA-targeting or CRISPR-mediated loss, continue to show reduced proliferation and migration in response to AI-10-104. In Chapter 4, these results are discussed and put into a greater literature context. Future directions of stemming from work are also outlined.

Chapter 2. Small molecule inhibition of the CBFβ/RUNX interaction decreases ovarian cancer growth and migration through alterations in genes related to epithelial-to-mesenchymal transition[1]

2.1 Introduction

Ovarian cancer is the second most common and deadliest gynecologic malignancy (Siegel et al., 2017). Despite numerous advances in the treatment of other cancers, the standard of care for ovarian cancer has not been significantly modified in the past 20 years, and 5-year survival remains unchanged. Unlike other epithelial cancers, ovarian cancer lacks many of the recurrent mutations that have been successful drug targets (Bowtell et al., 2015). Therefore, novel treatment strategies are urgently needed to combat this disease.

Core-Binding Factor Subunit Beta (CBFβ) and a RUNX protein (RUNX1, RUNX2, or RUNX3) form a heterodimeric transcription factor complex that is essential for proper tissue development and differentiation (Chuang et al., 2013). RUNX proteins contain a DNA-binding domain; however, their affinity for DNA is increased up to 40-fold upon CBFβ binding (Gu et al., 2000). The two proteins together form the functional transcription factor complex (Tang et al., 2000). While CBFβ and RUNX proteins are canonically involved in hematopoiesis (Okuda et al., 1996), osteogenesis (Komori et al., 1997), neurogenesis (Levanon et al., 2002), and gastric development (Brenner et al., 2004), they have an emerging oncogenic role in epithelial cancers (Chuang et al., 2017).

[1] This work has been accepted in *Gynecologic Oncology*. Carlton, A.L., Illendula, A., Gao, Y., Llaneza, D.C., Boulton, A., Shah, A., Rajewski, R.A., Landen, C.N., Wotton, D., and Bushweller, J.H. (2018). Small molecule inhibition of the CBFβ/RUNX interaction decreases ovarian cancer growth and migration through alterations in genes related to epithelial-to-mesenchymal transition. Gynecol. Oncol. doi: https://doi.org/10.1016/j.ygyno.2018.03.005.

RUNX1, RUNX2, and RUNX3 are overexpressed in a subset of epithelial ovarian cancers (Barghout et al., 2015; Keita et al., 2013; Wang et al., 2013). Genetic reduction of CBFβ, RUNX1, or RUNX2 in ovarian cancer cell lines reduces proliferation and decreases anchorage-independent growth (Davis et al., 2010; Greer et al., 2013; Keita et al., 2013; Wang et al., 2013). Upregulation of RUNX3 is associated with carboplatin resistance (Barghout et al., 2015). However, the downstream mechanisms underlying these effects remain unknown. Additionally, these experiments utilized shRNA-mediated knockdown (KD) to investigate the role of these proteins. While this is a useful tool for validation, it is not a viable therapeutic approach.

Recently, inhibitors of the CBFβ/RUNX protein-protein interaction have been developed. These compounds bind to CBFβ and block its ability to bind RUNX proteins (Illendula et al., 2016). With these novel tool compounds, we studied both the effects of CBFβ inhibition in ovarian cancer and the downstream mechanisms underlying these effects. CBFβ inhibition decreases ovarian cancer cell proliferation, migration, and anchorage-independent growth. This phenotype is driven by a small number of gene-expression changes. Knockdown of two differentially expressed genes recapitulates the phenotype observed with compound treatment. Together, these data validate CBFβ as a target in ovarian cancer and provide strong rationale for further development of clinically applicable CBFβ inhibitors.

2.2 Materials and methods

2.2.1 Cell culture and inhibitor treatment

A2780ip2, PEO1, PEO4, and SKOV3ip1 cell lines were from the Landen lab at the University of Virginia, OVCAR4 cells were from the Slack-Davis lab at the University of Virginia, BEAS-2B cells were a gift from Dr. Thao Dang, and OVCAR8 cells were from ATCC. A2780ip2, OVCAR4, OVCAR8, PEO1, PEO4, and SKOV3ip1 cells were cultured in RPMI-1640 (Gibco 11875-093) supplemented with 10% fetal bovine serum (FBS) (HyClone SH30396.03), 1% Anti-Anti (Gibco15240-062), and 100µg/mL Normocin (InvivoGen ant-nr-1). BEAS-2B cells were cultured in DMEM (Gibco 11965-092) supplemented with 10% FBS. All cell lines were grown in a humidified 37°C incubator with supplemented with 5% CO_2. Cell line identity was verified by STR profiling. Tool inhibitors were synthesized in the Bushweller lab as previously described (Illendula et al., 2016). Staurosporine was purchased from Sigma-Aldrich (S5921).

2.2.2 Cell viability assays

Cells (2500-5000 depending on the cell line) were seeded in a 96-well plate, and inhibitors were added the following day. After 3 days, CellTiter-Glo (Promega G7570) was added according to the manufacturer's protocol. For MTT assays, BEAS2-B cells (35,000) were plated in the presence of compounds. Relative cell number was assessed after 3 days by MTT (Invitrogen V13154) per the manufacturer's instructions. Luminescence and absorbance were measured using a PHERAStarPlus microplate reader. Live cell number was determined by trypan blue exclusion. To assess live/dead cell percentage, OVCAR8 cells were treated with compounds for 48 hours. Cells were

trypsinized, washed once, and then resuspended in 1x phosphate buffered saline (PBS). Fifteen minutes prior to analysis, propidium iodide (Sigma-Aldrich P4864) was added to a final concentration of 1μg/mL and cells were immediately analyzed by flow cytometry.

2.2.3 Western blotting

$3x10^6$ cells were lysed in RIPA buffer with protease inhibitor (Roche 11836170001), and equal volumes of lysate were analyzed by western blotting (Anderson et al., 2017). Primary antibodies used were: anti-HSP90 (1:2000, Cell Signaling Technology 4874), anti-CBFβ (1:1000, Santa Cruz Biotechnology 20693), anti-RUNX1 (1:1000, Santa Cruz Biotechnology 28679), anti-RUNX2 (1:500, Santa Cruz Biotechnology 390351), and anti-RUNX3 (1:500, Santa Cruz Biotechnology 101553).

2.2.4 EdU labeling and pHH3 IF staining

For EdU labeling, OVCAR8 or OVCAR4 cells were seeded in 4-well chamber slides and treated as described. Cells were pulse labeled with 10μM EdU for 45 minutes, then fixed with 4% paraformaldehyde (PFA). EdU was detected using the Click-iT EdU Kit (Invitrogen C10339) following the manufacturer's protocol. EdU intensity was measured using ImageJ. Immunofluorescence staining was performed as previously described with a primary antibody against phospho-HistoneH3(Ser10) (pHH3) (1:500, Millipore 06-570) (Anderson et al., 2017).

2.2.5 Cell cycle analysis

For unsynchronized cell cycle analysis, OVCAR8 cells were treated with 10μM AI-10-104 for 24 or 48 hours and collected. For the G_1/S arrest, OVCAR8 cells were treated with 2mM thymidine (Sigma-Aldrich T1895) for 17 hours, released for 8 hours, and then treated with 2mM thymidine for 14 hours. For the G_2/M arrest, OVCAR8 cells were treated with 2mM thymidine for 24 hours, released for 3 hours, and then treated with 5μg/mL nocodazole (Sigma-Aldrich T1895) for 12 hours. Following G_1/S or G_2/M cell cycle arrest, cells were released into media containing dimethyl sulfoxide (DMSO) or 5μM AI-10-104, and cells were collected at indicated times. Cells were stained with propidium iodide (Sigma-Aldrich P4864) to measure DNA content as previously described (Zerlanko et al., 2012).

2.2.6 Wound healing assays

OVCAR8 cells (250,000) were seeded in 6-well plates. The following morning, cells were washed once with PBS, and culture media was replaced with RPMI supplemented with 2.5% FBS and compounds. After 10 hours, confluent monolayers were scratched with a P1000 pipette tip, and the size of the wound was measured at 0, 14, and 24 hours. For siRNA-mediated knockdown, OVCAR8 cells (80,000) were seeded in 12-well plates. Sixteen hours later, cells were transfected with siRNAs as described in 2.10. Twenty-four hours after transfection, cells were washed once with 1x PBS, and culture media was replaced with RPMI supplemented with 2.5% FBS. After 10 hours, confluent monolayers were scratched with a P1000 pipette tip. Size of the wound was measured at 0 and 24 hours. Images were captured using an EVOS XL Core microscope. Wound size was

analyzed using MRI Wound Healing macro for ImageJ (http://dev.mri.cnrs.fr/projects/imagej-macros/wiki/Wound_Healing_Tool).

2.2.7 Colony formation in soft agar

OVCAR8 cells (2500), OVCAR4 (5000) or SKOV3ip1 cells (1000) were seeded into soft agar in 6-well plates in the presence of compounds. Media on the colonies was changed every 4th day. After 14 days (OVCAR8), 40 days (OVCAR4), or 24 days (SKOV3ip1), colonies were stained with 0.005% crystal violet (Sigma-Aldrich C6158) and imaged using a Gel Doc XR+ (BioRad). For compound addition experiments, OVCAR8 cells (5000) were seeded in soft agar. After 11 days, media on the colonies was changed to media supplemented with either DMSO or 10μM AI-14-91. Colonies were treated for 7 days and then stained as above. Colony number was counted using Quantity One 1-D Analysis software (BioRad), or by counting colony number in 4 fields of view per well. Colony size was measured using ImageJ.

2.2.8 OVCAR8 xenograft

Animal procedures were approved by the University of Virginia Animal Care and Use Committee. Animals were housed on a 12-hour light/dark cycle at 23°C with 30-50% relative humidity. 5.2x10^6 OVCAR8 cells were injected intraperitoneally (i.p.) into 7-8 week old female athymic nude mice (Envigo). Two days later, mice were randomized (n=10/group) and treated i.p. with either vehicle control or 100mg/kg AI-14-91 twice per day for 12 days. AI-14-91 was diluted to 25mg/mL in 0.1M Captisol (Ligand Pharmaceuticals) using the *in situ* formed hydrochloride salt. Compounds were 0.22μM

sterile filtered prior to use. Mice were weighed twice weekly, and behavior carefully noted, to assess for drug toxicity. Mice were euthanized 29-30 days after the initial xenograft and total tumor weight was measured.

2.2.9 RNA-Seq and RT-qPCR

OVCAR8 cells were treated for 0, 6 or 24 hours with 5μM AI-10-104, and RNA was sequenced as previously described (Anderson et al., 2017). RNA-Seq data were returned in Fastq format and analyzed using FastQC to determine quality. Combined reads for each sample were mapped to the genome using HISAT2 (Kim et al., 2015). Mapped reads were sorted using Samtools and read counts were obtained using featureCounts (Li et al., 2009; Tan et al., 2016).[2] Differential gene expression was analyzed using DESeq2 (Anders and Huber, 2010). Genes with an adjusted p value of < 0.05 were considered significantly altered. RT-qPCR validation of gene expression changes was performed on an independent set of RNA. EnrichR analysis was performed by submitting the list of differentially expressed genes (DEGs) to the EnrichR platform (Chen et al., 2013; Kuleshov et al., 2016). Gene Set Enrichment Analysis (GSEA) was performed using GSEA 3.0 (http://www.broad.mit.edu/gsea) (Subramanian et al., 2005). Gene sets were considered enriched when the FDR was <0.05.

RT-qPCR was performed as previously described (Anderson et al., 2017). Gene expression was normalized to GAPDH or RPL4 using the $\Delta\Delta C_T$ method. Primers were designed using Primer3 (Table 2.1). Digital droplet PCR (ddPCR) was performed using the QX200 system (BioRad) as described by the manufacturer. Briefly, cDNA and

[2] Adam Boulton processed the raw RNA-seq data into normalized read counts

primers were combined with EvaGreen MasterMix (BioRad 1864033) following the manufacturers protocol. Droplets were then generated using EvaGreen Droplet Generation Oil (BioRad 1864006) and the QX200 droplet generator (BioRad), and then PCR was performed following the manufacturers protocol. Droplets were then read using the QX200 droplet reader (BioRad). Copies of RNA/μL was determined using QuantaSoft (BioRad). Relative expression was determined by dividing the concentration of the gene of interest by the concentration of GAPDH, and then normalizing this ratio to the control.

Table 2.1 Primer sequences used for RT-qPCR

Gene	Forward	Reverse
COL7A1	TGGTGATGTTGGGAATGGCT	GGGCTGAGTAGTGAAGGATGC
IGFN1	ACCCTCATTGTCATAGAACCCAGC	GGGCACAGCCTCCATCCTTG
INHBA	CCGAGTCAGGAACAGCCAGGA	GCTGGAAGAGGCGGATGGTG
GAPDH	AATCCCATCACCATCTTCCA	AGAGATGATGACCCTTTTGG
MMP1	GCTTTCCTCCACTGCTGCTG	ACTTGCCTCCCATCATTCTTCAG
RLP4	CCGGAACACCATTCTTCG	ACCTACCACAGGCTTCTTGC

2.2.10 siRNA-mediated knockdown

OVCAR8 cells were plated in 12-well plates (80,000) or 4-well chamber slides (35,000). The following morning, cells were transfected with a pool of 4 siRNAs directed at non-targeting, inhibin beta a subunit (INHBA), or matrix metalloprotease 1 (MMP1) to a final concentration of 200 nM using Lipofectamine RNAiMax (Invitrogen 13778) per the manufacturer's protocol. siRNA sequences are provided in Table 2.2. Knockdown of target genes was confirmed by RT-qPCR. Protein loss following siRNA knockdown was confirmed by immunofluorescence staining for INHBA (1:66 , R&D Systems AF338) or MMP1 (1:60, AbCam ab52631) as previously described (Anderson et al., 2017).

Table 2.2 siRNA sequences and catalog numbers

Gene	GE Dharmacon Catalog Number	siRNA	Target Sequence
Non-Targeting	D-001206-13	1	UAGCGACUAAACACAUCAA
		2	UAAGGCUAUGAAGAGAUAC
		3	AUGUAUUGGCCUGUAUUAG
		4	AUGAACGUGAAUUGCUCAA
INHBA	M-011701-02	1	GCACAGACCUUUCCUCAUG
		2	GAACGGGUAUGUGGAGAUA
		3	CAACAUCUGCUGUAAGAAA
		4	GUAGUAGACGCUCGGAAGA
MMP1	M-005951-01	1	GGAGGUAUGAUGAAUAUAA
		2	GAUGAAAGGUGGACCAACA
		3	ACAGUAAGCUAACCUUUGA
		4	GCUAACCUUUGAUGCUAUA

2.2.11 Statistical methods

Each experiment was completed 3 independent times with n=3-6 technical replicates. Data shown are mean ± standard deviation (SD) of one representative experiment. Data was analyzed using Microsoft Excel and GraphPad PRISM 7.0. Groups were compared using a t-test, one-way ANOVA or two-way ANOVA with Holm-Sidak post-hoc tests, * $p<0.05$, ** $p<0.01$, *** $p<0.001$ control vs. experimental condition. IC_{50} values were calculated using the GraphPad PRISM curve fit – log inhibitor vs. normalized response.

2.3 Results

2.3.1 Ovarian cancer cell lines are sensitive to treatment with compounds that inhibit CBFβ/RUNX binding

A panel of 6 ovarian cancer cell lines was assessed for sensitivity to AI-10-104 and AI-14-91, active inhibitors of CBFβ's binding to RUNX proteins. All 6 ovarian cancer cell lines had reduced cell number after 3 days of treatment with either active compound (Figure 2.1A,B), and a range of sensitivities was observed. Treatment with AI-4-88, an inactive control compound with a similar chemical structure, had minimal effects on cellular proliferation at IC_{50} concentrations of AI-10-104 and AI-14-91 (Figure 2.1C). All cell lines express CBFβ and at least one RUNX protein (Figure 2.1D). There was a trend towards a positive correlation between CBFβ expression and sensitivity to active inhibitors, though SKOV3ip1 was an exception to this pattern. Given the high levels of heterogeneity within ovarian cancer cell lines, further studies should characterize what molecular features affect cell line sensitivity to compounds. Treatment of OVCAR8 cells with inhibitors did not cause a decrease in the protein levels of CBFβ or RUNX proteins (Figure 2.1E). Additionally, BEAS-2B cells, a normal epithelial cell line, treated with working concentrations of AI-10-104 had no effect on cell number after 3 days of treatment (Figure 2.1F).[3] Moving forward, experiments were performed primarily in the OVCAR8 cell line, and key experiments were replicated in the OVCAR4 cell line. These cell lines were chosen because they have high expression of CBFβ and have been shown to have a similar gene expression profile to high-grade serous ovarian cancer patient tumors (Domcke et al., 2013).

[3] Yan Gao performed the experiment using BEAS-2B cells

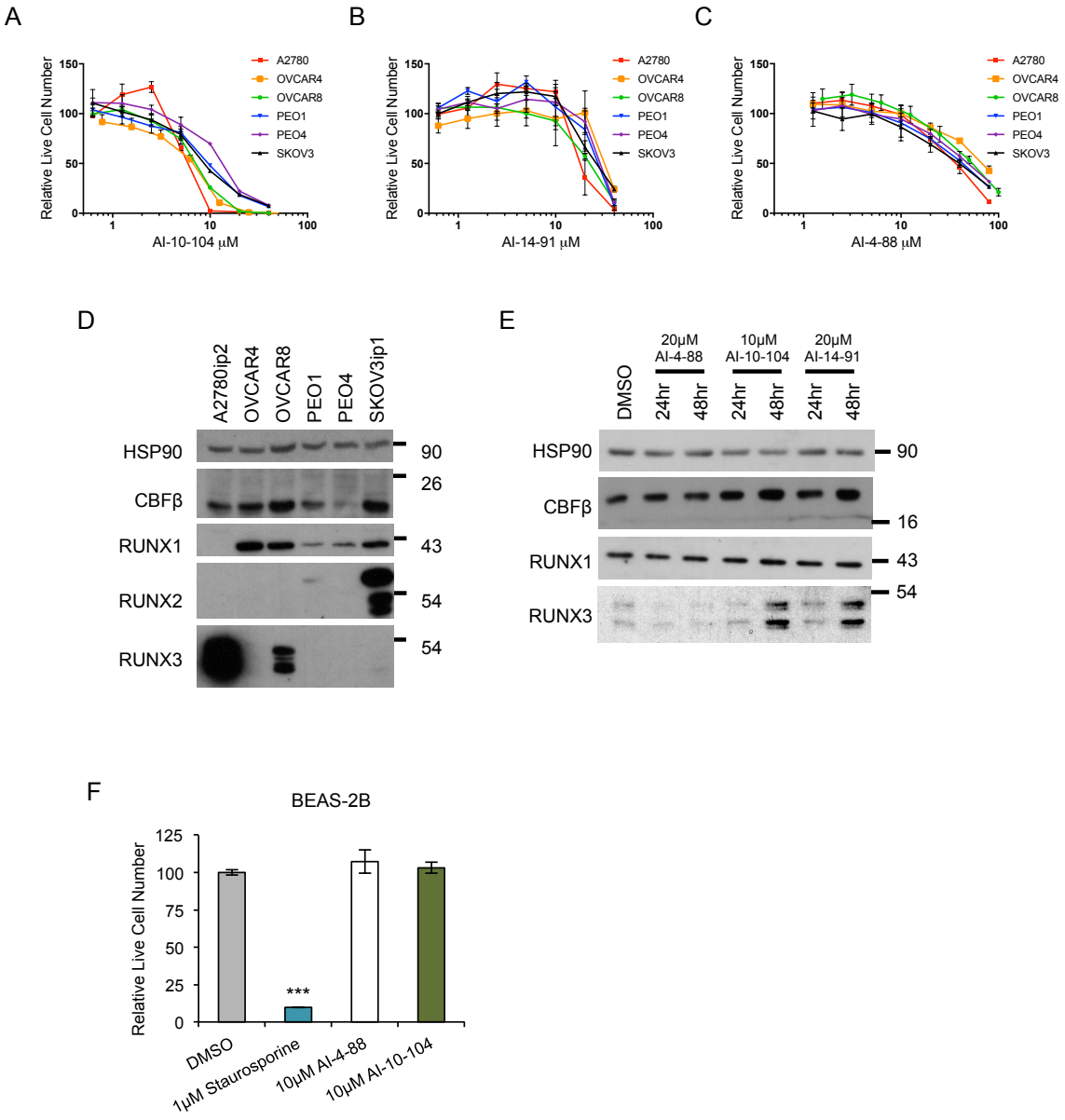
A
B
C
Relative Live Cell Number
A2780
OVCAR4
OVCAR8
PEO1
PEO4
SKOV3
AI-10-104 μM
AI-14-91 μM
AI-4-88 μM
D
A2780ip2
OVCAR4
OVCAR8
PEO1
PEO4
SKOV3ip1
HSP90
CBFβ
RUNX1
RUNX2
RUNX3
90
26
43
54
54
E
DMSO
20μM AI-4-88
10μM AI-10-104
20μM AI-14-91
24hr
48hr
HSP90
CBFβ
RUNX1
RUNX3
90
16
43
54
F
BEAS-2B
Relative Live Cell Number
***
DMSO
1μM Staurosporine
10μM AI-4-88
10μM AI-10-104

Figure 2.1 Effects of inhibitors on cell growth

A-C. Relative live cell number measured using CellTiter-Glo after 3 days of AI-10-104 (A), AI-14-91 (B), or AI-4-88 (C) treatment (n=3/dose). D. Western blot of 6 ovarian cancer cell lines for CBFβ, RUNX1, RUNX2, and RUNX3. One representative HSP90 blot is shown as a loading control. E. Western blot of OVCAR8 cells treated with indicated inhibitors for 24 or 48 hours for CBFβ, RUNX1, and RUNX3. HSP90 is shown as a loading control. F. Relative live cell number of BEAS-2B cells measured by MTT after 3 days of AI-4-88, AI-10-104 or staurosporine treatment (n=4/dose). ***$p<0.001$, by one-way ANOVA (F) with Holm-Sidak post-hoc tests.

To determine if the change in cell number was due to reduced growth or increased cell death, OVCAR8 cells were treated with either DMSO or 7μM AI-10-104, and the number of live cells was measured by trypan blue exclusion after 1, 3, and 5 days. Inhibitor treatment significantly reduced the number of live cells (Figure 2.2A). The 7μM dose was used because it is the average IC_{50} for the OVCAR8 cell line. To confirm that the number of dead cells did not increase with compound treatment, OVCAR8 cells were treated with high doses of compounds for 48 hours, and the percentage of dead cells was measured by flow cytometry. Treatment with 20μM AI-4-88, 10μM AI-101-04, or 20μM AI-14-91 caused minimal cell death, while causing significant reductions in total cell number (Figure 2.2B,C). There was a statistically significant increase in cell death with 20μM AI-14-91 treatment; however, the absolute percentage of dead cells increased from an average of 0.6% in the DMSO treatment to an average of 1.8% in the AI-14-91 treatment, which we do not believe has biological significance.

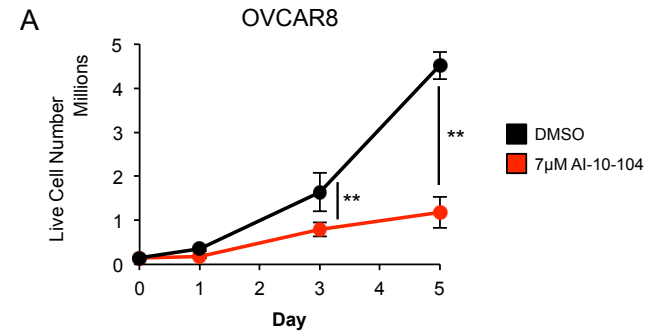
A
OVCAR8
Live Cell Number
Millions
5
4
3
2
1
0
0
1
2
3
4
5
Day
**
**
DMSO
7μM AI-10-104

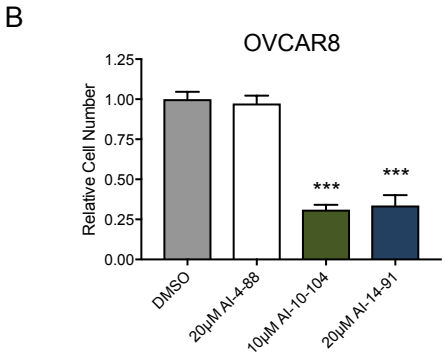
B
OVCAR8
Relative Cell Number
1.25
1.00
0.75
0.50
0.25
0.00
***
***
DMSO
20μM AI-4-88
10μM AI-10-104
20μM AI-14-91

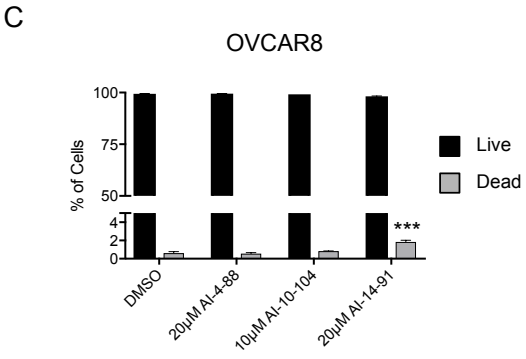
C
OVCAR8
% of Cells
100
75
50
4
2
0
***
Live
Dead
DMSO
20μM AI-4-88
10μM AI-10-104
20μM AI-14-91

Figure 2.2 Inhibitor treatment decreases OVCAR8 proliferation

A. OVCAR8 cells were treated with DMSO or 7μM AI-10-104. Number of live cells was counted by trypan blue exclusion at the indicated time. B. Relative OVCAR8 cell number after treatment with compounds for 48 hours. C. Percentage of live and dead OVCAR8 cells after compound treatment for 48 hours. Live/Dead analysis was performed by propidium iodide exclusion and measured by Flow Cytometry. ** $p<0.01$, ***$p<0.001$, by one-way ANOVA (B,C) or two-way repeated-measures ANOVA (A) with Holm-Sidak post-hoc tests.

2.3.2 AI-10-104 treatment reduces mitotic index and decreases EdU incorporation

Due to the reduced cell number following compound treatment, we investigated the mitotic index of OVCAR8 cells. Cells were treated with 10μM AI-10-104 for 24 or 48 hours and proliferation was measured by pHH3 staining, which marks cells in late G_2 and mitosis (Hendzel et al., 1997). Treatment with AI-10-104 significantly decreased the percentage of cells staining positive for pHH3, indicating a slowed proliferative rate (Figure 2.3A,B).

Due to the reduction in cell proliferation and mitotic index following tool compound treatment, we investigated the cell cycle profile of OVCAR8 cells exposed to AI-10-104 by propidium iodide staining. Asynchronously dividing OVCAR8 cells treated with AI-10-104 for 24 or 48 hours did not show a G_1 arrest, as has been previously described following RUNX1 knockdown in ovarian cancer (Keita et al., 2013). However, there was a significant increase in the number of cells in S-phase (Figure 2.3C,D).

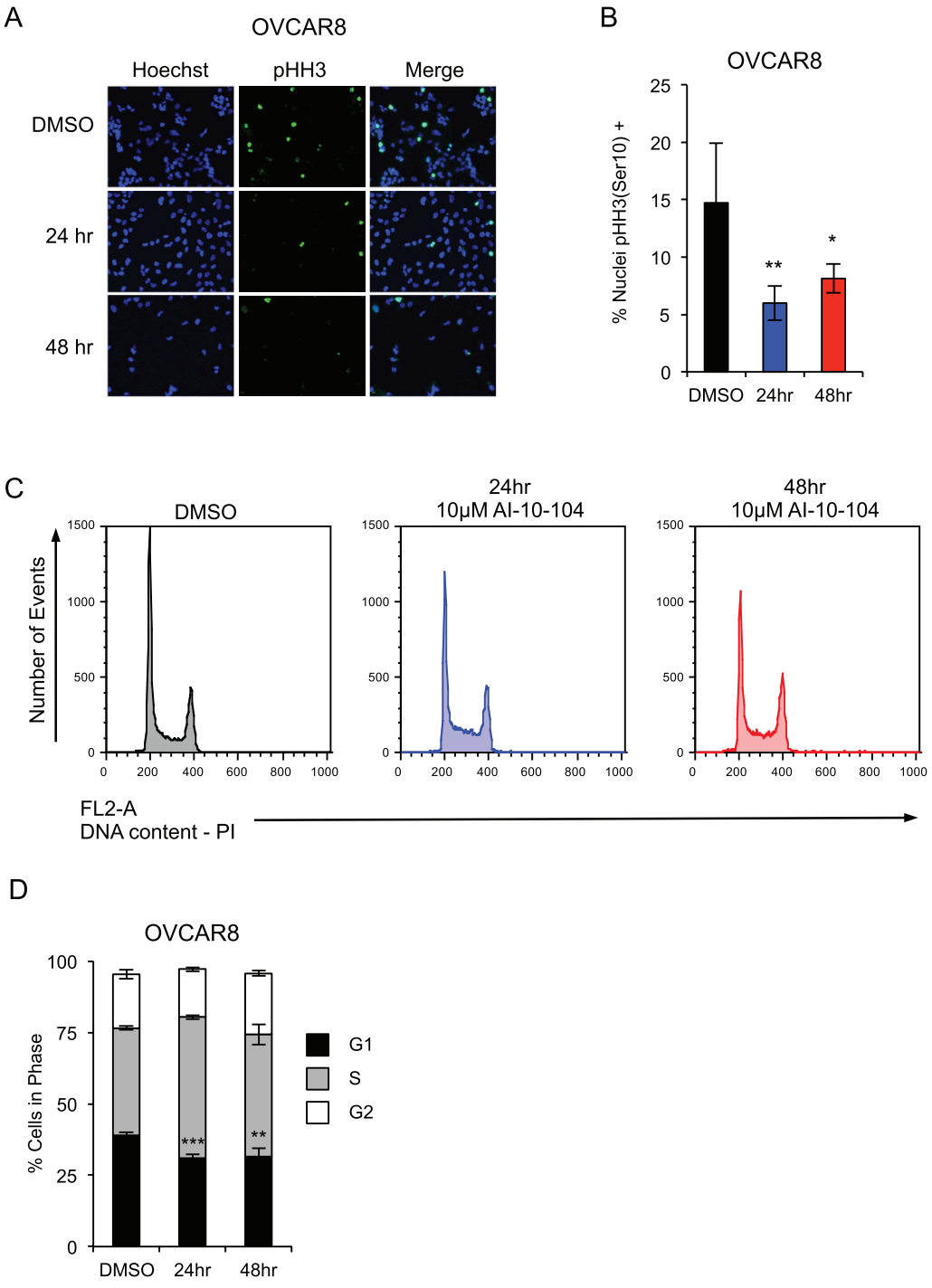
A
OVCAR8
Hoechst
pHH3
Merge
DMSO
24 hr
48 hr
B
OVCAR8
% Nuclei pHH3(Ser10) +
25
20
15
10
5
0
**
*
DMSO
24hr
48hr
C
DMSO
24hr
10μM AI-10-104
48hr
10μM AI-10-104
Number of Events
1500
1000
500
0
0
200
400
600
800
1000
FL2-A
DNA content - PI
D
OVCAR8
% Cells in Phase
100
75
50
25
0
***
**
G1
S
G2
DMSO
24hr
48hr

Figure 2.3 Effects of AI-10-104 on cell cycle kinetics

A. OVCAR8 cells were treated with 10μM AI-10-104 for 0, 24 or 48 hours and then stained with anti-pHH3(Ser10). Representative images are displayed. B. Quantification of pHH3 staining (n=4/time). C. Representative histograms of DNA content measured by propidium iodide straining of OVCAR8 cells treated with 10μM AI-10-104 for 0, 24 or 48 hours. D. Percentage of cells in each phase of the cell cycle measured by propidium iodide staining of DNA content and analyzed by Flow Cytometry (n=3/time). * $p<0.05$, ** $p<0.01$, ***$p<0.001$, by one-way ANOVA (B,D) with Holm-Sidak post-hoc tests.

To more accurately assess S-phase kinetics after tool compound treatment, OVCAR8 cells were treated with 10μM AI-10-104 for 24 or 48 hours. Cells were pulse labeled with EdU immediately prior to fixation. The proportion of cells incorporating EdU, a thymidine analog that marks active DNA replication, was significantly decreased after both 24 and 48 hours of compound treatment (Figure 2.4A,C). In addition to the decrease in the proportion of cells incorporating EdU, the intensity of each positive nucleus was significantly reduced, indicating a decreased rate of DNA replication (Figure 2.4D). These findings were replicated in the OVCAR4 cell line, which was treated with 10μM AI-10-104 for 48 or 72 hours. The proportion of OVCAR4 cells incorporating EdU was significantly decreased after 72 hours, with a strong trend towards a decrease at 48 hours ($p=0.08$) (Figure 2.4B,E). OVCAR4 cells were treated for longer than OVCAR8, because their doubling time is substantially longer.

2.3.3 AI-10-104 treatment slows S-phase progression in synchronized cells

To probe the apparent dichotomy between propidium iodide staining, indicating compound treatment increased the percentage of cells in S-phase, and EdU incorporation results, indicating the opposite, the cell cycle kinetics of synchronized cells was examined. OVCAR8 cells were arrested at the G_1/S boundary using a thymidine double block. Cells were then released from arrest into DMSO or 5μM AI-10-104. A low dose of compound was used to ensure that the observed effects were not influenced by cellular toxicity. Cell cycle progression was measured by propidium iodide staining at multiple time points over the next 30 hours.

As compound treated cells progressed through the cell cycle, their rate of S-phase completion was slowed relative to DMSO treated cells. A mild reduction in the rate of S-phase completion was observed at 6 hours – the first S-phase with compound treatment (Figure 2.4F). A more profound decrease in the rate of S-phase completion was observed 24 hours after release from the G_1/S boundary. Comparable results were obtained when cells were arrested at the G_2/M boundary by nocodazole and released into DMSO or AI-10-104 (Figure 2.4G).

These data indicate that while compound treated cells can progress through the cell cycle, the rate at which they do so is diminished due to a slow progression through S-phase. This S-phase delay leads to an increased percentage of cells in S-phase as measured by total DNA content. The apparent decrease in the proportion of cells in S-phase as measured by percent of EdU-positive cells is likely secondary to the decreased rate of incorporation. Cells with slow DNA replication velocity would both spend longer in S-phase and be less likely to incorporate EdU above the detection threshold.

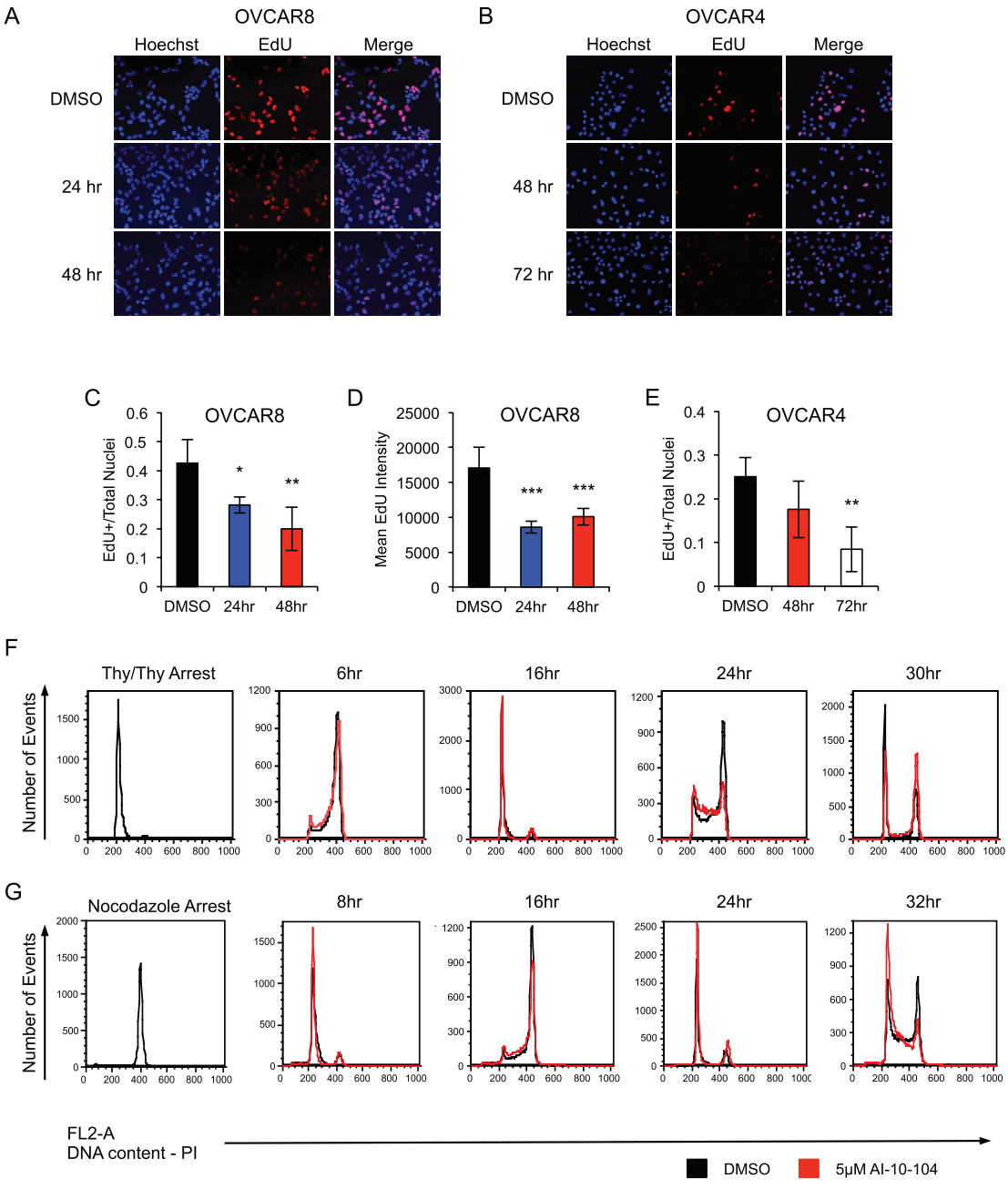
A
OVCAR8
Hoechst
EdU
Merge
DMSO
24 hr
48 hr
B
OVCAR4
Hoechst
EdU
Merge
DMSO
48 hr
72 hr
C
OVCAR8
EdU+/Total Nuclei
DMSO
24hr
48hr
D
OVCAR8
Mean EdU Intensity
DMSO
24hr
48hr
E
OVCAR4
EdU+/Total Nuclei
DMSO
48hr
72hr
F
Thy/Thy Arrest
6hr
16hr
24hr
30hr
Number of Events
G
Nocodazole Arrest
8hr
16hr
24hr
32hr
Number of Events
FL2-A
DNA content - PI
DMSO
5μM AI-10-104

Figure 2.4 AI-10-104 treatment alters S-phase kinetics

A. OVCAR8 cells were treated with 10μM AI-10-104 for 0, 24, or 48 hours then pulsed with EdU immediately prior to fixation. EdU incorporation was measured using Click-iT™ Imaging Kit. Representative images are shown. B. OVCAR4 cells were treated with 10μM AI-10-104 for 0, 48 or 72 hours then pulsed with EdU immediately prior to fixation. EdU incorporation was measured using Click-iT™ Imaging Kit. Representative images are shown. C. Quantification of EdU+ OVCAR8 cells relative to total nuclei (n=4/time). D. Quantification of mean EdU intensity of each positive OVCAR8 nucleus (n=4/time). E. Quantification of EdU+ OVCAR4 cells relative to total nuclei (n=4/time). F. OVCAR8 cells were arrested at the G_1/S boundary and released into DMSO or 5μM AI-10-104. DNA content was measured by propidium iodide staining at the indicated times. G. OVCAR8 cells were arrested at the G_2/M boundary with nocodazole. Cells were released into DMSO or 5μM AI-10-104, and DNA content was measured by propidium iodide staining was measured at indicated times. * $p<0.05$, ** $p<0.01$, ***$p<0.001$, by one-way ANOVA (C-E) with Holm-Sidak post-hoc tests.

2.3.4 AI-10-104 and AI-14-91 treatment impair wound healing and colony formation in soft agar

As CBFβ and RUNX proteins have been shown to modulate migration in ovarian and other epithelial cancers, we investigated the ability of tool inhibitors of the CBFβ/RUNX interaction to impair cell mobility, using a wound healing assay. Confluent monolayers of OVCAR8 cells were scratched and wound size was measured at 0, 14, and 24 hours. Treatment with AI-10-104 and AI-14-91 significantly impaired wound healing (Figure 2.5A,B).

To assess the ability of tool compounds to decrease anchorage-independent growth, OVCAR8 cells were plated in soft agar in the presence of either AI-10-104 or AI-14-91, and the number of colonies was counted after 14 days. Inhibitor treatment significantly reduced the number of colonies, from an average of 176 colonies per well in the control to an average of 12 colonies per well across all compound treatments (Figure 2.5C,F). Treatment with AI-4-88, the inactive control compound, did not appear to alter colony formation, indicating that this dramatic effect likely results from CBFβ/RUNX inhibition specifically. To ensure that this reduction in colony formation was not specific to the OVCAR8 cell line, colony formation in the presence of compounds was investigated in SKOV3ip1 and OVCAR4 cell lines. Similar significant reductions in colony formation were observed (Figure 2.5D,E,G,H).

Prior experiments assessed the ability of tool compounds to inhibit initial colony formation as well as subsequent colony growth. Thus, we assessed the ability of the tool

compounds to inhibit the growth of already-formed colonies. OVCAR8 cells were seeded in soft agar, and incubated for 11 days. Colonies were then treated with DMSO or 10μM AI-14-91 for 7 days. While the number of colonies did not change between treatments, the size of the inhibitor-treated colonies was significantly reduced (Figure 2.5I-K), indicating that tool compounds can decrease the growth rate of established colonies in addition to inhibiting the generation of new colonies.

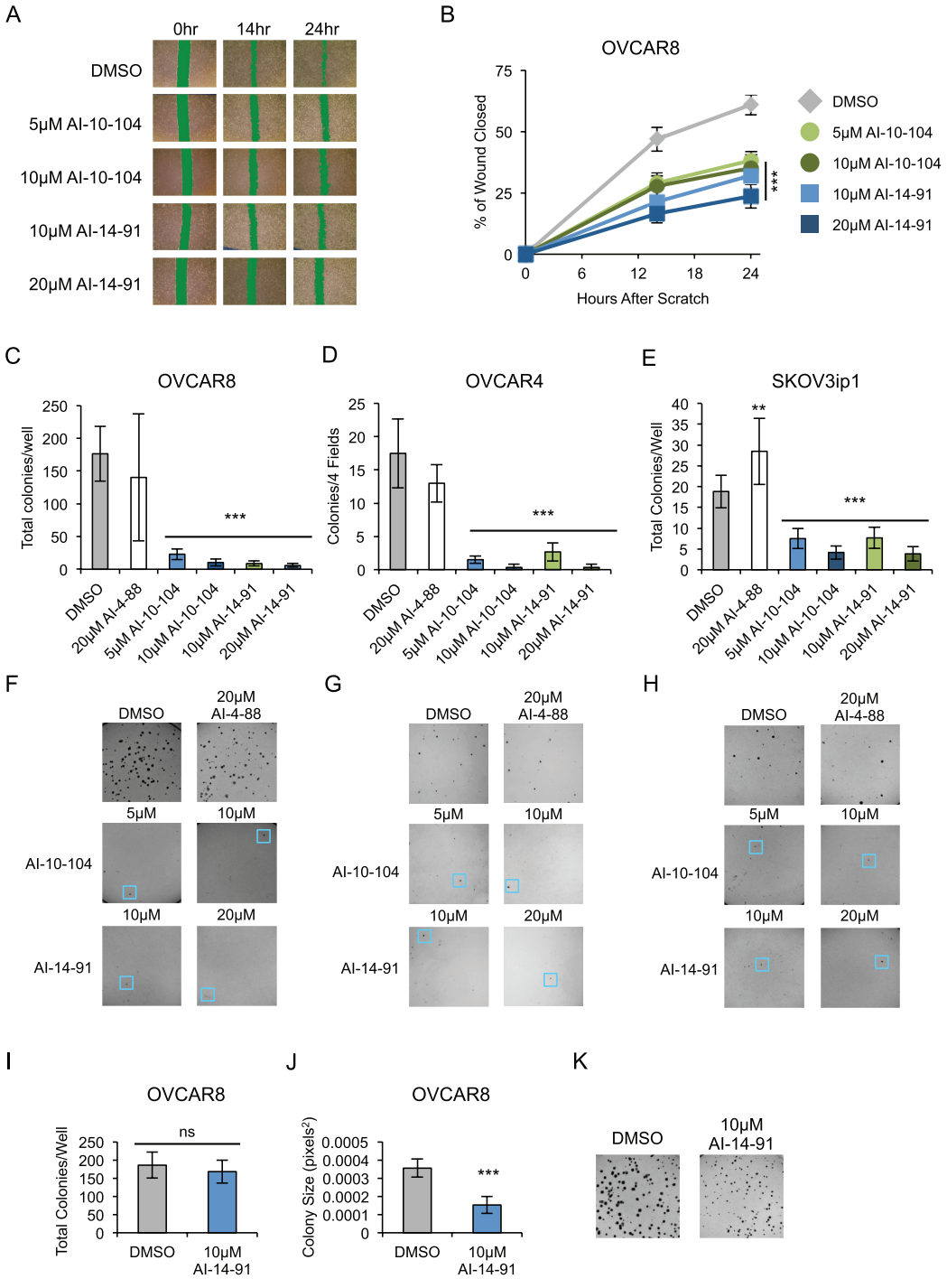
A
0hr
14hr
24hr
DMSO
5μM AI-10-104
10μM AI-10-104
10μM AI-14-91
20μM AI-14-91
B
OVCAR8
% of Wound Closed
Hours After Scratch
***
DMSO
5μM AI-10-104
10μM AI-10-104
10μM AI-14-91
20μM AI-14-91
C
OVCAR8
Total colonies/well
***
D
OVCAR4
Colonies/4 Fields
***
E
SKOV3ip1
Total Colonies/Well
**
***
F
G
H
DMSO
20μM AI-4-88
5μM
10μM
AI-10-104
10μM
20μM
AI-14-91
I
OVCAR8
Total Colonies/Well
ns
DMSO
10μM AI-14-91
J
OVCAR8
Colony Size (pixels²)
***
DMSO
10μM AI-14-91
K
DMSO
10μM AI-14-91

Figure 2.5 Effects of inhibitors on wound healing and colony formation

A-B. Confluent monolayers of OVCAR8 cells were scratched with a pipette tip. Size of the wound was imaged at 0, 14, and 24 hours. A. Representative images of wounds. Wound is highlighted in green. B. Quantification of wound closure (n=3 wounds/dose). C-H. Colony formation in soft agar of ovarian cancer cells treated with compounds. Total number of OVCAR8(C), OVCAR4 (D), SKOV3ip1 (E) colonies per well or 4 fields of view (n=6/dose). F-H. Representative images of OVCAR8 (F), OVCAR4 (G), and SKOV3ip1 (H) colonies treated with inhibitors. Small colonies on inhibitor treated plates are outlined in blue. I-K. OVCAR8 cells were seeded in soft agar. After 11 days, colonies were treated with DMSO or 10μM AI-14-91 for 7 days. I. Total number of colonies following compound treatment (n=6/dose). J. Average colony size (n=6/dose) K. Representative images of colonies following 7 days of compound treatment. * $p<0.05$, ** $p<0.01$, ***$p<0.001$, by t-test (I,J), one-way ANOVA (C-E), or two-way repeated measure ANOVA (B) with Holm-Sidak post-hoc tests.

To extend these results to an *in vivo* model of anchorage-independent growth, the effects of AI-14-91 were tested in a xenograft model of ovarian cancer. AI-10-104 is not suitable for use in animals (Illendula et al., 2016). Athymic nude mice were injected i.p. with OVCAR8 cells. Two days later, mice were randomized and treated with vehicle control or AI-14-91 at 100mg/kg twice per day for 12 days. Thirty days following xenografting, total tumor weight from the peritoneal cavity was measured. There was no significant change in total tumor weight; however, this is likely due to the limited half-life and low potency of AI-14-91 (Figure 2.6A). Pharmacokinetic data indicates that CBFβ was likely only inhibited for ~2 hours following each injection (Illendula et al., 2016). Treatment with AI-14-91 did not cause any overt toxicity or weight loss (Figure 2.6B).

A

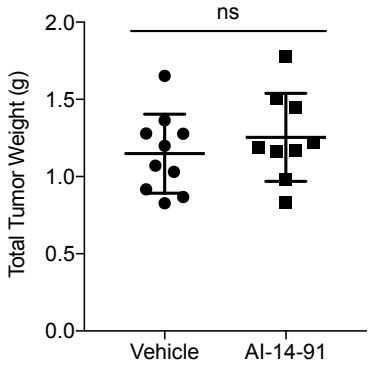
ns
2.0
1.5
1.0
0.5
0.0
Total Tumor Weight (g)
Vehicle
AI-14-91

B

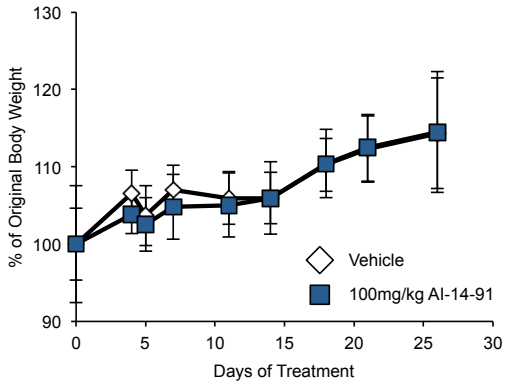
130
120
110
100
90
% of Original Body Weight
0
5
10
15
20
25
30
Days of Treatment
Vehicle
100mg/kg AI-14-91

Figure 2.6 AI-14-91 does not reduce xenograft growth in mice

A. Total tumor weight of Nude mice xenografted with OVCAR8 cells i.p. and treated with AI-14-91 at 100mg/kg twice daily for 12 days (n=10 mice/treatment). Tumors were collected 29-30 days after xenografting. Horizontal bar and error bars represent mean ± SD and each dot represents one individual mouse. B. Percent change in bodyweight during in vivo experiment.

2.3.5 Inhibition of CBFβ with AI-10-104 alters the transcription of a small network of genes

As CBFβ constitutes an integral component of the CBFβ/RUNX transcription factor complex, we hypothesized that CBFβ controlled the expression of a network of genes regulating proliferation, migration, and anchorage-independent growth. To assess the network of genes controlled by CBFβ in ovarian cancer, we performed RNA-Seq on OVCAR8 cells treated with 5μM AI-10-104 for 0, 6 or 24 hours. We chose a short time course to identify the most proximal effects of CBFβ/RUNX inhibition and used a low dose of compound to reduce the chance of any confounding toxicity. Analysis of differential gene expression using DESeq2 revealed a small set of genes altered by compound treatment (Figure 2.7A,B, Table 2.3). Alterations in a panel of DEGs, including INHBA, MMP1, COL7A1, and IGFN1 were confirmed by RT-qPCR (Figure 2.7C). Additionally, these changes in gene expression were replicated in the OVCAR4 cell line indicating these findings are not unique to the OVCAR8 cells (Figure 2.7D).

A

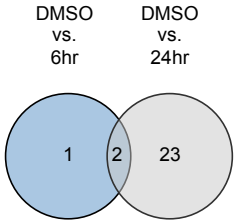

B

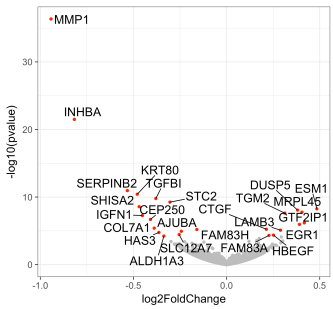

C

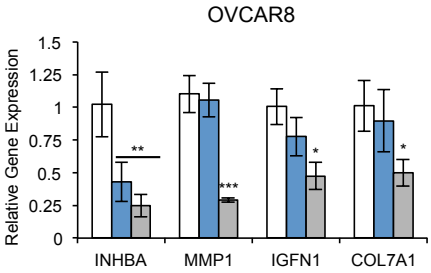

D

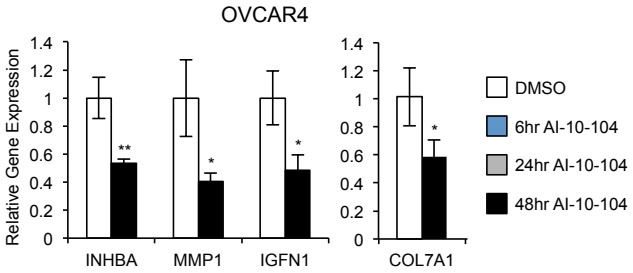

E

ChEA 2016	p adj	Z-score
PPAR_26484153_Chip-Seq_NCI H1993_Human	0.0056	-1.960
SMAD2_18955504_ChIP ChIP_HaCaT_Human	0.0113	-1.805
SMAD3_18955504_ChIP-ChIP_HaCaT_Human	0.0113	-1.798
TP63_23658742_ChIP-Seq_EP156T_Human	0.0113	-1.084
ATF3_23680149_ChIP-Seq_GBM1-GSC_Human	0.0253	-1.571

Figure 2.7 AI-10-104 changes the expression of a small network of genes

A. Venn diagram of differentially expressed genes (DEGs) following 6 or 24 hours of treatment with 5μM AI-10-104 measured by RNA-Seq. Differential gene expression was analyzed using DESeq2 with a significance cutoff of padj<0.05 (n=3 samples/condition). B. Volcano plot of DEGs. C-D. Confirmation of DEGs in OVCAR8 and OVCAR4 cells treated with AI-10-104 for the indicated time. C. RT-qPCR analysis of gene expression in OVCAR8 cells. Expression of each gene is normalized to GAPDH (n=3 samples/dose). D. ddPCR (INHBA, MMP1, IGFN1) or RT-qPCR (COL7A1) analysis of gene expression in OVCAR4 cells. Expression of each gene is normalized to GAPDH (n=3 samples/dose). E. Significantly enriched TF consensus sequences in DEGs assessed from the ChEA 2016 database using EnrichR. * $p<0.05$, ** $p<0.01$, ***$p<0.001$, by t-test (D) or one-way ANOVA (C) with Holm-Sidak post-hoc tests.

Table 2.3 Differentially expressed genes after 24 hours of AI-10-104 treatment in OVCAR8 cells

Gene	baseMean	log2FC	lfcSE	stat	pvalue	padj
MMP1	1331.385294	-0.94257	0.07409	-12.72212	4.46E-37	9.01E-33
INHBA	273.731519	-0.81742	0.08432	-9.69390	3.20E-22	3.24E-18
SERPINB2	60.31759451	-0.53278	0.07843	-6.79272	1.10E-11	7.42E-08
KRT80	420.3199442	-0.47973	0.07258	-6.60965	3.85E-11	1.95E-07
SHISA2	43.55317982	-0.46950	0.07889	-5.95125	2.66E-09	7.69E-06
IGFN1	435.9450881	-0.45211	0.08319	-5.43487	5.48E-08	9.24E-05
CEP250	1245.750903	-0.40879	0.07874	-5.19172	2.08E-07	3.24E-04
COL7A1	359.8382783	-0.38867	0.08427	-4.61206	3.99E-06	5.04E-03
TGFBI	3213.697744	-0.37982	0.05943	-6.39086	1.65E-10	6.67E-07
HAS3	131.2655138	-0.36320	0.08448	-4.29909	1.72E-05	1.65E-02
ALDH1A3	973.1846338	-0.33688	0.08391	-4.01455	5.96E-05	4.82E-02
STC2	4185.092571	-0.30418	0.04906	-6.20039	5.63E-10	1.90E-06
SLC12A7	204.007367	-0.25474	0.06161	-4.13461	3.56E-05	3.27E-02
AJUBA	5014.75897	-0.24292	0.05540	-4.38517	1.16E-05	1.17E-02
FAM83H	15.62240046	-0.15967	0.03536	-4.51595	6.30E-06	7.08E-03
CTGF	5616.236625	0.21339	0.04707	4.53404	5.79E-06	6.88E-03
FAM83A	1597.738973	0.22765	0.05594	4.06928	4.72E-05	3.97E-02
HBEGF	1153.939125	0.25150	0.06148	4.09047	4.30E-05	3.78E-02
LAMB3	1591.821551	0.28946	0.06483	4.46521	8.00E-06	8.51E-03
TGM2	19092.3076	0.31226	0.05594	5.58244	2.37E-08	4.36E-05
DUSP5	1519.20176	0.38132	0.06626	5.75524	8.65E-09	1.94E-05
EGR1	295.7482519	0.39090	0.08025	4.87113	1.11E-06	1.50E-03
MRPL45	498.8270675	0.40472	0.07180	5.63710	1.73E-08	3.50E-05
GTF2IP1	248.4123422	0.41714	0.08388	4.97325	6.58E-07	9.51E-04
ESM1	193.3305656	0.48459	0.08315	5.82761	5.62E-09	1.42E-05

DEGs were analyzed for transcription factor enrichment using EnrichR. Five transcription factor consensus sequences from the ChEA 2016 data set were significantly enriched, including SMAD2 and SMAD3 (Figure 2.7E). GSEA revealed enrichment of seven hallmark gene signatures, including signatures for the “Mitotic Spindle” and “Epithelial-to-Mesenchymal Transition” (EMT)(Figure 2.8A,B).

A

NAME	NES	FDR q-val	NOM p-val
MITOTIC_SPINDLE	-2.09063	0.000000	0.000000
UV_RESPONSE_DN	-2.07574	0.000000	0.000000
KRAS_SIGNALING_DN	-1.70310	0.016237	0.001984
COAGULATION	-1.64335	0.019735	0.002049
EPITHELIAL_MESENCHYMAL_TRANSITION	-1.63664	0.017005	0.000000
MYOGENESIS	-1.55551	0.029755	0.002179
APICAL_JUNCTION	-1.52653	0.032474	0.008565

B

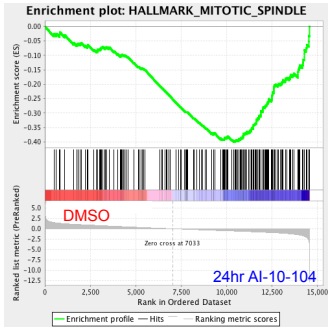

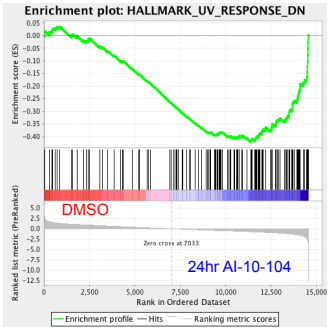

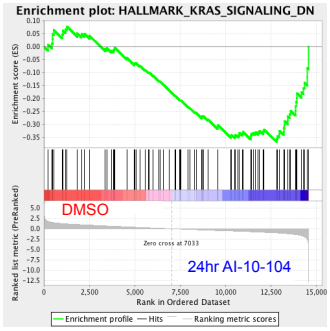

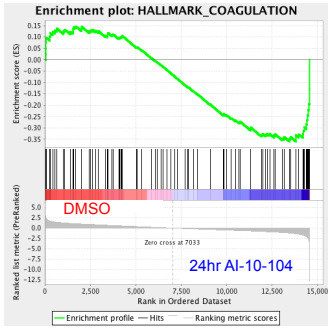

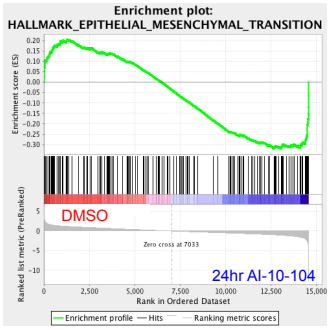

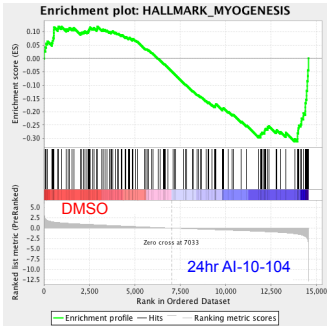

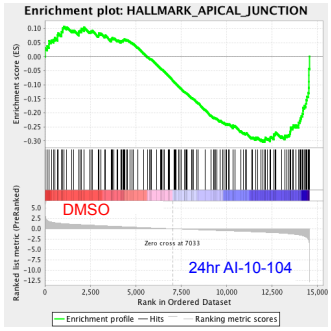

Figure 2.8 Enriched Hallmark Gene Sets from GSEA analysis

A. Table of enriched hallmark gene sets from GSEA analysis of differentially expressed genes. B. GSEA enrichment plots for the 7 significantly enriched hallmark gene sets.

2.3.6 siRNA-mediated knockdown of differentially expressed genes decreases EdU incorporation and impairs wound healing

The differentially expressed genes *INHBA* and *MMP1* were chosen for further analysis, as they are likely candidates to explain the phenotypes observed following tool compound treatment. These genes are included in the GSEA EMT gene list, are SMAD2/3 target genes, and have been putatively shown to be CBFβ or RUNX regulated in cancer (Keita et al., 2013; Mendoza-Villanueva et al., 2011; Mullen et al., 2011; Wang et al., 2013). Additionally, INBHA is the monomeric subunit of Activin A, which has been shown to promote ovarian oncogenesis by stimulating the migration of fallopian tube secretory epithelial cells (Dean et al., 2017).

To assess the influence of the above genes on cell cycle progression, OVCAR8 cells were seeded in 4-well chamber slides and transfected with a pool of 4 non-targeting siRNAs or a pool of 4 siRNAs targeting INHBA or MMP1. Three days after transfection, cells were pulse labeled with EdU. siRNA-mediated knockdown of MMP1 significantly reduced the proportion of cells incorporating EdU, as observed following tool compound treatment (Figure 2.9A,B). siRNA-mediated knockdown of INBHA showed a trend towards decreased EdU incorporation; however, it did not meet statistical significance. siRNA knockdown was confirmed by RT-qPCR (Figure 2.9E). To confirm that RNA knockdown was accompanied by a corresponding decrease in protein expression, OVCAR8 cells were transfected with non-targeting siRNAs or siRNAs targeting INHBA or MMP1. Protein levels of INHBA and MMP1, as measured by immunofluorescence,

were decreased after siRNA targeting, indicating that RNA knockdown corresponds to decreased protein expression (Figure 2.9C,D).

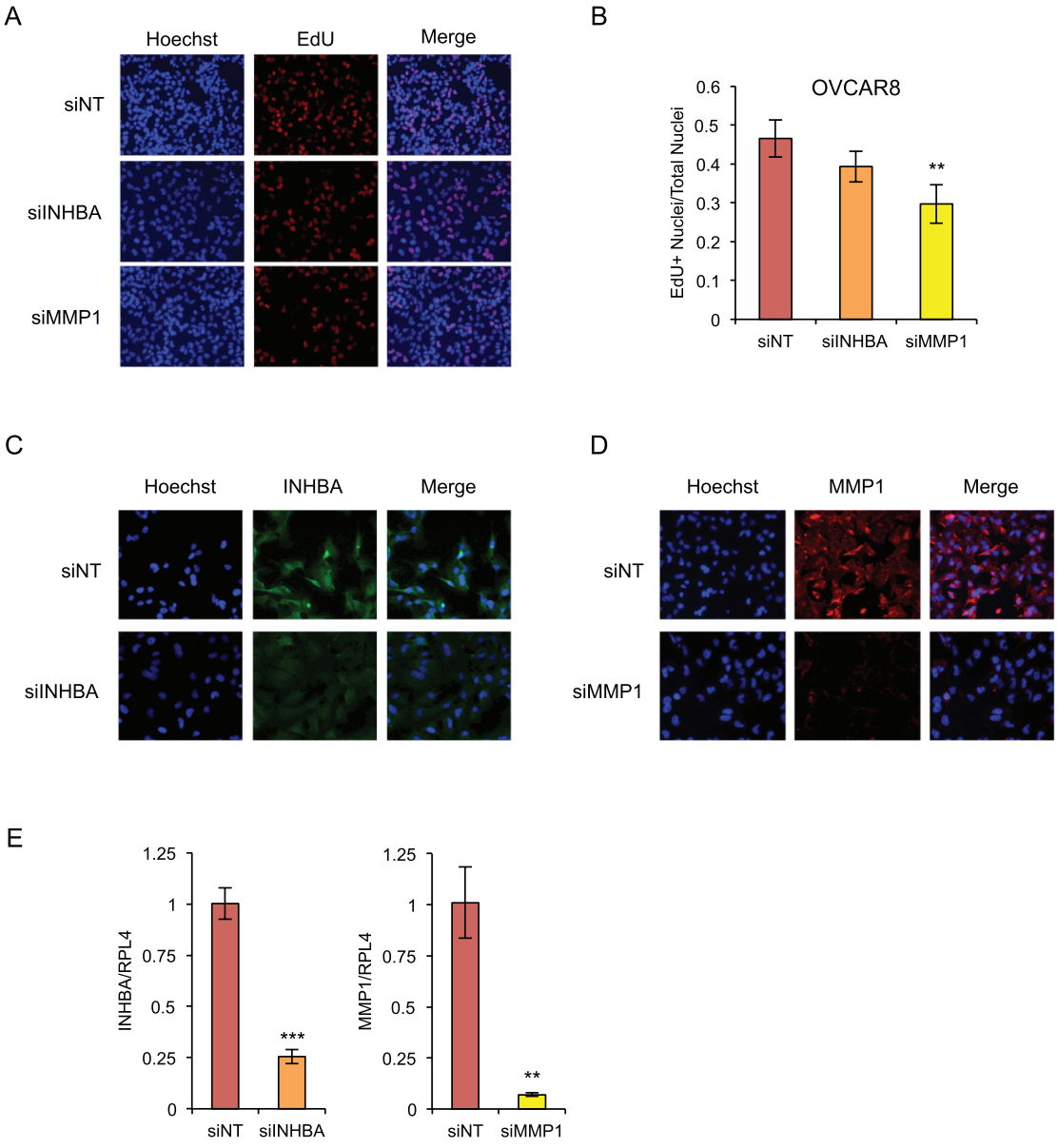
A
Hoechst
EdU
Merge
siNT
siINHBA
siMMP1
B
OVCAR8
EdU+ Nuclei/Total Nuclei
0.6
0.5
0.4
0.3
0.2
0.1
0
**
siNT
siINHBA
siMMP1
C
Hoechst
INHBA
Merge
siNT
siINHBA
D
Hoechst
MMP1
Merge
siNT
siMMP1
E
INHBA/RPL4
1.25
1
0.75
0.5
0.25
0
***
siNT
siINHBA
MMP1/RPL4
1.25
1
0.75
0.5
0.25
0
**
siNT
siMMP1

Figure 2.9 siRNA-mediated knockdown of compound-altered genes mimics compound treatment

A-B. siRNA mediated KD of INHBA or MMP1 was performed on OVCAR8 cells in 4-well chamber slides. Cells were pulsed with EdU for 45 minutes immediately before fixation. A. Representative images of EdU incorporation following siRNA-mediated KD. B. Quantification of ratio of EdU+ nuclei/total nuclei (n=4 chambers/siRNA). C. OVCAR8 cells were transfected with non-targeting siRNAs or INHBA-targeting siRNAs. Protein levels of INHBA were measured by immunofluorescence. Nuclei are counterstained with Hoechst. D. OVCAR8 cells were transfected with non-targeting siRNAs or MMP1-targeting siRNAs. Proteins levels of MMP1 were measured by immunofluorescence. Nuclei are counterstained with Hoechst. E. Knockdown measured by RT-qPCR of genes from Figure 2.9A,B. ** $p<0.01$, *** $p<0.001$ by t-test (E) or one-way ANOVA (B) with Holm-Sidak post-hoc tests.

To assess the role of these genes in migration, OVCAR8 cells were transfected with a pool of 4 non-targeting siRNAs or a pool of 4 siRNAs targeting INHBA or MMP1. Confluent monolayers were scratched, and wound healing was assessed after 24 hours (Figure 2.10A,B,E). siRNA targeting of either gene significantly decreased wound healing, consistent with the phenotype observed following tool CBFβ/RUNX inhibitor treatment.

2.3.7 Dual knockdown of INHBA and MMP1 enhances wound healing inhibition

As *INHBA* and *MMP1* are both included in the hallmark EMT gene list, we assessed if dual targeting of these genes would have combinatorial effects on wound healing. To measure the relative contribution of each gene to this process, genes were targeted independently or in combination, and the effect on wound healing was measured.

OVCAR8 cells were transfected with a total of 20pmol of siRNAs targeting either a single gene or both genes together. When targeting individual genes, half of the siRNA was non-targeting. As expected, siRNA-mediated knockdown of each gene independently decreased wound healing, even when the amount of siRNA transfected was reduced by 50%. Knockdown of both genes together yielded an even greater reduction in wound healing (Figure 2.10C,D,F). These results indicate that each gene has a non-redundant contribution to wound healing, suggesting that CBFβ may control multiple mediators of EMT.

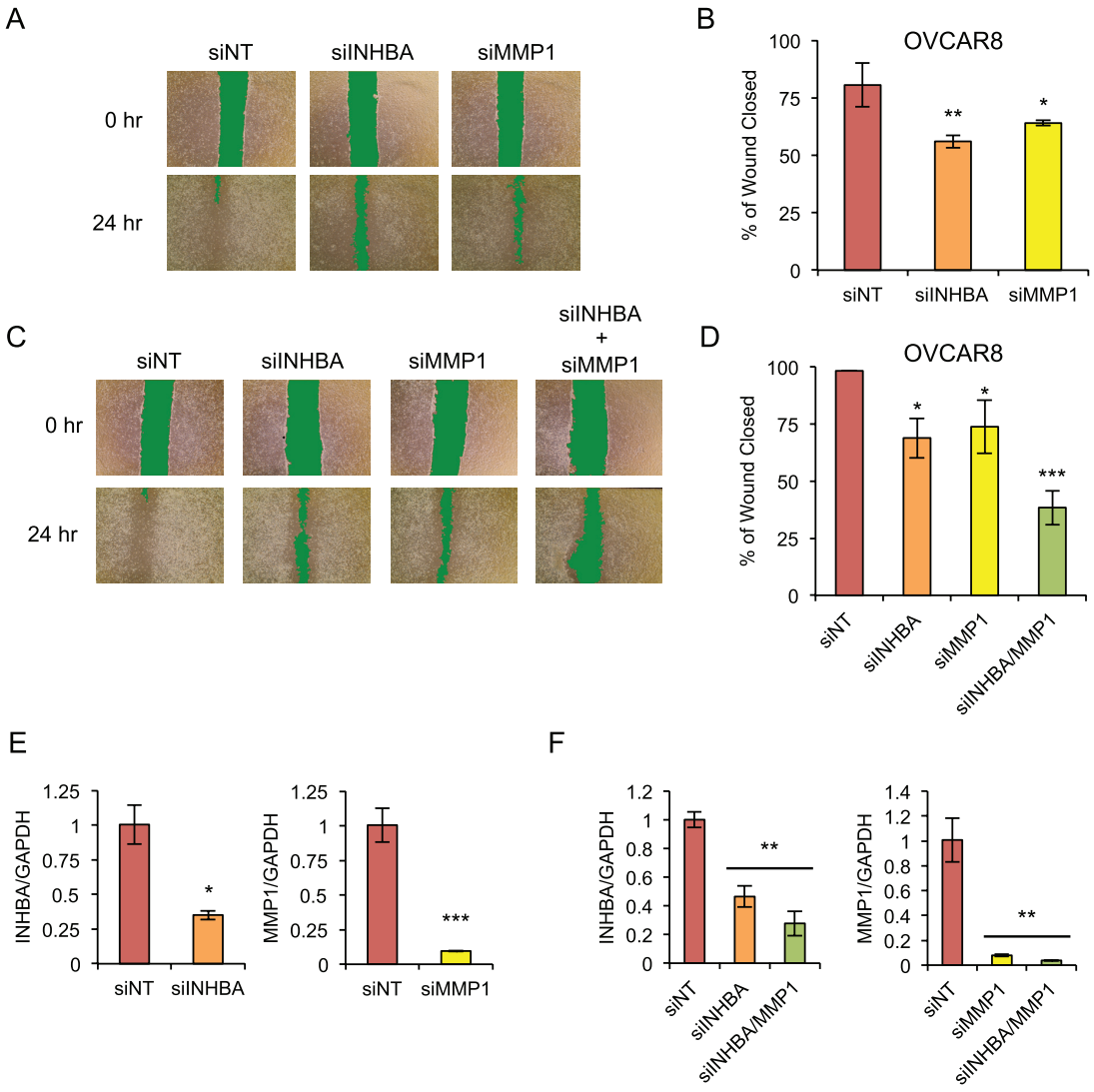
A
siNT
siINHBA
siMMP1
0 hr
24 hr
B
OVCAR8
% of Wound Closed
100
75
50
25
0
**
*
siNT
siINHBA
siMMP1
C
siNT
siINHBA
siMMP1
siINHBA + siMMP1
0 hr
24 hr
D
OVCAR8
% of Wound Closed
100
75
50
25
0
*
*
***
siNT
siINHBA
siMMP1
siINHBA/MMP1
E
INHBA/GAPDH
1.25
1
0.75
0.5
0.25
0
*
siNT
siINHBA
MMP1/GAPDH
1.25
1
0.75
0.5
0.25
0
***
siNT
siMMP1
F
INHBA/GAPDH
1.2
1
0.8
0.6
0.4
0.2
0
**
siNT
siINHBA
siINHBA/MMP1
MMP1/GAPDH
1.4
1.2
1
0.8
0.6
0.4
0.2
0
**
siNT
siMMP1
siINHBA/MMP1

Figure 2.10 siRNA-mediated knockdown of INHBA and MMP1 impair wound healing

A-B. siRNA-mediated KD of INHBA or MMP1 was performed. Confluent monolayers of KD cells were scratched with a pipette tip, and percent wound closure was assessed at 24 hours. A. Representative images of wounds at 0 and 24 hours. Wounds are highlighted in green. B. Quantification of wound closure after 24 hours (n=3 wounds/siRNA). C-D. Compound-affected genes were knocked down alone or in combination, and effects on wound healing were assessed. C. Representative images of wounds following single or combined siRNA-mediated KD. Wounds are highlighted in green. D. Percent wound closure after 24 hours following single or combined KD (n=3 wounds/siRNA). E. Knockdown measured by RT-qPCR of genes from Figure 2.10A,B. F. Knockdown as measured by RT-qPCR of genes from Figure 2.10C,D. * $p<0.05$, ** $p<0.01$, ***$p<0.001$ by t-test (E) or one-way ANOVA (B,D,F) with Holm-Sidak post-hoc tests.

2.4 Discussion

In this study, we demonstrate that CBFβ inhibition leads to decreased growth, migration, and anchorage independent growth of ovarian cancer cells in multiple cell lines. Additionally, CBFβ/RUNX inhibition causes a decrease in INHBA and MMP1 mRNA, and knockdown of these genes recapitulates the effects of inhibitor treatment. This work further validates the oncogenic role CBFβ plays in ovarian cancer and uses a clinically applicable small molecule inhibition strategy.

These results particularly emphasize the role of CBFβ in migration and anchorage-independent growth. Doses of inhibitors needed to significantly impair wound healing or colony formation were much lower than those required for growth inhibition. This result is of particular importance in ovarian cancer as anchorage-independent growth and migration are strong models of metastasis. The majority of women with ovarian cancer are diagnosed with metastatic disease, and these metastases are a primary driver of ovarian cancer morbidity and mortality (Bowtell et al., 2015). CBFβ/RUNX inhibition may be uniquely useful as an adjuvant therapy to inhibit further development of metastatic lesions.

While AI-14-91 had significant effects on cells grown in culture, it did not inhibit tumor growth in an *in vivo* xenograft model of ovarian cancer. AI-14-91, while a useful chemical probe, has several significant limitations for *in vivo* use. AI-14-91 has low potency and a short half-life. These two limitations combined lead to an estimated ~2 hours of CBFβ inhibition per dose. Thus, even with twice daily dosing, the protein-

protein interaction between CBFβ and RUNX was likely only inhibited for ~4 hours per day (Illendula et al., 2016). Compounds with increased potency should be evaluated for their success in this model. In addition to ongoing structure-activity-relationship work, alternate strategies could be employed to increase the potency of current compounds, such as generating a PROTAC (proteolysis targeting chimera) compound. PROTACs are bivalent compounds which bind to their target protein and an E3 ubiquitin ligase, leading to target protein degradation (Neklesa et al., 2017). This irreversible inhibition of CBFβ would combine the beneficial features seen with chemical inhibition, as well as likely recapitulate data generated using shRNAs.

While we were surprised at the relatively small number of DEGs following compound treatment, this result is not unprecedented. Analysis of gene expression changes after treatment with Kartogenin, a CBFβ/FilaminA inhibitor, revealed only 39 DEGs, and siRNA-mediated knockdown of CBFβ in a metastatic breast cancer cell line yielded 161 DEGs, many fewer than would be predicted following knockdown of a transcription factor (Johnson et al., 2012; Mendoza-Villanueva et al., 2011). While the specific genes altered in these studies do not have large overlap, this is likely due to the differing cell lineages. However, more interestingly, perturbation of CBFβ, whether chemical or genetic, revealed recurrent alterations in EMT and extracellular matrix formation. Kartogenin was identified during a screen for compounds that promote chondrogenesis, and Kartogenin treatment increases collagen production. GO analysis of genes altered by siRNA targeting of CBFβ in metastatic breast cancer revealed enrichment of the "extracellular matrix organization" and "regulation of cell adhesion biological

processes", mimicking our results. These data externally validate our findings demonstrating the contribution of CBFβ specifically to EMT.

The relatively small changes in gene expression across all 3 experiments likely indicate that CBFβ controls a very specific and narrow transcriptional network. It is also possible that there is an undefined non-transcriptional function of CBFβ. CBFβ has reported protein-protein interactions with several components of the cytoskeleton, including Collagen Alpha-1(VII) Chain (*COL7A1*), whose transcript levels were decreased after CBFβ/RUNX inhibitor treatment. Additionally, CBFβ has been identified at the midbody during cytokinesis, though its function there is not well defined (Lopez-Camacho et al., 2014a). These interactions may provide additional mechanistic insight into the role of CBFβ as a regulator of cellular proliferation and migration. Future studies should investigate alterations in protein-protein interactions following inhibitor treatment. These experiments may provide insight into these potential non-transcriptional effects of CBFβ.

In summary, CBFβ is a druggable target in ovarian cancer, and chemical inhibition of its interaction with RUNX proteins decreases proliferation, migration, and anchorage-independent growth. These effects are partially explained by alterations in gene expression. Future work identifying higher potency compounds and extending these findings to an *in vivo* model will both help improve ovarian cancer treatment and provide novel therapeutic strategies for a difficult to target disease.

Chapter 3. Genetic reduction of CBFβ alters gene expression and decreases the proliferation and migration of ovarian cancer cell lines

3.1 Introduction

CBFβ and a RUNX protein (RUNX1, RUNX2 or RUNX3) form a heterodimeric transcription factor complex. RUNX proteins bind DNA and activate or repress transcription at target genes (Chuang et al., 2013; Tang et al., 2000). While RUNX proteins are capable of DNA binding alone, their affinity for DNA is increased up to 40-fold when bound to CBFβ (Gu et al., 2000). The structure and function of RUNX proteins are extensively characterized. RUNX proteins function as molecular scaffolds to assemble other transcription factors, leading to alterations in target gene transcription (Chuang et al., 2013).

Many studies have examined the role of RUNX proteins in development and disease. RUNX proteins play essential roles in development; RUNX1 is essential for hematopoiesis, RUNX2 is essential for bone development, and RUNX3 contributes to gastric and neurologic development (Brenner et al., 2004; Komori et al., 1997; Levanon et al., 2002; Okuda et al., 1996). The RUNX proteins also have complex roles in cancer and can be oncogenic or tumor-suppressive depending on the context (Ito et al., 2015). In most epithelial cancers, RUNX1 and RUNX2 are oncogenic and promote proliferation, migration and invasion of cancer cells (Chuang et al., 2017).

Significantly less is understood about the role of CBFβ, the non-DNA binding partner of RUNX proteins. While the structure of CBFβ is known, its interactions with other proteins remain elusive (Lopez-Camacho et al., 2014b). Additionally, CBFβ has both nuclear and cytoplasmic localization, but the functional consequences of this are not well understood (Tanaka et al., 1998, 1997; Yoshida et al., 2005). Recent studies have indicated that CBFβ has an oncogenic role in cancer, promoting proliferation, migration and invasion of cancer cells (Chen et al., 2018; Mendoza-Villanueva et al., 2010, 2011; Ostenfeld et al., 2010). However, the downstream mechanisms by which these phenotypes occur are poorly described.

CBFβ and RUNX proteins have recently shown to be oncogenic in ovarian cancer (Greer et al., 2013; Keita et al., 2013; Lee et al., 2011; Wang et al., 2013). However, the molecular mechanism by which this oncogenicity occurs remains unknown. In this chapter, we will knockdown CBFβ expression using multiple methods, and the effects on gene transcription and cellular phenotypes will be assessed. Additionally, the effects of genetic reduction of CBFβ will be compared to the effects of chemical inhibition of the CBFβ/RUNX protein-protein interaction by AI-10-104, and key similarities and differences will be highlighted.

3.2 Materials and methods

3.2.1 Cell culture and inhibitor production

Cells were cultured in RPMI-1640 (Gibco 11875-093) (OVCAR8) or DMEM (Gibco 11965-092) (293T) supplemented with 10% FBS (HyClone SH30396.03), 1% Anti-Anti (Gibco 15240-062), and 100μg/mL Normocin (InvivoGen ant-nr-1) in a humidified 37°C incubator with 5% CO_2. OVCAR8 and 293T cells were obtained from ATCC. Cell line identity was verified by STR profiling. Tool inhibitors were synthesized in the Bushweller lab as previously described (Illendula et al., 2016).

3.2.2 siRNA transfection for RNA-Seq

200,000 OVCAR8 cells were plated in a 6-well plate. The following morning, cells were transfected with non-targeting (GE Dharmacon D-001206-13) or CBFβ-targeting (GE Dharmacon M-011602-00) siRNAs using Lipofectamine RNAiMax (Invitrogen 13778) per the manufacturers' specifications. Total RNA was collected after 72 hours using the Absolutely RNA kit (Agilent 400800). RNA quality was confirmed using a Bioanalyzer and CBFβ knockdown was confirmed by RT-qPCR. Poly(A) RNA-seq libraries were generated at HudsonAlpha with Illumina barcodes and sequenced (Illumina HiSeq) to a target depth of ~25 million paired-end 50-bp reads per sample, resulting in 17 to 21 million mapped reads per sample. RNA-Seq data were returned in Fastq format and analyzed using FastQC to determine quality. Combined reads for each sample were mapped to the genome using HISAT2 (Kim et al., 2015). Mapped reads were sorted using Samtools, and read counts were obtained using featureCounts (Li et al., 2009; Liao et al., 2014). Differential gene expression was analyzed using DESeq2 (Anders and

Huber, 2010). Genes with an adjusted p value of < 0.05 and log2foldchange of >0.05 were considered significantly altered. RT-qPCR validation of gene expression changes was performed on an independent set of RNA. EnrichR analysis was performed by submitting the list of differentially expressed genes (DEGs) to the EnrichR platform (Chen et al., 2013; Kuleshov et al., 2016). GSEA was performed using GSEA 3.0 (http://www.broad.mit.edu/gsea) (Subramanian et al., 2005). Gene sets were considered enriched when the FDR was <0.05.

3.2.3 RT-qPCR

Cells were treated as indicated and total RNA was collected using the Absolutely RNA kit (Agilent 400800). cDNA was made from equal amounts of RNA per the manufacturers' specifications (Applied Biosystems 4387406). PCR was conducted on a Bio-Rad MyIQ cycler using the SensiMix/SYBR green/FITC master mix (Bioline QT615). Primers were designed using Primer3. Gene expression was normalized to GAPDH using the ΔΔCT method. Primer sequences used in this chapter are listed in Table 3.1.

Table 3.1 Primer sequences used for RT-qPCR

Gene	Forward	Reverse
CBFB	CAGGGAGAACAGCGACAAACAC	AGACAGCCCATACCATCCAGTC
GAPDH	AATCCCATCACCATCTTCCA	AGAGATGATGACCCTTTTGG
INHBA	CCGAGTCAGGAACAGCCAGGA	GCTGGAAGAGGCGGATGGTG
MMP1	GCTTTCCTCCACTGCTGCTG	ACTTGCCTCCCATCATTCTTCAG
RUNX1	ATCCAATTGCCTCTCCCTTCTGTGC	TCAGGTCGGGTGCCGTTGA
SERPINE1	CAGAGGTGGAGAGAGCCAGA	CCGTTGAAGTAGAGGGCATT
UGCG	CTCAACAAGAAGGCAACTGA	GGAGCACTTCATATTTGGGAT

3.2.4 AI-10-104 treatment

$1x10^6$ OVCAR8 cells were plated in 10cm plates. The following morning, cells were treated with the indicated dose of AI-10-104 and total RNA was collected after 24 hours. RT-qPCR was then preformed as described in section 2.2.3.

3.2.5 siRNA proliferation

225,000 OVCAR8 cells were plated in 6-well plates and the following day cells were transfected with a pool of non-targeting siRNAs or a pool of CBFβ-targeting siRNAs using Lipofectamine RNAiMax (Invitrogen 13778) per the manufacturers' instructions. After 48 hours, cells were plated in 96-well plates (2500 cells/well). For relative growth assays, relative cell number was measured at 0, 24, and 72 hours using CellTiter-Glo (Promega G7570). For AI-10-104 treatment, 24 hours after cell were seeded in a 96-well plate, cells were treated with AI-10-104 and relative live cell number was measured after 72 hours. Luminescence was measured using a PHERAStarPlus microplate reader. To confirm knockdown, OVCAR8 cells were collected 2 and 6 days after transfection, and CBFβ expression was monitored by western blot.

3.2.6 Wound healing

For siRNA-mediated KD, OVCAR8 cells (80,000) were seeded in 12-well plates. Sixteen hours later, cells were transfected with siRNAs as described in section 3.2.5. Twenty four hours after transfection, cells were washed once with 1x PBS, and culture media was replaced with RPMI supplemented with 2.5% FBS. After 10 hours, confluent monolayers

were scratched with a P1000 pipette tip. Size of the wound was measured at 0, 14, and 24 hours.

For CRISPR cells 500,000 cells were seeded in 6-well plates. The following morning, cells were washed once with 1x PBS, and culture media was replaced with RPMI supplemented with 2.5% FBS and compounds. After 10 hours, confluent monolayers were scratched with a P1000 pipette tip, and the size of the wound was measured at 0 and 14 hours.

Images were captured using an EVOS XL Core microscope. Wound size was analyzed using MRI Wound Healing macro for ImageJ (http://dev.mri.cnrs.fr/projects/imagej-macros/wiki/Wound_Healing_Tool).

3.2.7 Western blotting

OVCAR8 cells were lysed in RIPA buffer with protease inhibitor (Roche 11836170001) or 1% NP-40/1x PBS/1x Loading Buffer, and equal volumes of lysate were analyzed by western blotting (Anderson et al., 2017). Primary antibodies used were: anti-HSP90 (1:2000, CST-4874), anti-α-TUBULIN (1:2000, Sigma-Aldrich-T9026), and anti-CBFβ (1:1000, SCBT-20693).

3.2.8 CRISPR cell line generation

Guide RNAs targeting the first exon of CBFβ were cloned into pLentiCRISPRv2 (addgene 52961), and the empty pLentiCRISPRv2 was used as a non-targeting control.

The sequence for *CBFB* guide RNA 1 is: CTCTGGTCGGGCACGACGCG, and the sequence for *CBFB* guide RNA 2 is: GAGAAGCAAGTTCGAGAACG. To produce lentivirus, 293T cells were transfected with pLentiCRISPRv2, pMD2.1 (addgene 12259), and psPAX2 (addgene 12260) using polyethylenimine (PEI) (Polysciences 23966-2) at a ratio of 4μg PEI:1μg DNA. Media on the transfected cells was changed after 16 hours and cell culture media was collected and 0.45μM filtered 48 hours after transfection. Filtered media was mixed 1:1 with normal culturing media supplemented with 4μg/mL polybrene (Millipore TR-1003-G) and added to OVCAR8 cells. 72 hours after infection, cells were passaged into 1μg/mL puromycin (InvivoGen ant-pr-1). OVCAR8 CRISPR cells were maintained in normal culture medium supplemented with 1μg/mL puromycin.

3.2.9 CRISPR cell line proliferation

100,000 CRISPR OVCAR8 cells were seeded in a 6-well plate. Three to four days later, cells were trypsinized and live cell number was counted by trypan blue exclusion; additionally, 100,000 cells were replated for the next passage. Fold change was calculated at each passage and total fold change was calculated by multiplying the fold change after each passage together.

3.2.10 Statistical methods

Each experiment was completed 3 independent times with n=3-6 technical replicates. Data shown are mean ± SD of one representative experiment, unless otherwise specified. Data was analyzed using Microsoft Excel and GraphPad PRISM 7.0. Groups were compared using a t-test, one-way ANOVA or two-way ANOVA with Holm-Sidak post-

hoc tests, * $p<0.05$, ** $p<0.01$, *** $p<0.001$, control vs. experimental condition. IC_{50} values were calculated using the GraphPad PRISM curve fit – log inhibitor vs. normalized response.

3.3. Results

3.3.1 siRNA-mediated knockdown of CBFβ alters a large network of genes

While CBFβ has been demonstrated to modulate proliferation and anchorage-independent growth in ovarian cancer, the mechanism underlying these phenotypes remains unknown. As CBFβ and its cognate binding partner RUNX form a transcription factor complex, we were interested if the phenotypic changes observed following CBFβ knockdown could be explained by alterations in gene expression. To address this question, OVCAR8 cells were transfected with non-targeting or CBFβ-targeting siRNAs, and, 72 hours later total RNA was collected and sequenced.

RNA-Seq revealed that a large number of genes were altered following CBFβ knockdown as analyzed by DESeq2. Genes were considered significantly altered when padj <0.05 and absolute value (log2foldchange) >0.5. 872 genes had increased expression and 469 genes had decreased expression (Figure 3.1A, Table 3.2, Table 3.3), and significantly altered genes are displayed in a volcano plot (Figure 3.1B). Principle component analysis revealed good separation between the non-targeting and CBFβ samples, with 63% of the variance in PC1, and 19% of the variance in PC2 (Figure 3.1C). Alterations in genes that were upregulated (SERPINE1 and UGCG) and downregulated (RUNX1) were confirmed by RT-qPCR to validate the RNA-Seq findings (Figure 3.1D).

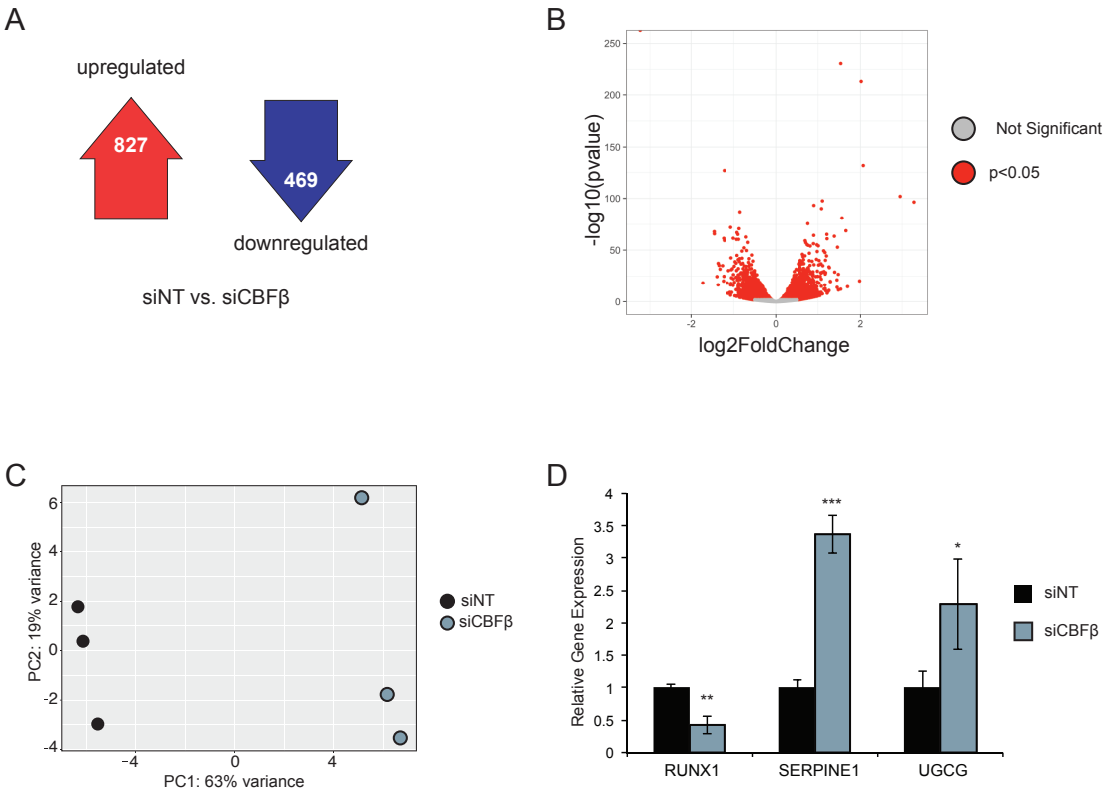
A
upregulated
827
469
downregulated
siNT vs. siCBFβ
B
-log10(pvalue)
log2FoldChange
Not Significant
p<0.05
C
PC2: 19% variance
PC1: 63% variance
siNT
siCBFβ
D
Relative Gene Expression
RUNX1
SERPINE1
UGCG
siNT
siCBFβ

Figure 3.1 Differentially expressed genes following siRNA-mediated knockdown of CBFβ in OVCAR8 cells

A. Number of upregulated and downregulated differentially expressed genes following siRNA knockdown of CBFβ. B. Volcano plot of differentially expressed genes. Genes with a padj<0.05 are colored in red. C. Graph of principle component analysis of samples used to determine differentially expressed genes. D. RT-qPCR validation of gene expression changes in RUNX1, SERPINE1, and UGCG following siRNA-mediated knockdown of CBFβ. * $p<0.05$, ** $p<0.01$, ***$p<0.001$ by t-test (D).

Table 3.2 Genes significantly downregulated after CBFβ knockdown

CBFB	ARHGAP19	PPP1R16B	PRPH	ITGBL1	SPRY4	DENND1B
SPX	EXO1	TLE6	ERRFI1	MKI67	CLIP4	IL20RB
ANXA3	TRPV3	ZNF675	RALA	NT5C3B	ISOC1	LINC01128
TAF11	GADD45A	NRN1L	SMOX	EXPH5	STYK1	KIF21B
SYTL3	CDC42BPG	TRAF3IP2	BCYRN1	AK2	CHAF1B	MRPS31P5
CDK15	AEN	SYDE1	RAET1L	SDCCAG8	CDKN2D	RFX8
PTPRB	MSS51	NAV3	VPS25	ITPKA	DOT1L	EMID1
HBEGF	GRB7	VWDE	TRIB3	S100A2	FRMD5	RIPK4
SFTA1P	ASNS	MIR4435-2HG	PDGFB	RFT1	VDR	YBX1
E2F2	TINAGL1	MAP7	TSC22D2	SLC25A45	DDB2	RNF38
AOX1	EPCAM	ABHD4	FRS3	PDXP	PTPN22	GNAQ
ZNF714	FAM195B	STK24	KCTD4	LOC100996437	LOC374443	PSMB10
TSC22D3	MYO1D	FAM111B	SVIP	ZNF428	LINC00152	DHFR
RAB5B	UTAT33	DUSP14	CDT1	CA5B	TFCP2L1	CALB1
S1PR1	LAMC2	KNSTRN	DNAJC9	PTDSS1	NMU	ZNF551
TRIM55	SURF2	RNF43	SNCA	TIFA	NAPB	PCNA
AREG	WHAMMP1	RUNX1	FAM83A	HMSD	CRY2	LSM7
ETV5	MGLL	MBOAT1	PAWR	DCBLD1	WBP1L	PDZD8
VEPH1	CLK2	ANKRD1	GDF15	PSAT1	SLC2A1	PLAC8
LCK	ALOXE3	ZNF165	NME1	USP3	TMEM176B	DDAH1
E2F1	IMPDH1	DDX49	CXCR4	ATP6V0A4	BEX1	SNX11
CLDN1	SCML2	ITGB2	SERPINA1	FAM225A	KBTBD8	SBDSP1
UNC13D	OR2A7	SLC22A15	SNHG15	GOLT1A	ZNF566	LOC101928841
ZNF430	C3orf52	TUFT1	NRK	PTPN9	EIF5A2	CEL
MYEOV	SEMA3E	FAM126B	EED	COL16A1	MAPK13	ZNF548
ETV4	ZNF431	FAM107B	PALM2	EPN2	MMD	ARID5B
ABCC9	GCNT2	MCM10	MCM3	USP53	LINC00665	GAP43
ARID3B	RASSF3	ITGB4	ZNF157	LPAR1	KLF5	MPDZ
IL6	ZDHHC4	TADA2A	TBC1D4	SKP2	NR4A1	GFPT1
PPP1R15A	SPNS3	SFRP5	MAFF	ARHGDIB	ADORA2B	MTHFD1L
ACTR3B	PLEK2	CENPM	SEC61A2	SYNE3	MND1	FERMT3
CCNE2	MEF2C	SUV39H1	BCAT1	ORC3	ESPL1	DDIT3
SLC7A11	SLC39A4	ROS1	ABCA1	ASB1	IKZF4	ARNTL
TNFRSF10D	MISP	SYBU	DCK	NT5C3A	PSMD14	HKDC1
MYO5B	PTPRR	ABHD5	CDC45	CCDC28B	41163	GTPBP1
UPP1	DBF4B	CHIC2	POLR2A	TNPO1	SLFN5	PRRC2B
SERPINB7	IRAK2	RIMS2	U2AF1L4	TOMM34	KRTDAP	KAT2B
TUBA4A	EIF3J	CDS1	PMS2P4	OSBPL10	RBMS3	C19orf57
LETM2	ASF1B	PMAIP1	NME2	CD163L1	NHP2	LAMP3
RAB39B	LOC100506178	MTUS1	NCR3LG1	ALYREF	ANKEF1	SENP1
SNAPC1	PARD6A	USP43	MDFI	FLNC	PNMT	RANGRF
SAMD3	NFATC2	CLSPN	MCM4	PXMP2	PNPO	ARHGEF34P
SUN3	NKIRAS2	PPARG	PTPRG-AS1	TGIF2	CTCFL	HOXC11
ATAD2	SNHG1	PRR34-AS1	ZNF71	GINS2	FAM101B	PXN
GRPEL2	ARHGAP33	FGD6	BTRC	EZH2	C12orf49	AKAP12
CDC25A	NDUFB2	C16orf87	EXOSC5	OSR2	AMN1	CCDC64
ERBB2IP	PARD6B	ESPN	TERT	RASGEF1B	CDC14A	PDIK1L
ATF3	DSCC1	IL12A	LCP1	SPOCD1	LSM3	PCP2
MAPRE3	SESN2	HMGA1	GRAMD3	INA	NEDD4L	DCAF17
MB21D2	PKP2	DUT	NGF	CTNNAL1		
PROSER2	NRG1	CDKN1A	TMEM40	IL31RA		

PAGR1	SLC25A19	RNF7	RAB2B	ULBP2
SDC2	PPP1R14A	ACER3	DDX46	NOC2L
YARS	CENPW	STAMBPL1	VAMP8	AZIN1
FOXO3B	POLA2	TRIML2	NUDT17	COL17A1
RGL2	CMTM7	F8A1	VRK3	RIC1
C5orf30	KRT18	RASEF	CPED1	LIMA1
COX17	DGKD	E2F8	PAK6	STRN4
ADAMTSL1	UAP1	SLC25A6	CYTH3	ANAPC15
S100A10	ZWINT	SNRPA1	MYL12B	ADI1
GREB1L	ROMO1	NFIL3	TXNRD1	NDUFAF5
AKNA	HSD11B2	NDUFV3	MED20	CACFD1
RAD51AP1	MCM5	TEX14	EPB41L4A-AS1	CBWD1
FUT6	PBX3	NLRC5	ZNF333	MARS
PPL	CDCP2	DCAF7	SRGAP2C	ANKRD28
NABP2	ABCA17P	SPATA5	PSMC3IP	UBE2R2
DMTN	COLGALT2	MCM6	PRADC1	PACSIN2
BOK	CLTB	SPSB4	GLB1L2	BAZ2A
WASH7P	ZSCAN16-AS1	ZC4H2	MRPL35	CNTNAP3P2
RUSC2	RPL23AP7	GDNF	SLC17A5	FAM229A
HIC2	DNAJC5	UCHL3	LOC642423	DPP3
C9orf91	KCTD13	PCBP4	AGO2	
SKAP1	INPP5A	EPHX4	PLD6	
ZNF223	SCML1	HLA-A	C16orf59	
CMSS1	ZHX2	AVIL	PLEKHA8P1	

Table 3.3 Genes significantly upregulated after CBFβ knockdown

DICER1-AS1	PTN	KLHL42	ABAT	MORF4L2	PCDHB14	LOC100996693
CA8	ZFP36L1	TRIM6	MYADM	AHNAK2	TAF6L	CRYL1
IGF2BP3	SRD5A1	LINC00638	LRRK1	GOLT1B	TMCC1-AS1	IARS2
LINC00520	GNG4	PRKCG	UCKL1	ZNF337-AS1	KRT15	TMEM109
LINC01004	OLFML2A	GLT8D1	LOC145783	FZD8	CENPBD1	ZDHHC1
LINC00963	MN1	NRAV	ACE	GYPE	EML1	CDK6
ATP6AP1L	ANGPTL2	TJP3	WNT5A	NYNRIN	SOD3	MATN1-AS1
ZNF300	CSGALNACT2	HOGA1	BCAN	CDON	MME	EPHB3
OTUD4	ZNF271P	C15orf27	SCUBE3	CCDC8	PSMD5-AS1	TMEM97
PTGFR	UNC5A	NPHP4	PRDM12	LOC100507351	TMEM170B	ANKRD34A
FBXL17	SAMD14	NAGS	TGFB2	USH1G	PANK1	ADRA1B
TIMM10B	VANGL1	APOL1	P4HA3	CALU	SCN4B	CCDC142
DCAF12L2	UHMK1	C10orf55	SCAMP1-AS1	DIRC2	TMEM206	MAMSTR
CREB3L2	ZKSCAN3	TTLL1	SIX3	ZFP62	PTGIS	RHOQ
TCEAL8	LRRC14	PROM2	RHBDL2	KIF1A	SLC10A3	DROSHA
JUNB	LINC00667	PIGK	ZNF471	PLBD1	RNF112	TMBIM4
CUL7	TMEM102	PRUNE2	SPARC	ITGB1	DKFZP434I0714	CKAP4
PTH1R	AEBP1	TECPR2	STRN	APAF1	LOC100130417	MEGF6
FNDC3B	WDR78	C7orf13	CYP2J2	DES	LIMCH1	ANK2
LOC101928414	CCZ1	ICK	LZTR1	TSPY26P	CPEB4	BOC
DNAJC18	CPXM1	KDELC2	RAB6B	AIF1L	WNT11	ZNF771
ZEB2	MRPL36	HSD17B14	DPY19L2P2	LYSMD2	TMEM92	ICAM3
SLC16A9	INSIG1	MAFA	LRRIQ1	C17orf100	MYLK	ZCCHC3
PGBD4	GMCL1	FGF14-AS2	AK8	LOC339803	LOXL1	PSD4
D2HGDH	LRG1	PHYH	NEK11	GLIS1	CD82	TPK1
ISM2	ZNF467	PDE6B	TMEM185B	C14orf159	TPGS1	HS6ST3
CROT	RGS9BP	SEMA3F	SLC16A1	NHLRC1	EMB	DEPTOR
FAM89B	CC2D1B	TCTN1	SYNC	CST3	MAGED2	B4GALT7
LAMA1	MANF	HSPB2	USP8	FJX1	PPP6R3	CACNG8
UQCR10	TMED9	NOG	MAN1A1	ZNF75D	FLJ42351	SNX32
PLXNB3	GGCX	FANCF	FOXRED2	CCDC103	OBSL1	SLC4A11
APOBEC3G	SPIRE2	SOCS1	PPIL6	B4GAT1	COL6A2	DAPK2
IL1A	ADGRG2	SEC22B	CCDC74B	KIAA1143	MAN1C1	COPZ2
ISM1	P4HA2	ZNF583	BICC1	BTG2	ARHGEF6	INTS5
PRKAR2B	ZNF425	CLDN9	CACNA1F	C9orf116	MYLK3	LINC01410
IFIT3	SFPQ	SLC30A1	SSR4P1	EXOC3-AS1	RCN1	MFAP5
PIGV	UBE3B	SLC38A3	GBP2	ADAM23	SELM	SLC22A17
LINC01573	PARM1	CCNB3	TMEM189	SRPX	NTNG2	PCBP3
LAPTM5	NOP14-AS1	CEBPD	ADAMTS13	CALHM2	PLBD2	CXCL1
JMJD8	DYNLL2	TMEM37	GMPPA	CDIP1	TRIB2	MLEC
TCTN2	MAGI2	TMEM121	EFNB3	CARNS1	PIEZO2	ID1

SAMHD1	SRRM2-AS1	EPOR	NPY	ADCK1	CLDN23	VWA1
SMAD6	GNB1L	LINC01560	ARTN	ROR1	SERPINA3	LRRC73
CCDC40	RASSF5	CENPB	RCAN2	LOXL3	LOC90246	MAGEH1
STAM2	HCK	BVES	MANSC1	HEG1	CPZ	CTHRC1
HMCN1	NKD2	AK5	EPHA4	CHSY3	HVCN1	EDEM3
PDIA4	VGF	KCNQ1OT1	GPR173	PHYHIP	SLC47A1	WNT4
C2orf72	HIPK3	TTC30B	ADGRG1	ZNF70	C1RL	NINJ2
WDR88	EFEMP2	ITGA1	LINC01089	LRP11	LIMD2	ARHGAP18
SUSD3	PRRT2	SLC1A1	HYDIN	PLEKHB2	DPY19L1	HCG11
MOCS3	ADGRA2	FBXO36	C5AR1	IER5L	PRDM13	C19orf66
VIPR2	ATF6B	DCHS1	WDR60	ADAMTS10	TRPC1	PLAT
TGOLN2	ITGB3	NEAT1	ABHD16B	CCDC89	P4HA2-AS1	MBTPS1
USP51	KLRG1	C1S	LPXN	SDK1	CDH11	CTSB
MIR17HG	IL11RA	C1orf233	IGIP	CDHR2	MBNL1	PDGFRL
RAMP2-AS1	ARSG	SRD5A3	CCDC144A	FAM114A1	ARFIP1	CYP1B1
ARHGEF40	ITGA7	CREB3L1	PCDHB13	SRR	SYNPO	PPAPDC2
LOC100287042	RTKN	ADGRL3	CTSA	EID2B	FAM167B	PKP1
KCNJ4	SERPING1	ZNF286A	MCC	CSF1	CPS1	CTBP1-AS2
LINC00094	IGDCC4	GAS7	LTBP2	TGFBR1	PPT1	CYBRD1
CD72	ELF3	CYB561	CANX	PTRF	CPLX1	C11orf1
CYP4V2	ZNF213-AS1	GATA2-AS1	CCDC158	POGLUT1	PDZK1IP1	CHST13
MAN1B1-AS1	SLC25A22	CD24	ADAMTS2	AJAP1	FLRT2	SCN4A
PIGM	GPRC5C	PGLS	MDGA2	PPP1R3G	LTBP1	ZDHHC14
LINC01003	HPS6	DHRS3	IGFBP6	SLC38A10	ZNF862	SETBP1
LAMB2	AGGF1	CTNNB1	RNF207	LOC727751	C15orf52	C11orf95
BPHL	C9orf69	CHST12	LAMC1	ZNF114	KCTD11	LAD1
ANKS1B	MAGEF1	GRN	ATG10	GHR	PGAM4	JHDM1D-AS1
LOC388849	ACTA2	NFKBIA	HSD3BP4	ZNF572	PCDHGB5	C20orf195
TAGLN	FCGRT	CNTN1	FAM43A	PSMG3-AS1	SLC31A1	LBX2-AS1
C19orf73	ERVMER34-1	ERO1B	VMA21	NTN3	LOC100996455	CYB561A3
CCL20	P3H4	UGCG	IL4I1	IL6R	EMP2	TNFRSF9
PRSS35	FAM8A1	PNRC1	ITGB8	C3	ILF3-AS1	LINGO1
PMP22	RMI2	NEK9	FAM89A	RTN4RL1	GALNT9	PTPRU
LINC01588	SFXN2	ST14	ECSCR	LDHD	LINC01547	ADAMTSL4
KDELR3	TBC1D10C	TMEM39A	FAM53B	FLJ10038	SQSTM1	TYMP
CSGALNACT1	FAM134B	GHET1	RASD2	FAM66C	ARHGAP31	RNASET2
LINC00294	PROB1	GPC1	TMEM214	SLC25A21-AS1	ODF3B	KCNC3
ACHE	TIGD6	NEURL2	AHRR	PURB	COL18A1	FN1
RNF39	TTC39B	LMNB1	PNMA2	HINT3	LINC00909	PRR5L
COX6B2	FAM73A	OTOP2	LOC101929705	FBXL12	LNP1	LOC100129917
ATP8A1	ARMC2	C9orf163	LOC284454	RELN	SEMA5A	DYRK2
PRKCDBP	SIRPB1	ZNF780B	MAMDC2	SLC38A7	MRGPRF	MTMR6
GGACT	C14orf79	IGSF11	DUSP19	C19orf38	CLCN5	VARS2

IP6K3	MYO1F	COL25A1	TMEM198B	WDR5B	FBXL7	RIN2
KCNH3	BNIP3L	FADS2	NLRP6	ORAI3	GPR137C	NXN
TCEA2	ARSI	KCNJ8	FZD9	MAGED1	FYCO1	ADAMTS7
LINC00526	CLDN4	SEMA3B	SLC41A2	MIR503HG	SOD2	TMEM255A
CEP19	PSG10P	HSPB6	TCF21	PRDM5	MT1E	GPR78
MYL5	LOC100049716	CSDC2	LRRC16B	TEX19	CHST4	TMEM87B
DYNC2H1	DNER	PLXND1	CASC10	FKBP14	KRT17	DCHS2
P3H1	C17orf97	CNPY4	TP53INP1	PALM3	SUMF1	FNDC3A
LRRC6	PLTP	MAP3K4	LAMB3	RORC	NKILA	CCR10
PPP1R3F	LOC100129461	ZNF32	EHD3	EIF4EBP2	SH3D19	PTGDS
LINC00657	ID3	ACVRL1	CASP7	KCNK15	TRNP1	TAMM41
SAMD11	PPAP2B	C11orf71	FKBP7	LEMD1	PSG4	PLA2G16
IRF2BP1	MYO7A	C1QTNF6	SNAP25	LINC00942	TMCO1	HSPA1B
ZNF503-AS2	LMLN	ZBED8	PBXIP1	LINC01106	PLEKHH1	DDX60
LOC728392	GJD3	ZNF84	RCN3	SLIT3	C5	A4GALT
C16orf52	BEAN1	LINC00339	ELMOD1	LCMT2	KRCC1	RNF149
ZNF846	SLC2A6	GEMIN5	LINC00472	RASGRF1	WIPI1	MDFIC
KLF14	FOXL1	ZEB1-AS1	KLF9	THBS3	SCN1B	LINC01521
SFT2D3	CA12	ZMYND10	MSC-AS1	TIE1	PSG5	LOC100268168
KLHL24	HTRA3	THG1L	OASL	THAP7-AS1	PSG1	NFIB
FBLN2	TGFBR3	SESN3	FAM109B	GRIN2D	APLP2	XXYLT1
NPBWR1	TMEM200B	BNC2	PLAU	ADAM12	IGFN1	PSG9
PTGES	BGN	SLC7A10	LAMP1	ZCCHC24	TTPAL	MT1X
CCDC78	SFXN1	RAB42	SLC26A2	MARVELD1	PSG2	
ZNF365	L1CAM	APCDD1L-AS1	B3GALT6	LRRC10B	PSG11	
PPARA	TRAM1L1	FBXL19-AS1	SERPINE1	LINC00346	IGFBP3	
HYAL1	WNT5B	KDR	SLC16A13	MAP1A	NT5E	
SIAE	SIK1	LMBR1L	FAM98A	RAB31	SBSN	
RAP2B	PLSCR4	DOLK	TBC1D8B	CXCL8	PSG7	
H1F0	GRB10	KLF2	OLMALINC	COL1A1	MATK	
C6orf120	SLC2A10	EBI3	WISP2	HTRA1	SGK1	
ST8SIA1	CARF	KAZALD1	ERG	LAMP2	HN1L	
TMEM67	TTC30A	FAM227A	TOB2P1	OLFML3	ITPRIPL2	
PRRT3	L3HYPDH	GLB1L	HES1	APCDD1L	PAPSS2	
CBFA2T3	PCDH7	EXOC3L1	MAGEL2	MDK	CEBPA-AS1	
SOGA1	HDAC4	ZNF268	IL2RB	LOC642852	WDFY1	

3.3.2 Many consensus transcription factor sequences, miRNA targets, KEGG pathways, and gene sets are enriched in differentially expressed genes following CBFβ knockdown

The lists of downregulated and upregulated differentially expressed genes following CBFβ knockdown were submitted to EnrichR to identify enriched promoter sequences, miRNA targets, and KEGG pathways. Seventeen transcription factor binding sequences from the ChEA 2016 collection were enriched in the list of downregulated genes (Figure 3.2A, Table 3.4). The top two enriched promoter sequences were E2F7 and SMAD2/3. E2F7 is a transcription factor that represses the expression of genes related to the G_1/S transition, and the SMAD2/3 complex has a well-characterized role in migration and anchorage-independent growth (Bruin et al., 2003; Lamouille et al., 2014; Westendorp et al., 2012). These promoter sequences are consistent with the phenotypes observed after CBFβ knockdown in ovarian cancer cells. The targets of 10 miRNAs were enriched in the downregulated gene list (Figure 3.2B, Table 3.5). The targets of one micro-RNA, miR193-b, were dramatically more enriched than the targets of the other 9 miRNAs, suggesting increased expression of this microRNA. Studies have shown that miR193-b functions as a tumor suppressor in ovarian cancer. miR193-b has decreased expression in ovarian cancer tumors relative to adjacent normal tissue, and miR193-b is downregulated in ovarian cancer cell lines (Li et al., 2015a). Additionally, miR193-b is downregulated in a co-culture model of ovarian cancer metastasis, and re-expression of miR193-b decreases ovarian cancer cell line proliferation, colony formation, migration, invasion, and i.p. xenograft growth (Mitra et al., 2015; Zhang et al., 2017).

Table 3.4 TF consensus sequences enriched in DEGs

TF consensus sequences enriched in downregulated genes:

ChEA Data Set	Adjusted P-value	Z-score	Combined Score
E2F7_22180533_ChIP-Seq_HELA_Human	0.0000	-3.8469	63.6086
SMAD2_18955504_ChIP-ChIP_HaCaT_Human	0.0000	-1.8108	29.2157
SMAD3_18955504_ChIP-ChIP_HaCaT_Human	0.0000	-1.8047	29.1184
ATF3_27146783_Chip-Seq_COLON_Human	0.0000	-1.5343	23.7641
AR_21909140_ChIP-Seq_LNCAP_Human	0.0007	-2.8475	34.6478
E2F1_21310950_ChIP-Seq_MCF-7_Human	0.0017	-2.3526	25.9576
GATA6_25053715_ChIP-Seq_YYC3_Human	0.0053	-1.5373	14.9875
NUCKS1_24931609_ChIP-Seq_HEPATOCYTES_Mouse	0.0070	-2.2337	20.8611
JUND_26020271_ChIP-Seq_SMOOTH_MUSCLE_Human	0.0124	-1.4954	12.9316
ESR1_21235772_ChIP-Seq_MCF-7_Human	0.0154	-3.1197	25.9660
BRD4_25478319_ChIP-Seq_HGPS_Human	0.0260	-1.3175	10.1534
WT1_19549856_ChIP-ChIP_CCG9911_Human	0.0350	-3.1944	23.3834
E2F4_17652178_ChIP-ChIP_JURKAT_Human	0.0374	-3.1417	22.4141
SOX2_20726797_ChIP-Seq_SW620_Human	0.0374	-1.8093	12.8478
ELF5_23300383_ChIP-Seq_T47D_Human	0.0456	-2.1159	14.4603
ZNF217_24962896_ChIP-Seq_MCF-7_Human	0.0488	-1.7588	11.7093
E2A_27217539_Chip-Seq_RAMOS-Cell_line_Human	0.0488	-1.4940	9.9215

TF consensus sequences enriched in upregulated genes:

ChEA Data Set	Adjusted P-value	Z-score	Combined Score
SUZ12_20075857_ChIP-Seq_MESCs_Mouse	0.0000	-0.9352	22.6195
MTF2_20144788_ChIP-Seq_MESCs_Mouse	0.0001	-1.2921	19.0633
TCF21_26020271_ChIP-Seq_SMOOTH_MUSCLE_Human	0.0035	-1.5663	17.2499
SUZ12_27294783_Chip-Seq_ESCs_Mouse	0.0161	-1.4588	13.4257
SUZ12_18974828_ChIP-Seq_MESCs_Mouse	0.0191	-1.7365	15.2975
ESR2_21235772_ChIP-Seq_MCF-7_Human	0.0214	-2.7324	22.9360
KDM2B_26808549_Chip-Seq_K562_Human	0.0214	-1.5067	12.5951
SUZ12_18692474_ChIP-Seq_MESCs_Mouse	0.0250	-1.7999	14.4698
RING1B_27294783_Chip-Seq_NPCs_Mouse	0.0250	-1.4920	11.8659
RNF2_27304074_Chip-Seq_ESCs_Mouse	0.0325	-1.6938	12.6864
KDM2B_26808549_Chip-Seq_SUP-B15_Human	0.0325	-1.4733	11.1341
ESR1_21235772_ChIP-Seq_MCF-7_Human	0.0463	-3.1049	21.8103
SUZ12_18692474_ChIP-Seq_MEFs_Mouse	0.0463	-1.9610	13.6624

Four KEGG pathways were significantly enriched in the downregulated gene list (Figure 3.2C, Table 3.5). The most enriched KEGG pathway was “Cell Cycle”, which is consistent with the enrichment of the E2F7 promoter sequence and the reported decreased proliferation with knockdown of CBFβ in ovarian cancer (Greer et al., 2013). The other three significantly enriched pathways were “DNA Replication”, “pyrimidine metabolism”, and “vitamin B6 metabolism”. There are no direct reported links between CBFβ and these pathways; however, correlative evidence supports this association as treatment of OVCAR8 cells with inhibitors of the CBFβ/RUNX interaction cause decreased EdU incorporation and an S-phase delay (Carlton et al., 2018).

A

Top 10 TF binding motifs enriched in downregulated genes

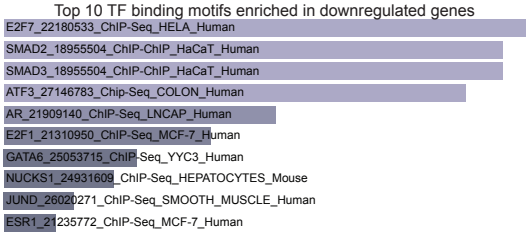

B

Top 10 miRNA targets enriched in downregulated genes

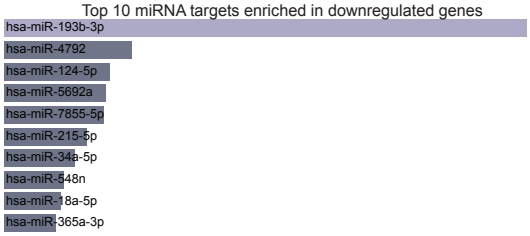

Top 10 TF binding motifs enriched in upregulated genes

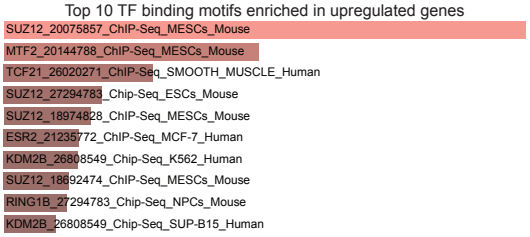

Top miRNA targets enriched in upregulated genes

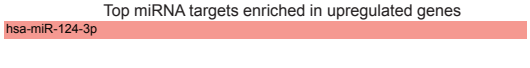

C

Top KEGG pathways enriched in downregulated genes

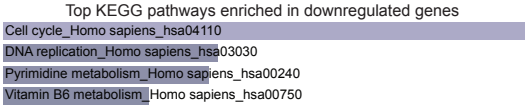

Top KEGG pathways enriched in upregulated genes

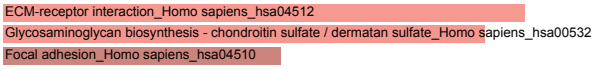

D

Top in downregulated

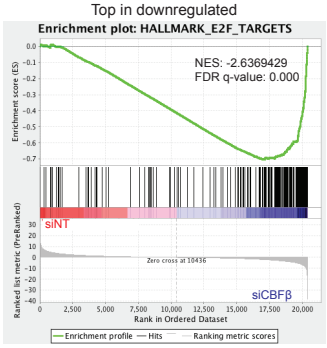

Top in upregulated

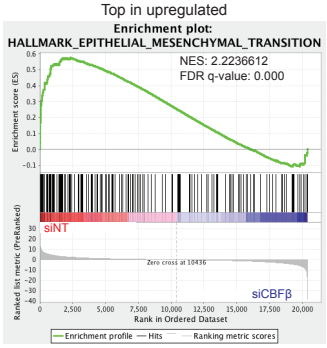

Figure 3.2 EnrichR and GSEA analysis of differentially expressed genes following siRNA-mediated knockdown of CBFβ

A. Top 10 significantly enriched transcription factor consensus binding sequences from ChEA 2016 in genes altered by CBFβ knockdown. B. Top 10 miRNAs with target genes enriched in genes altered following CBFβ knockdown. C. Significantly enriched KEGG 2016 pathways in genes significantly altered by CBFβ knockdown. D. GSEA plots for the most positively and negatively enriched hallmark gene sets.

Table 3.5 miRNA targets and KEGG pathways enriched in DEGs

micro-RNA targets enriched in differentially expressed genes:

Downregulated			
Term	Adjusted P-value	Z-score	Combined Score
hsa-miR-193b-3p	0.000002	-6.364176	132.635715
hsa-miR-5692a	0.019724	-2.959103	30.258419
hsa-miR-124-5p	0.019724	-2.265232	23.430580
hsa-miR-4792	0.019724	-2.102638	22.869661
hsa-miR-7855-5p	0.019724	-2.142214	21.808870
hsa-miR-215-5p	0.025388	-5.168214	50.368181
hsa-miR-34a-5p	0.028942	-5.105124	48.297422
hsa-miR-548n	0.032666	-2.905159	26.673014
hsa-miR-18a-5p	0.032666	-2.643167	24.021732
hsa-miR-365a-3p	0.032785	-2.108787	18.935270
hsa-miR-140-3p	0.043465	-2.568671	21.872023
hsa-miR-4766-3p	0.043465	-2.174124	18.520821
Upregulated			
Term	Adjusted P-value	Z-score	Combined Score
hsa-miR-124-3p	0.0000002	-9.7981039	227.6714857

KEGG pathways enriched in differentially expressed genes:

Upregulated			
KEGG pathway	Adjusted P-value	Z-score	Combined Score
Cell cycle_Homo sapiens_hsa04110	0.000001	-1.733198	33.892112
Vitamin B6 metabolism_Homo sapiens_hsa00750	0.000423	-0.952546	11.882088
DNA replication_Homo sapiens_hsa03030	0.008089	-1.803483	15.923183
Pyrimidine metabolism_Homo sapiens_hsa00240	0.008089	-1.734793	15.379174
Downregulated			
KEGG pathway	Adjusted P-value	Z-score	Combined Score
ECM-receptor interaction_Homo sapiens_hsa04512	0.000976	-1.712524	21.173265
Glycosaminoglycan biosynthesis - chondroitin sulfate / dermatan sulfate_Homo sapiens_hsa00532	0.000976	-1.158566	13.611521
Focal adhesion_Homo sapiens_hsa04510	0.015315	-1.871717	16.077509

The list of upregulated genes is also enriched for several ChEA 2016 TF consensus sequences, miRNA targets, and KEGG pathways. Thirteen ChEA 2016 TF consensus sequences are enriched in upregulated genes following CBFβ knockdown (Figure 3.2A, Table 3.4). Of note, 4 out of the 13 enriched sequences are for SUZ12 promoters (each representing a unique ChIPSeq data set), indicating a particularly strong association with this gene. SUZ12 is one member of the trimeric PRC2 complex consisting of SUZ12, EED, and EZH1/2; together this complex leads to H3K27 tri-methylation and target gene repression (Conway et al., 2015). Only one report links SUZ12 and ovarian cancer, and this study indicates that SUZ12 plays an oncogenic role (Li et al., 2012a). Two of the remaining nine enriched promoter sequences are for KDM2B. KDM2B is another epigenetic regulator that causes demethylation of H3K36me2 and H3K4me3 marks, leading to target gene repression (Tzatsos et al., 2009). Like SUZ12, the link between KDM2B and ovarian cancer is not well characterized. However, the one report investigating this link indicates that KDMB2 plays an oncogenic role in ovarian cancer via EZH2 upregulation, perhaps linking the roles of SUZ12 and KDMB2 after CBFβ knockdown (Kuang et al., 2017). The list of upregulated genes was enriched for targets of only one miRNA, miR-124-3p. miR-124-3p has a putative tumor suppressive role in ovarian cancer leading to decreased migration and invasion (Figure 3.2B, Table 3.5) (Yuan et al., 2017; Zhang et al., 2013).

Three KEGG pathways were enriched in the list of upregulated genes: “ECM-receptor interaction”, “glycosaminoglycan biosynthesis – chondroitin sulfate/dermatan sulfate”, and “focal adhesion” (Figure 3.2C, Table 3.5). The enrichment of these KEGG pathways

was a bit surprising. As knockdown of CBFβ is associated with decreased anchorage-independent growth, one would expect these pathways to be enriched in the downregulated genes instead (Greer et al., 2013; Mendoza-Villanueva et al., 2010). Further work to understand both why these pathways are upregulated and the functional significance of this upregulation is needed.

Additionally, GSEA was performed on the list of differentially expressed genes. Several gene sets were significantly enriched; gene sets were considered enriched when FDR q-value < 0.05. Nine gene sets were enriched in the CBFβ knockdown samples (Figure 3.2E, Table 3.6). The gene set with the most significant enrichment was "E2F targets", complementing the promoter analysis from EnrichR. The most enriched gene set in the control samples was "Epithelial to Mesenchymal Transition". Again, this result complements the EnrichR analysis, showing that some of the most upregulated KEGG pathways were "ECM-receptor interaction" and "Focal Adhesion". A complete list of enriched hallmark gene sets is listed in table 3.6.

Table 3.6 Significantly enriched hallmark gene sets by GSEA

List of significantly enriched gene sets from GSEA analysis of differentially expressed genes following siRNA-mediated knockdown of CBFβ in OVCAR8 cells

Hallmark Gene Set	NES	FDR q-value
HALLMARK_EPITHELIAL_MESENCHYMAL_TRANSITION	2.2236612	0
HALLMARK_COAGULATION	1.9405582	0.001464286
HALLMARK_PROTEIN_SECRETION	1.6282951	0.020862365
HALLMARK_CHOLESTEROL_HOMEOSTASIS	1.581853	0.02308685
HALLMARK_INFLAMMATORY_RESPONSE	1.5789926	0.01916948
HALLMARK_GLYCOLYSIS	1.5635659	0.020600654
HALLMARK_WNT_BETA_CATENIN_SIGNALING	1.5309405	0.023271145
HALLMARK_ANGIOGENESIS	1.5062953	0.026189985
HALLMARK_COMPLEMENT	1.4875038	0.028381266
HALLMARK_UV_RESPONSE_DN	1.4749184	0.028601663
HALLMARK_APICAL_JUNCTION	1.4743501	0.026106408
HALLMARK_TGF_BETA_SIGNALING	1.4697288	0.025727944
HALLMARK_MYOGENESIS	1.4662336	0.024379533
HALLMARK_TNFA_SIGNALING_VIA_NFKB	1.39503	0.046117824
HALLMARK_E2F_TARGETS	-2.6369429	0
HALLMARK_G2M_CHECKPOINT	-2.4194002	0
HALLMARK_MYC_TARGETS_V1	-2.2761824	0
HALLMARK_OXIDATIVE_PHOSPHORYLATION	-2.147033	0
HALLMARK_MYC_TARGETS_V2	-1.9983912	0
HALLMARK_DNA_REPAIR	-1.9577159	0
HALLMARK_MITOTIC_SPINDLE	-1.8763366	4.00E-04
HALLMARK_P53_PATHWAY	-1.6414553	0.004419468
HALLMARK_MTORC1_SIGNALING	-1.5670732	0.008836918

3.3.3 Differentially expressed genes following CBFβ knockdown in ovarian cancer share minimal overlap with genes either altered by RUNX knockdown or CBFβ/RUNX inhibitor treatment in ovarian cancer

Prior work has investigated gene expression changes following stable knockdown of RUNX1 and RUNX2 in the SKOV3 ovarian cancer cell line. Therefore, we were interested in identifying potential overlap between the differentially expressed genes following CBFβ knockdown and the genes differentially expressed after RUNX1 or RUNX2 knockdown. As previously reported, knockdown of RUNX1 or RUNX2 in ovarian cancer both decrease proliferation, migration, invasion and anchorage-independent growth. However, there is substantial diversity in the differentially expressed genes following knockdown of these genes (Wang et al., 2013). We examined the RUNX1, RUNX2, and CBFβ knockdown data sets, pooling upregulated and downregulated genes together. In this analysis a total of 2307 genes were differentially expressed in any data set. Eight percent (195/2307) of differentially expressed genes were shared in one pairwise comparison between data sets, and 0.2% (5/2307) of genes were differentially expressed in all three data sets (Figure 3.3A). Additionally, of these shared differentially expressed genes, 55% are altered in opposing directions in pairwise comparisons (Figure 3.3B). The lack of overlap between these three data sets is striking, and further work to characterize these differences should be completed. Only one gene, PSG11, was altered in the same direction in all three data sets showing upregulation after knockdown of CBFβ, RUNX1 and RUNX2. Little is reported about PSG11, which is a protein secreted by the trophoblast during pregnancy. One report indicates the treatment of human monocytes with PSG11 stimulated the release of TGFβ1, IL-6, and IL-10, but

did not probe any downstream consequences (Snyder Sara K. et al., 2003). The only study reporting a link between PSG11 and cancer indicates that high mRNA expression of PSG11 predicts increased mortality in ovarian cancer (Zhang et al., 2014). PSG11 is also listed as a RUNX2 target gene in the EnrichR platform. Further work should be conducted to understand the function this gene plays in ovarian cancer.

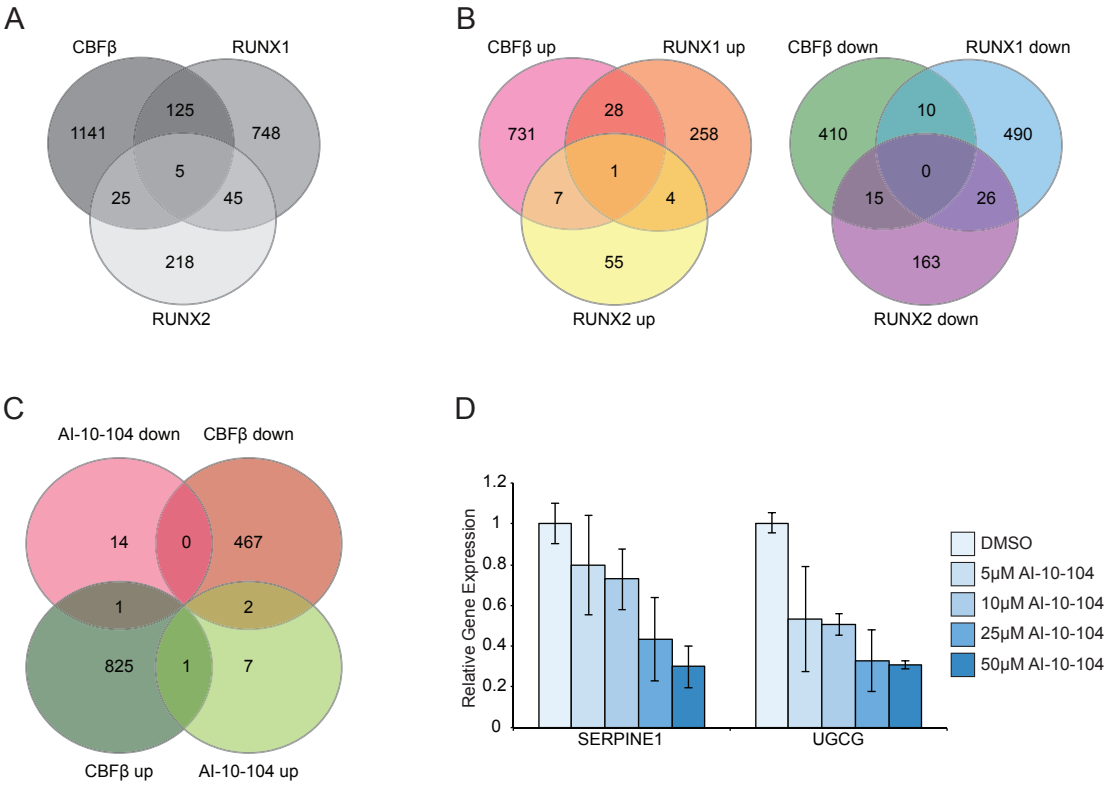
A
CBFβ
RUNX1
1141
125
748
5
25
45
218
RUNX2
B
CBFβ up
RUNX1 up
731
28
258
1
7
4
55
RUNX2 up
CBFβ down
RUNX1 down
410
10
490
0
15
26
163
RUNX2 down
C
AI-10-104 down
CBFβ down
14
0
467
1
2
825
1
7
CBFβ up
AI-10-104 up
D
Relative Gene Expression
1.2
1
0.8
0.6
0.4
0.2
0
SERPINE1
UGCG
DMSO
5μM AI-10-104
10μM AI-10-104
25μM AI-10-104
50μM AI-10-104

Figure 3.3 Genes differentially expressed after CBFβ knockdown share little overlap with genes controlled by RUNX1 and RUNX2 in ovarian cancer

A. Venn diagram comparing significantly altered genes following CBFβ, RUNX1 and RUNX2 knockdown in ovarian cancer cell lines. B. Venn diagrams comparing significantly upregulated and downregulated genes following CBFβ, RUNX1 and RUNX2 cell lines in ovarian cancer cell lines. C. Venn diagram comparing genes significantly altered by CBFβ knockdown and AI-10-104 treatment for 24 hours. D. RT-qPCR of SERPINE1 and UGCG in OVCAR8 cells treated with the indicated dose of AI-10-104 for 24 hours. Gene expression is normalized to GAPDH.

We were also interested in comparing the differentially expressed genes following CBFβ knockdown to the differentially expressed genes following treatment with AI-10-104, a validated inhibitor of the CBFβ/RUNX protein-protein interaction (Illendula et al., 2016). As we reported earlier, treatment of OVCAR8 cells with AI-10-104 changed the expression of a very small number of genes. There was little overlap between the genes altered by AI-10-104 treatment and siRNA-mediated knockdown of CBFβ, and of the few shared genes, many were regulated in opposing directions (Figure 3.3C). One possible explanation for the minimal overlap between these two data sets is that the concentration of AI-10-104 was not high enough to mimic the effects of protein knockdown. To address this question, OVCAR8 cells were treated with increasing doses of AI-10-104 for 24 hours and expression of SERPINE1 and UGCG was assessed by RT-qPCR. These genes were chosen because they were validated by RT-qPCR following siRNA knockdown of CBFβ, are well-studied RUNX target genes, and had increased expression following knockdown. We chose upregulated genes to ensure that decreased global RNA transcription due to toxicity would not confound our results. Treatment with escalating doses of AI-10-104 did not increase the mRNA levels of SERPINE1 or UGCG, indicating that the lack of overlap between these two data sets is not due to an incorrect dose of AI-10-104 (Figure 3.3D).

3.3.4 siRNA-mediated knockdown of CBFβ does not alter growth or migration of OVCAR8 cells

Literature reports characterizing the role of CBFβ in ovarian cancer have used shRNA-mediated knockdown to investigate phenotypes. One report indicated that only double

shRNA-mediated knockdown of CBFβ decreased ovarian cancer growth, while other methods of knockdown had no effect on cellular phenotypes (Greer et al., 2013). To confirm this finding, we assessed the growth of OVCAR8 cells transfected with a pool of non-targeting or CBFβ-targeting siRNAs. OVCAR8 cells were transfected with non-targeting or CBFβ-targeting siRNAs, and live cell number was measured after 24 and 72 hours by CellTiter-Glo. Across an average of two independent experiments, siRNA-mediated knockdown of CBFβ did not alter the growth of OVCAR8 cells (Figure 3.4A). To assess the effects of CBFβ knockdown on cellular migration, OVCAR8 cells were transfected with non-targeting or CBFβ-targeting siRNAs. After 24 hours, confluent monolayers were scratched with a pipette tip and wound size was measured at 0, 14, and 24 hours. siRNA-mediated knockdown of CBFβ did not alter OVCAR8 cell migration, though there was a trend towards decreased migration at both 14 and 24 hours ($p=0.08$) (Figure 3.4B). siRNA-targeting of CBFβ decreased both CBFβ protein and mRNA levels, indicating that our lack of phenotypic effects was not secondary to poor knockdown (Figure 3.4C,D). While the cells transfected with a pool of CBFβ-targeting siRNAs have over 95% reduction of CBFβ by RT-qPCR, there is still a substantial amount of CBFβ mRNA present. Cells transfected with CBFβ-targeting siRNAs express CBFβ at an average C_t value of 27.2, a reduced, but still present level, which could help explain the lack of effect following CBFβ knockdown.

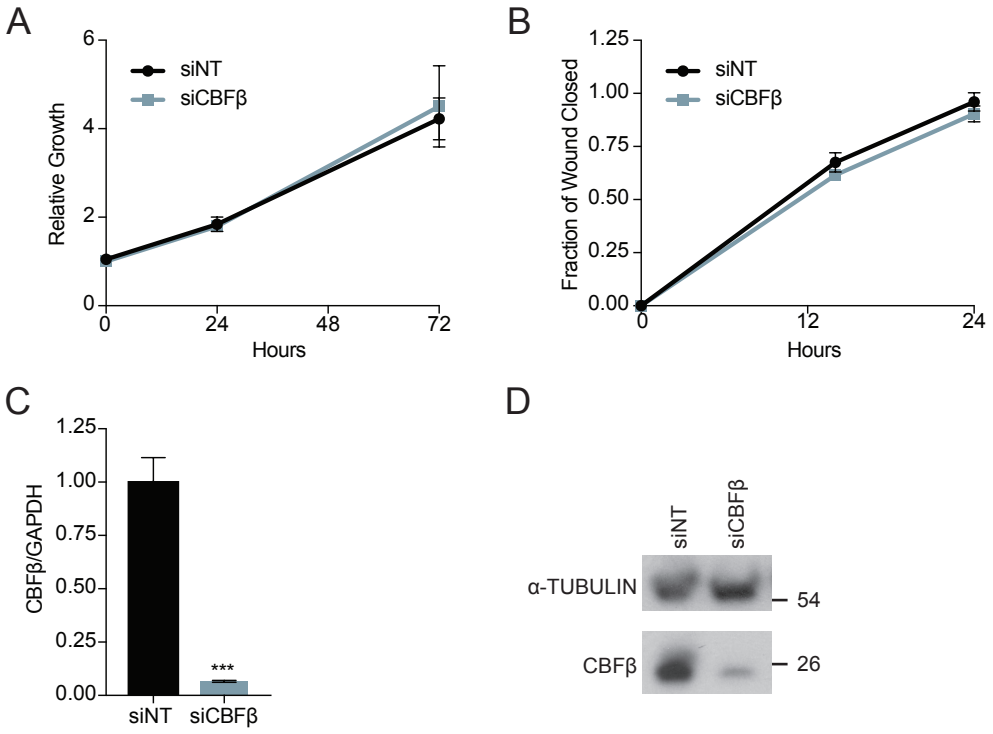
A
Relative Growth
siNT
siCBFβ
Hours
B
Fraction of Wound Closed
siNT
siCBFβ
Hours
C
CBFβ/GAPDH
***
siNT
siCBFβ
D
siNT
siCBFβ
α-TUBULIN
54
CBFβ
26

Figure 3.4 siRNA-mediated knockdown of CBFβ does not alter ovarian cancer growth or migration

A. Relative growth of OVCAR8 cells transfected with non-targeting or CBFβ-targeting siRNAs as assessed by CellTiter-Glo after 0, 24, and 72 hours. B. OVCAR8 cells transfected with non-targeting or CBFβ-targeting siRNAs were plated in confluent monolayers and scratched with a pipette tip. Relative fraction of wound closed was measured at 0, 14, and 24 hours. C. RT-qPCR analysis of CBFβ mRNA levels 48 hours after transfection with non-targeting or CBFβ-targeting siRNAs. Gene expression is normalized to GAPDH. D. Protein expression of CBFβ 48 hours after transfection with non-targeting or CBFβ-targeting siRNAs. α-tubulin is shown as a loading control. ***$p<0.001$ by t-test (C) or two-way repeated-measured ANOVA (B) with Holm-Sidak post-hoc tests.

3.3.5 CRISPR-mediated knockdown of CBFβ partially mimics the effects of CBFβ/RUNX inhibitor treatment

As our own data and other literature reports indicate that near complete knockdown of CBFβ is required to decrease ovarian cancer growth, we generated OVCAR8 cells stably expressing an empty vector or vector containing CRISPR guide RNAs targeting CBFβ. These cell lines have complete loss of CBFβ at the protein level (Figure 3.5A). Unlike prior literature reports using shRNA-mediated knockdown, these cells were able to proliferate (Greer et al., 2013). Growth of OVCAR8 cells lacking CBFβ was measured in a serial passage assay; a fixed number of cells were plated every 3-4 days and fold change at each passage was recorded. Cells with CBFβ knockdown had significantly decreased growth relative to control cells (Figure 3.5B).

Treatment of OVCAR8 cells with AI-10-104 significantly decreased the expression of INHBA and MMP1, and siRNA-mediated knockdown of those genes decreased proliferation and migration. Therefore, we were interested to see if these same gene expression changes would be present with CRISPR-mediated reduction of CBFβ. Cell lines without CBFβ had decreased expression of INHBA while the expression of MMP1 was unchanged (Figure 3.5C). We were a bit surprised that the expression of MMP1 was not decreased with CRISPR-mediated loss of CBFβ; however, this may be due the difference between protein-interaction inhibition and stable knockdown.

We also investigated if genes that were altered with short-term siRNA-mediated knockdown of CBFβ (RUNX1, SERPINE1, and UGCG) would be recapitulated with

CRISPR-mediated stable CBFβ loss. RT-qPCR analysis revealed that expression of RUNX1 was significantly increased in cells with stable CBFβ loss, directly opposing the effects of CBFβ-targeting siRNAs (Figure 3.5D). While this result appears surprising, it likely reflects the differing methods of CBFβ reduction used in each experiment. When CBFβ was targeted using siRNAs, gene expression was assessed after 72 hours, likely capturing primary alterations in gene expression. As expected in this experimental setting, the levels of RUNX1 were decreased, as RUNX1 can regulate its own transcription and without CBFβ one would predict this auto regulation to decrease (Martinez et al., 2016). However, under stable CBFβ knockdown it is not totally unprecedented that RUNX1 levels would increase. This increase in RUNX1 mRNA levels is likely a compensatory attempt to overcome CBFβ loss. This compensatory upregulation of RUNX proteins in response to loss of one member of the family has recently been characterized in multiple other cancer cell lines (Morita et al., 2017b). The levels of SERPINE1 and UGCG were not significantly altered in cells with stable CBFβ loss. It is possible that these genes would be altered in the short-term after CBFβ loss, but compensatory secondary alterations dampened those responses (Figure 3.5D).

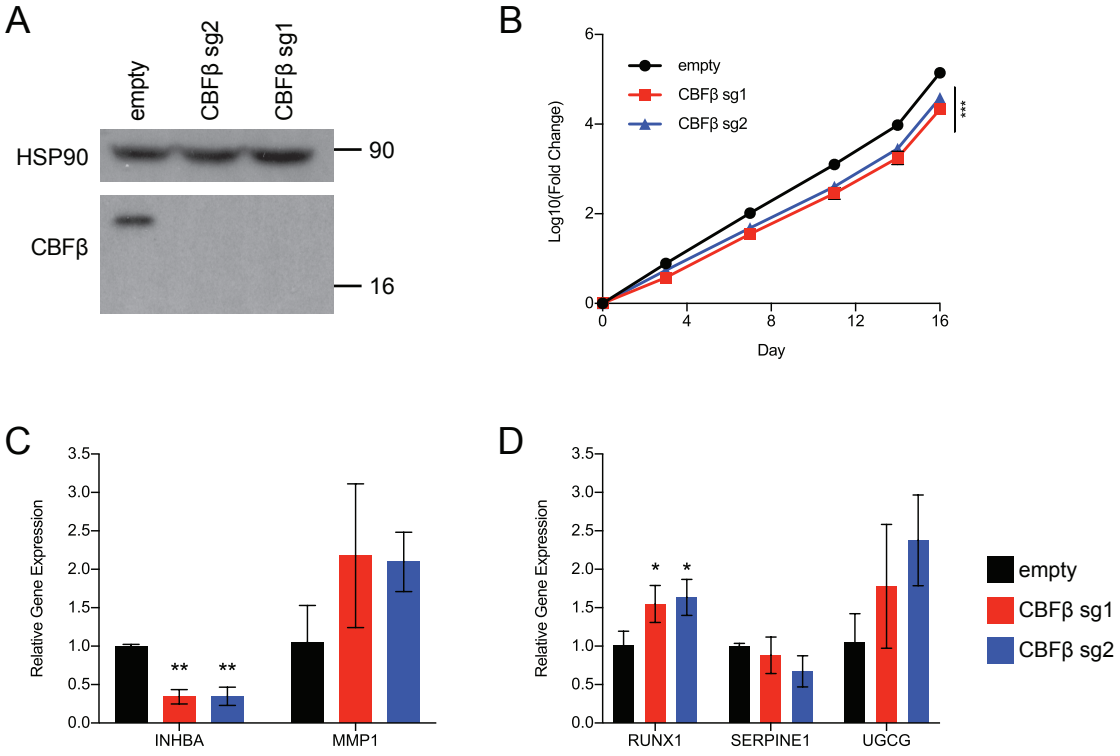
A
empty
CBFβ sg2
CBFβ sg1
HSP90
90
CBFβ
16
B
empty
CBFβ sg1
CBFβ sg2
Log10(Fold Change)
Day
***
C
Relative Gene Expression
**
**
INHBA
MMP1
D
Relative Gene Expression
*
*
RUNX1
SERPINE1
UGCG
empty
CBFβ sg1
CBFβ sg2

Figure 3.5 CRISPR-mediated knockdown of CBFβ decreases ovarian cancer growth and causes gene expression alterations

A. Western blot showing protein expression of CBFβ in OVCAR8 cells stably expressing an empty vector or a vector containing CBFβ-targeting guide RNAs. HSP90 is shown as a loading control. B. OVCAR8 cells stably expression an empty vector or CBFβ-targeting CRISPR guide were serially passaged and fold change in cell number over time was measured. Data on the Y-axis have been Log_{10} transformed. C. RT-qPCR for INHBA and MMP1 in cells with stable knockdown of CBFβ. Gene expression is normalized to GAPDH. D. RT-qPCR analysis for RUNX1, SERPINE1, and UGCG in OVCAR8 cells with stable knockdown of CBFβ. Gene expression is normalized to GAPDH. *$p<0.05$, **$p<0.01$, ***$p<0.01$, control vs. experimental condition, by two-way repeated-measures two-way ANOVA (B), or one-way ANOVA (C,D) with Holm-Sidak post-hoc tests.

3.3.6 Cells with CBFβ knockdown retain sensitivity to AI-10-104

AI-10-104 is a validated inhibitor of the protein-protein interaction between CBFβ and RUNX proteins (Illendula et al., 2016). Therefore, we were interested to see if cells lacking CBFβ had a diminished response to treatment with AI-10-104. To address this question, OVCAR8 cells were transfected with non-targeting or CBFβ-targeting siRNAs and then treated with AI-10-104 for 72 hours; live cell number was assessed using CellTiter-Glo. Cells with siRNA-mediated knockdown of CBFβ did not have an altered response to AI-10-104 averaged across three independent experiments (Figure 3.6A,B). Given the limitations of siRNA-targeting of CBFβ, we investigated if AI-10-104 would have differential effects on the CRISPR cell lines with complete knockout of CBFβ. Cells lacking CBFβ were treated with AI-10-104 for 72 hours, and then live cell number was measured by CellTiter-Glo. Compared with the control cell line, cells with complete knockout of CBFβ had lower total cell numbers, as measured by luminescence, after compound treatment (Figure 3.6C). However, when relative live cell number was calculated by normalizing each cell line to DMSO, all three cell lines had the same response to CBFβ/RUNX inhibitor treatment (Figure 3.6D). This result confirms that loss of CBFβ affects cellular proliferation, as evidenced by the reduced growth of cells treated with DMSO only. However, the effect of AI-10-104 on cells lacking its target CBFβ may indicate that the effect of AI-10-104 on proliferation is mediated by additional targets in addition to CBFβ.

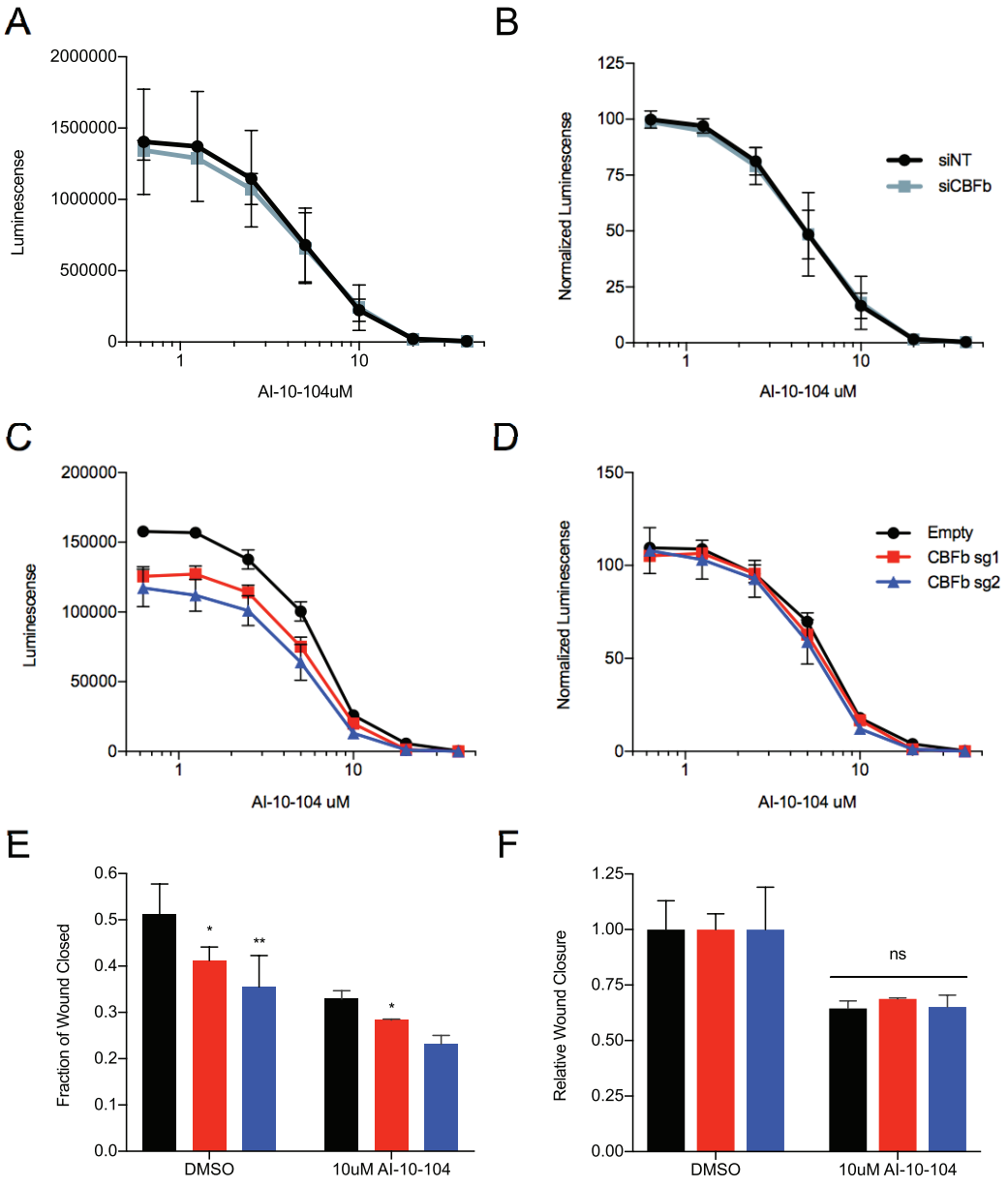
A
Luminescense
2000000
1500000
1000000
500000
0
1
10
AI-10-104uM
B
Normalized Luminescense
125
100
75
50
25
0
siNT
siCBFb
AI-10-104 uM
C
Luminescense
200000
150000
100000
50000
AI-10-104 uM
D
Normalized Luminescense
150
Empty
CBFb sg1
CBFb sg2
AI-10-104 uM
E
Fraction of Wound Closed
0.6
0.5
0.4
0.3
0.2
0.1
0.0
DMSO
10uM AI-10-104
F
Relative Wound Closure
1.25
1.00
0.75
0.50
0.25
0.00
ns
DMSO
10uM AI-10-104

Figure 3.6 Cells with CBFβ knockdown retain sensitivity to the CBFβ/RUNX protein-protein inhibitor AI-10-104

A. OVCAR8 cells transfected with non-targeting or CBFβ-targeting siRNAs were treated with AI-10-104 for 72 hours and relative live cell number was measured by CellTiter-Glo. B-C. OVCAR8 cells stably expressing an empty plasmid or a plasmid containing CBFβ-targeting CRISPR guide RNAs were treated with AI-10-104 for 72 hours and relative live cell number was measured by CellTiter-Glo. C. Total luminescence after 72 hours. D. Relative live cell number after 72 hours. D-E. OVCAR8 cells with stable CBFβ knockdown or control cells were plated and then treated with DMSO or AI-10-104. Confluent monolayers were scratched with a pipette tip and wound size was measured at 0 and 24 hours. D. Fraction of wound closed after 14 hours. E. Relative wound healing after 14 hours. *$p<0.05$, **$p<0.01$, control vs. experimental condition by two-way ANOVA (E,F) with Holm-Sidak post-hoc tests.

Ovarian cancer cells treated with AI-10-104 also have significantly impaired wound healing. As AI-10-104 causes greater effects on wound healing than it does on proliferation, we wanted to determine if CBFβ loss would blunt the effect of AI-10-104 on this phenotype. OVCAR8 control cells and cells lacking CBFβ were plated and treated with DMSO or 10μM AI-10-104. Confluent monolayers were then scratched with a P1000 pipette tip. Fractional wound closure was measured after 14 hours. Loss of CBFβ significantly decreased wound healing alone (Figure 3.6E). However, similar to proliferation, when each cell line was normalized to its own DMSO control, there was no change in relative inhibition of wound healing (Figure 3.6F). In combination with the effects of AI-10-104 on proliferation in cells lacking CBFβ, these results indicate that AI-10-104 may have additional protein targets that contribute to its effects on proliferation and migration of ovarian cancer cells.

3.4 Discussion

In this chapter, we examined the effects of CBFβ knockdown on ovarian cancer cells using multiple methods. siRNA-mediated knockdown of CBFβ altered a large number of genes and these differentially expressed genes were associated with processes relevant to cancer pathogenesis. Comparison of differentially expressed genes following siRNA-mediated knockdown of CBFβ to RUNX1 shRNA knockdown, RUNX2 shRNA knockdown, and RUNX/CBFβ inhibitor treatment demonstrated little overlap between data sets. siRNA-mediated knockdown of CBFβ did not alter cellular proliferation or migration; however, CRISPR-mediated loss of CBFβ significantly reduced ovarian cancer cell proliferation and migration. Lastly, ovarian cancer cells with either siRNA-mediated or CRISPR-mediated reduction of CBFβ retain their sensitivity to CBFβ/RUNX inhibitors.

We were surprised at the lack of overlap between our data set and other published data sets examining RUNX proteins in ovarian cancer. There are a few key differences between these experiments, which may help explain the lack of shared results. First, our CBFβ knockdown experiment was performed in OVCAR8 cells, and the RUNX1 and RUNX2 knockdown experiments were performed in SKOV3 cells. There is great heterogeneity between ovarian cancer cell lines, and some believe that SKOV3 cells are not HGSOC at all (Domcke et al., 2013). These large baseline differences in gene expression may be a barrier to observing meaningful overlap, were it to exist.

Another contributor to this variation may be the method used to knock down CBFβ. Genes controlled by CBFβ were analyzed 72 hours after siRNA transfection, with the goal of analyzing the early effects of CBFβ knockdown, while minimizing secondary effects. In contrast, the RUNX1 and RUNX2 expression analyses were performed in cell lines with stable knockdown. These differences in methodology may have introduced substantial variability, making our results difficult to compare directly.

Interestingly, approximately half of the shared differentially expressed genes were altered in opposing directions; this may be in part due to the use of stably maintained cell lines. As RUNX proteins are known to regulate the expression of each other, and stable knockdown of one RUNX protein has been shown to lead to compensatory upregulation of other family members, it is possible that some primary alterations in gene expression are being masked by long-term compensation (Martinez et al., 2016; Spender et al., 2005). Further work investigating the kinetics of gene expression changes following single or combined RUNX and CBFβ knockdown would help clarify these findings and may shed light on these unexpected changes in gene expression.

Despite the lack similarity in the gene expression changes following CBFβ knockdown, RUNX1/2 knockdown, and CBFβ/RUNX inhibitor treatment in ovarian cancer cells, the phenotype observed following all of these conditions was shared. Similar to ovarian cancer cells with RUNX1 or RUNX2 stable knockdown, cells with stable CBFβ knockdown have decreased proliferation and migration (Carlton et al., 2018; Greer et al., 2013; Keita et al., 2013; Wang et al., 2013). This phenotype following stable loss of

CBFβ also matches the phenotype observed after treatment of ovarian cancer cells with AI-10-104. Future work should investigate what shared features between these 3 models are driving these consistent phenotypes.

Lastly, cells lacking CBFβ retained their sensitivity to AI-10-104, the CBFβ/RUNX inhibitor, which binds directly to CBFβ. This result was in some ways surprising. One would hypothesize that when the target of a drug is absent, the effect of the drug should be blunted. This result indicates that AI-10-104 may have additional targets beyond CBFβ, which merits further study.

In sum, siRNA-mediated knockdown of CBFβ causes large-scale changes in gene expression and the differentially expressed genes are enriched for several cancer-related processes. The method of CBFβ knockdown, siRNA vs. CRISPR, affects the observed alterations in gene expression. Genetic reduction of CBFβ decreases the proliferation and migration of ovarian cancer cell lines and also alters gene expression. Lastly, ovarian cancer cells lacking CBFβ retained sensitivity to AI-10-104, a CBFβ/RUNX protein-protein interaction inhibitor, which binds to CBFβ. Further studies to tease apart these expected and unexpected phenotypes will help provide clarity to these results.

Chapter 4. Discussion

In this dissertation, we showed that treating ovarian cancer cell lines with CBFβ/RUNX inhibitors decreases proliferation, migration and anchorage-independent growth. Compound treatment alters the expression of a small number of genes and knockdown of two differentially expressed genes replicates the effects of inhibitor treatment. Additionally, siRNA-mediated knockdown of CBFβ alters a large number of genes, and these differentially expressed genes are related to several cancer processes. Loss of CBFβ protein inhibits proliferation and migration, similar to the effects of inhibitor treatment.

4.1 Non-transcriptional role of CBFβ

Previous studies had used genetic methods to reduce CBFβ, RUNX1, RUNX2 or RUNX3 in ovarian cancer cell lines and have shown decreases in proliferation, migration, and anchorage-independent growth (Barghout et al., 2015; Keita et al., 2013; Wang et al., 2013). Treatment with AI-10-104 and AI-14-91 replicated these results as expected. However, treatment with AI-10-104 altered the expression of a very small number of genes, whereas knockdown of RUNX1 or RUNX2 resulted in wide-scale alterations in gene expression. Studies investigating the role of CBFβ in other cancers and developmental processes similarly have short lists of genes under the control of CBFβ (Johnson et al., 2012; Mendoza-Villanueva et al., 2011). These data implicate a possible secondary role for CBFβ independent of an interaction with RUNX proteins in regulating gene transcription. A few lines of correlative evidence may provide insight into what these functions may be.

In the cytoplasm, the cytoskeletal protein, FilaminA, has been the best characterized binding partner of CBFβ (Yoshida et al., 2005). CBFβ shuttles between the nucleus and the cytoplasm, and its localization is at least partially dependent on FilaminA binding (Yoshida et al., 2005). FilaminA is an actin-crosslinking member of the cellular cytoskeleton, and FilaminA function is necessary for proper cellular migration, particularly during the development of mesenchymal tissues (Lian et al., 2017; Shao et al., 2016). FilaminA binds to a wide variety of other proteins and is considered a link between the cellular milieu and cellular morphology (Robertson, 2005). Loss of FilaminA function leads to several inherited diseases and is often associated with congenital abnormalities stemming from a failure of cells to migrate properly during embryogenesis (Lange et al., 2015). Additionally, FilaminA has been shown to regulate both signal transduction and migration, and has also been implicated in several cancers (Shao et al., 2016). Given that AI-10-104 treatment blocks the interaction between CBFβ and RUNX, and RUNX binding is required for CBFβ nuclear import, AI-10-104 would be predicted to increase the cytoplasmic concentration of CBFβ. This increased level of cytoplasmic CBFβ may alter the interaction dynamics between CBFβ and Filamin A. As inhibition of CBFβ using AI-10-104 had dramatic effects on cellular migration and anchorage-independent growth, compared with the relatively moderate effects on proliferation, it is possible that the interaction of CBFβ with FilaminA may be an undefined contributor to the effects of CBFβ on cancer cell migration.

CBFβ has also been shown to have putative interactions with nuclear proteins, which may contribute to a non-RUNX dependent function of CBFβ. LC-MS analysis of protein

immunoprecipitated by CBFβ revealed peptides from SMAD4, JUNB, JUN, and FOS (Lopez-Camacho et al., 2014a). As all of these proteins are also known to bind to RUNX proteins, it is not clear if they were bound directly to CBFβ or if they were immunoprecipitated out of tertiary complexes with CBFβ/RUNX proteins (Chuang et al., 2013). However, the direct interaction between MyoD and CBFβ regulates skeletal muscle differentiation; therefore, it is possible that direct interactions between CBFβ and these other nuclear transcription factors are mediating cellular processes (Philipot et al., 2010). More detailed biochemical studies investigating the proteomic network binding to CBFβ should help clarify the role of these protein interactions.

4.2 Contradictory nature of studies involving CBFβ and RUNX proteins:

Our data investigating the effects of CBFβ/RUNX chemical inhibition paint the role of CBFβ as oncogenic, and this is supported by other studies. However, siRNA-mediated knockdown of CBFβ led to a mix of gene expression alterations, some indicating an oncogenic role, but others indicating a tumor-suppressive role. These, at times, contradictory roles of CBFβ and other RUNX proteins reflect a more general theme in the literature. CBFβ and RUNX proteins have been studied intensively since the early 1990's. Submission of RUNX or CBFβ to PubMed returns a list of over 3600 articles. With regard to cancer, it is possible to cherry pick nearly any argument about the role of RUNX or CBFβ in cancer and find at least one study to support it.

Deeper investigation into some of these contradictions reveals interesting findings. For example, the role of RUNX1 in breast cancer remains unclear. RUNX1 is mutated in approximately 3% of breast cancer patients and amplified an additional approximately

3% (Pereira et al., 2016). Additionally RUNX1 protein expression has been reported to both stimulate and inhibit the proliferation and invasion of breast cancer cell lines (Browne et al., 2015; Hong et al., 2017; Jeselsohn et al., 2017; Wang et al., 2011). Careful reading of this literature identifies that many of the studies in which RUNX1 is shown to be tumor-suppressive use MCF10A cells as their primary experimental model. Further work to understand why the loss of RUNX1 causes an apparent unique phenotype in this cell line is needed. A possible explanation for these opposing results comes from a second study, which determined that loss of RUNX1 in combination with wild-type p53 reduced breast progenitor cell proliferation. However, loss of RUNX1 in combination with a p53 mutation increased breast progenitor cell proliferation, indicating that the status of other cooperating mutations may influence the cumulative effects of RUNX proteins (Bragt et al., 2014). In summary, the role of RUNX1 in breast cancer appears dependent on both the experimental model used and the accompanying mutations present. Further work to tease apart the complex interplay between these findings is needed.

Another example of apparently contradicting roles of RUNX proteins involves the effects of RUNX3 in pancreatic adenocarcinoma (PDAC), which is exemplified in this trio of studies. First, a report in 2008 identified hypermethylation of the RUNX3 promoter in 20/32 (62.5%) of patients with PDAC. This hypermethylation was correlated with decreased survival, leading to the assertion that RUNX3 is a tumor suppressor in PDAC (Nomoto et al., 2008). In contrast, a second study examined the expression of RUNX3 immunohistochemistry, finding that RUNX3 was expressed at some level in 46/78 (60%) patient tumors. In this study, protein expression of RUNX3 was associated with the

development of distant metastases (Rossi et al., 2017). Overall survival was not assessed in this cohort. A third study which assessed the role of RUNX3 in mouse models of prostate cancer illustrates how each of the above studies can contradict each other, while both reflecting a degree of truth (Whittle et al., 2015). In this study, two mouse models of pancreatic cancer were compared to each other. Mice with *TP53* and *KRAS* mutations under the control of a p48-driven Cre recombinase had widely disseminated disease. In contrast, similar mice with *TP53* and *KRAS* mutations, in addition to heterozygous deletion of *SMAD4*, had larger local tumors, but little-to-no distant metastases. Tumors with high metastatic potential had markedly increased expression of RUNX3 compared with non-invasive tumors. As expected, knockdown of RUNX3 in cell lines derived from invasive tumors reduced migration, and overexpression of RUNX3 in cell lines derived from non-invasive tumors increased migration and metastatic ability. This data alone supports the idea that RUNX3 is an oncogene; however, the story is decidedly more complicated. Knockdown of RUNX3 in invasive cells increased proliferation and overexpression of RUNX3 in non-invasive cells inhibited proliferation. These unexpected effects on proliferation represent a rheostat between proliferation and metastasis, whereby RUNX3 inhibits proliferation, while simultaneously promoting metastatic capacity. These complex and context dependent roles of RUNX proteins may help explain these often-contradictory roles they have in cancer progression.

4.3 Interplay between CBFβ/RUNX and p53

An emerging theme in the often-contradictory literature about the role of the CBFβ/RUNX complex in cancer is the impact of p53 functional status. Initial studies looking at the role of *Runx1* in MEFs determined that Runx1 only stimulated MEF

proliferation in a *Tp53*$^{-/-}$ background (Wotton et al., 2004). Additionally, RUNX1 was identified as oncogenic in lymphocytes but only when p53 was altered (Shimizu et al., 2013). Other groups have shown that p53 directly interacts with both RUNX1 and RUNX3, giving a plausible mechanism by which these phenotypes occur (Wu et al., 2013; Yamada et al., 2010). p53 has also recently been shown to directly regulate the expression of CBFβ, and mutated p53 increased CBFβ protein levels to a greater degree than wild-type p53 (Morita et al., 2017a). However, RUNX2 knockdown was found to inhibit the proliferation of p53 wild-type osteosarcoma cell lines, but RUNX2 knockdown had no effect on cell lines with p53 mutations (van der Deen et al., 2013). Additionally, the effects of a polyamide conjugated RUNX inhibitor were tested in a panel of cancer cell lines. This RUNX inhibitor was only effective in p53 wild-type cell lines, though the mechanism underlying this result was not explored (Morita et al., 2017b). While the literature clearly indicates a relationship between RUNX signaling and p53, the directionality and functional consequences remain unclear. Further work to characterize these interactions and their diversity across cancers is needed.

4.4 Implications for targeted therapy

Despite the contradictory nature of the CBFβ/RUNX literature, it is clear that a proportion of cancers, in particular ovarian cancers, may respond to CBFβ/RUNX inhibition. Several studies have shown that CBFβ/RUNX inhibition, using a variety of inhibitors, can be efficacious in cancer and safe for use in animals (Illendula et al., 2015, 2016; Morita et al., 2017b; Oo et al., 2017). What is also clear is that there is likely a subset of cancers for which CBFβ/RUNX inhibition may be tumor promoting. Therefore, the challenge lies in determining strategies to best identify which patients and which

cancers, would benefit from treatment. The challenge of matching the correct targeted therapy with the correct patient is well described in the literature. Several clinical trials of targeted therapies have lacked clear benefit in the intended target population and proven beneficial in unexpected populations. A well-studied example of this is the efficacy of PARP inhibitors in ovarian cancer. PARP inhibition in combination with *BRCA* mutations leads to synthetic lethality of breast and ovarian cancer cells (Bryant et al., 2005). Therefore, clinical trials testing the efficacy of PARP inhibitors in women with germline *BRCA* mutations were initiated. Based on the success of PARP inhibitors in women with germline *BRCA* mutations, the use of these drugs was extended to the additional ~40% of women whose ovarian tumors had a somatic defect in DNA repair (Cancer Genome Atlas Research Network, 2011). The results of a large-scale Phase III clinical trial of PARP inhibitors showed increased progression-free survival for women with *BRCA* mutations or alterations in DNA repair, as predicted. However, not all women responded to treatment. More surprisingly, PARP inhibitors also increased progression-free survival in women lacking either genetic alteration in their tumor (Coleman et al., 2017). Several ongoing clinical trials are currently evaluating which patients may benefit most from this therapy and seeking to identify biomarkers of response.

As the studies of PARP inhibitors demonstrate, the tumor biomarkers currently used are not always accurately predicting which patients will be responsive to treatment. It is currently unclear how to determine whether or not a given tumor will be a suitable candidate for CBFβ/RUNX inhibitor treatment. Tumors with high levels of CBFβ or RUNX expression appear to be good candidates for treatment. However, the method by

which “expression” is detected will need to be refined. For example, in cBioPortal, amplification or increased mRNA expression of RUNX2 is not associated with ovarian cancer survival (Gao et al., 2013). However, studies looking at RUNX2 protein level by immunohistochemistry have come to the opposing conclusion (Li et al., 2012b). Deciding which methodology should be used to codify CBFβ /RUNX status will require further study. A second group has proposed that RUNX proteins are most oncogenic when they are expressed at moderate levels. This study posits that total RUNX levels across all three members are most correlated with oncogenicity. Due to cross-regulation of RUNX family members, moderate levels of RUNX expression lead to the fewest compensatory alterations, and therefore result in the highest total RUNX expression. Validating this hypothesis, AML patients with intermediate expression of RUNX1 had the poorest overall survival (Morita et al., 2017c). Additional work to characterize which tumors may best respond to CBFβ/RUNX inhibition will be needed before transitioning this treatment strategy to the clinic.

4.5 Future directions

4.5.1 Short-term

In these studies, we investigated the transcriptional network controlled by CBFβ using both chemical and genetic methods. Chemical inhibition of the CBFβ/RUNX protein/protein interaction caused minimal changes in gene expression, and surprisingly the RUNX TF consensus sequence was not enriched in the significantly altered genes. However, despite the lack of transcriptional changes, chemical inhibition of this interaction still produces significant alterations in cellular phenotypes. Therefore, we will

investigate the effects of CBFβ point mutations on proliferation and migration of ovarian cancer cells.

CBFβ point mutations, which alter the protein's function, will be analyzed. Four point mutations will be evaluated: G61A (reduces RUNX binding), N104A (reduces RUNX binding), G61A/N104A double mutant (almost no RUNX binding), and K111E (decreases AI-10-104 binding) (Illendula et al., 2016; Tahirov et al., 2001). OVCAR8 cells with CRISPR loss of CBFβ using sg1 will be stably infected with plasmids containing these CBFβ point mutants. The CBFβ sg1 targets the second codon of CBFβ. To make the infected mutant plasmids resistant to this guide RNA, mutations were made to the wobble codons, such that the plasmid sequence is no longer targeted by sg1. This process should generate cell lines that only express CBFβ from the plasmid.

We hope to address two questions using these cell lines. First, are cells with a drug-binding point mutation in CBFβ still responsive to AI-10-104? Second, do CBFβ mutants with diminished RUNX binding cause the same phenotypic changes as AI-10-104?

To answer this first question, the effects of AI-10-104 on OVCAR8 cellular proliferation and migration will be tested in both CBFβ-WT and CBFβ-K111E cell lines. If the effects of the AI-10-104 treatment are mediated through its binding to CBFβ, we would expect cells with the CBFβ-K111E cells to have a blunted response to compound.

To address this second question, the effects of CBFβ-WT and CBFβ-mutants on proliferation and migration will be examined in OVCAR8 cells. If the primary effects of AI-10-104 are mediated by blocking CBFβ /RUNX binding, we would predict that expression of these mutants in ovarian cancer cell lines would produce the same phenotype as compound treatment.

Second, we observed that the effects of knockdown of CBFβ differed at times from treatment with AI-10-104. This is perhaps not surprising, as whole protein loss and protein functional inhibition have key differences. To see if non-chemically mediated loss of CBFβ/RUNX binding could produce the same effects as AI-10-104 treatment,

A second outstanding question from the work characterizing AI-10-104 and AI-14-91 is what effects these compounds have on normal cells. While the effects of AI-10-104 were tested in an epithelial cell line, it did not reflect the ovarian cancer cell of origin. To address this question, the effects of inhibitor treatment should be evaluated in an immortalized fallopian tube secretory epithelial cell (FTSEC) line. As the majority of HGSOC likely originates from the fallopian tube, this cell line is the most relevant "normal" cell line use as a control. One would predict, and hope, that treatment of these cells with AI-10-104 and AI-14-91 would not affect proliferation, or do so to a much lesser degree than in HGSOC cell lines. While we predict that these cells will be less sensitive to inhibitor treatment than cancer cells, there are a few potential explanations for the alternate result. In order to generate a stable cell line culture, FTSEC cells are immortalized with the SV-40 T antigen. As this immortalization process alters p53

function, it is possible that our inhibitors would have effects on these cells, given the complex relationship between RUNX and p53 outlined above (Pipas, 2009).

4.5.2 Medium-term

One limitation of the work that has been completed to far is the moderate potency of AI-10-104 and AI-14-91. One strategy to increase potency is generation of a PROTAC compound, which leads to irreversible target degradation. The Bushweller lab is generating modified PROTAC versions of AI-14-91, and the effects of these inhibitors should be evaluated.

First, these compounds need to be verified in a FRET assay to ensure that they still bind to CBFβ. Compounds that have been validated in an *in vitro* model will subsequently be tested in cells. First, OVCAR8 cells will be treated with compounds to determine the IC_{50} by CellTiter-Glo. Next, validation of the PROTAC function of these compounds needs to be completed. Next protein expression of CBFβ will be examined by western blot after treatment of cell lines with a range of doses of compound centered at the IC_{50} at a variety of time points. The expected result of this experiment would be that at the IC_{50} for proliferation, the expression of CBFβ would be reduced.

Following these key functional validations, the effects of these new PROTAC compounds on proliferation, EdU incorporation, migration, and anchorage-independent growth will be investigated in the OVCAR4 and OVCAR8 cell lines. As discussed previously, there are some key differences between inhibitor-treated cells and cells with whole-protein knockdown of CBFβ. As treatment with PROTAC compounds will

combine both approaches, it will be interesting to determine which phenotype is most dominant. These experiments should be completed in at least two cell lines to ensure that the observed effects are more widely generalizable.

Assuming that the PROTAC compounds pass the functional and phenotypic validation outlined above, we would next propose to use these compounds as an unbiased tool to determine what, if any, other proteins our inhibitors bind to. To address this question, cells will be treated with PROTAC compounds at the appropriate dosage for the appropriate time and then total protein will be subjected to mass spectrometry analysis. The time point selected for this experiment should be as short as possible to minimize the odds of capturing confounding secondary changes in protein levels. This experiment should reveal decreased levels of CBFβ. Any other proteins that have decreased levels are candidate targets for compound binding. Validation of any additional protein targets should be completed.

In tandem, another unbiased method to determine novel protein targets, affinity chromatography, should be completed. In this method, a biotinylated version of the compound is loaded into a column. Protein lysates are then run over the column and after washing, bound proteins are eluted. These eluted proteins are then identified by mass spectrometry and are lead drug-target candidates (Lomenick et al., 2011). First, validated biotinylated versions of AI-10-104 and AI-14-91 need to be synthesized. When they are available, affinity chromatography should be conducted as a second independent method to identify alternative drug targets. The results of this analysis, and its intersection with

the PROTAC-based analysis, will provide a large body of information from which identify and characterize secondary targets of these compounds.

4.5.3 Long-term

In the long-term, it is essential that CBFβ/RUNX inhibitors with an increased half-life should be evaluated in mouse models of ovarian cancer. If the PROTAC compounds pass technical and phenotypic validation, they would be the best choice to use in these experiments. As the levels of CBFβ will be decreased irreversibly after PROTAC compound treatment, one would predict that the functional half-life of these compounds would be much greater than our previous compounds. First, the safety and basic pharmacokinetics (maximum tolerated dose and compound half-life) of these new PROTAC compounds should be evaluated to ensure they are safe to use in animals.

After determining the ideal treatment structure and dose, these compounds should be tested in an i.p. xenograft mouse model of ovarian cancer. The effects of these compounds on total tumor weight would be measured, as well as number of tumors, if feasible. If these compounds prove to be efficacious in a xenograft mouse model of ovarian cancer, extension of these findings to another model of ovarian cancer would strengthen the argument for this treatment strategy. One approach would be to test the effects of these compounds on patient-derived xenograft models of ovarian cancer. A second strategy would be to assess the effects of these compounds in a genetic model of ovarian cancer.

If PROTAC compounds are not available to test in an animal model, another approach to test the effects of CBFβ/RUNX inhibition in an animal model could be to generate mice with i.p. ovarian cancer xenografts and then treat them with AI-14-91 dosed with a continuous infusion pump. Use of the continuous infusion pump would ensure that animals maintain plasma concentrations of compound with inhibitory activity for a sustained duration of time. The effects of AI-14-91 treatment on tumor size and weight would be measured. Overall, these animal studies will provide more clinically relevant rationale for the use of CBFβ/RUNX inhibitors in ovarian cancer and guide future researchers towards the most efficacious way to integrate these inhibitors into current clinical practice.

5. References

Anders, S., and Huber, W. (2010). Differential expression analysis for sequence count data. Genome Biol. *11*, R106.

Anderson, A.E., Taniguchi, K., Hao, Y., Melhuish, T.A., Shah, A., Turner, S.D., Sutherland, A.E., and Wotton, D. (2017). Tgif1 and Tgif2 Repress Expression of the RabGAP Evi5l. Mol. Cell. Biol. *37*.

Aronson, B.D., Fisher, A.L., Blechman, K., Caudy, M., and Gergen, J.P. (1997). Groucho-dependent and -independent repression activities of Runt domain proteins. Mol. Cell. Biol. *17*, 5581–5587.

Astudillo, L., Da Silva, T.G., Wang, Z., Han, X., Jin, K., VanWye, J., Zhu, X., Weaver, K., Oashi, T., Lopes, P.E.M., et al. (2016). The small molecule IMR-1 inhibits the Notch transcriptional activation complex to suppress tumorigenesis. Cancer Res. *76*, 3593–3603.

Balduini, C.L., and Savoia, A. (2012). Genetics of familial forms of thrombocytopenia. Hum. Genet. *131*, 1821–1832.

Banerji, S., Cibulskis, K., Rangel-Escareno, C., Brown, K.K., Carter, S.L., Frederick, A.M., Lawrence, M.S., Sivachenko, A.Y., Sougnez, C., Zou, L., et al. (2012). Sequence analysis of mutations and translocations across breast cancer subtypes. Nature *486*, 405–409.

Bangsow, C., Rubins, N., Glusman, G., Bernstein, Y., Negreanu, V., Goldenberg, D., Lotem, J., Ben-Asher, E., Lancet, D., Levanon, D., et al. (2001). The RUNX3 gene--sequence, structure and regulated expression. Gene *279*, 221–232.

Baniwal, S.K., Khalid, O., Gabet, Y., Shah, R.R., Purcell, D.J., Mav, D., Kohn-Gabet, A.E., Shi, Y., Coetzee, G.A., and Frenkel, B. (2010). Runx2 transcriptome of prostate cancer cells: insights into invasiveness and bone metastasis. Mol. Cancer *9*, 258–258.

Barghout, S.H., Zepeda, N., Vincent, K., Azad, A.K., Xu, Z., Yang, C., Steed, H., Postovit, L.-M., and Fu, Y. (2015). RUNX3 contributes to carboplatin resistance in epithelial ovarian cancer cells. Gynecol. Oncol. *138*, 647–655.

Behbakht, K., Sill, M.W., Darcy, K.M., Rubin, S.C., Mannel, R.S., Waggoner, S., Schilder, R.J., Cai, K.Q., Godwin, A.K., and Alpaugh, R.K. (2011). Phase II trial of the mTOR inhibitor, temsirolimus and evaluation of circulating tumor cells and tumor biomarkers in persistent and recurrent epithelial ovarian and primary peritoneal malignancies: a Gynecologic Oncology Group study. Gynecol. Oncol. *123*, 19–26.

Beral, V., Doll, R., Hermon, C., Peto, R., and Reeves, G. (2008). Ovarian cancer and oral contraceptives: collaborative reanalysis of data from 45 epidemiological studies including 23,257 women with ovarian cancer and 87,303 controls. Lancet Lond. Engl. *371*, 303–314.

Bernardin-Fried, F., Kummalue, T., Leijen, S., Collector, M.I., Ravid, K., and Friedman, A.D. (2004). AML1/RUNX1 Increases During G1 to S Cell Cycle Progression Independent of Cytokine-dependent Phosphorylation and Induces Cyclin D3 Gene Expression. J. Biol. Chem. *279*, 15678–15687.

Bhojwani, D., Pei, D., Sandlund, J.T., Jeha, S., Ribeiro, R.C., Rubnitz, J.E., Raimondi, S.C., Shurtleff, S., Onciu, M., Cheng, C., et al. (2012). *ETV6-RUNX1*-positive childhood acute lymphoblastic leukemia: improved outcome with contemporary therapy. Leukemia *26*, 265–270.

Biggs, J.R., Peterson, L.F., Zhang, Y., Kraft, A.S., and Zhang, D.-E. (2006). AML1/RUNX1 phosphorylation by cyclin-dependent kinases regulates the degradation of AML1/RUNX1 by the anaphase-promoting complex. Mol. Cell. Biol. *26*, 7420–7429.

Blanke, C.D., Rankin, C., Demetri, G.D., Ryan, C.W., von Mehren, M., Benjamin, R.S., Raymond, A.K., Bramwell, V.H.C., Baker, L.H., Maki, R.G., et al. (2008). Phase III randomized, intergroup trial assessing imatinib mesylate at two dose levels in patients with unresectable or metastatic gastrointestinal stromal tumors expressing the kit receptor tyrosine kinase: S0033. J. Clin. Oncol. Off. J. Am. Soc. Clin. Oncol. *26*, 626–632.

Bodelon, C., Wentzensen, N., Schonfeld, S.J., Visvanathan, K., Hartge, P., Park, Y., and Pfeiffer, R.M. (2013). Hormonal risk factors and invasive epithelial ovarian cancer risk by parity. Br. J. Cancer *109*, 769–776.

du Bois, A., Floquet, A., Kim, J.-W., Rau, J., del Campo, J.M., Friedlander, M., Pignata, S., Fujiwara, K., Vergote, I., Colombo, N., et al. (2014). Incorporation of Pazopanib in Maintenance Therapy of Ovarian Cancer. J. Clin. Oncol. *32*, 3374–3382.

du Bois, A., Kristensen, G., Ray-Coquard, I., Reuss, A., Pignata, S., Colombo, N., Denison, U., Vergote, I., Del Campo, J.M., Ottevanger, P., et al. (2016). Standard first-line chemotherapy with or without nintedanib for advanced ovarian cancer (AGO-OVAR 12): a randomised, double-blind, placebo-controlled phase 3 trial. Lancet Oncol. *17*, 78–89.

Bondeson, D.P., Mares, A., Smith, I.E.D., Ko, E., Campos, S., Miah, A.H., Mulholland, K.E., Routly, N., Buckley, D.L., Gustafson, J.L., et al. (2015). Catalytic in vivo protein knockdown by small-molecule PROTACs. Nat. Chem. Biol. *11*, 611–617.

Bowtell, D.D.L. (2010). The genesis and evolution of high-grade serous ovarian cancer. Nat. Rev. Cancer *10*, 803–808.

Bowtell, D.D., Böhm, S., Ahmed, A.A., Aspuria, P.-J., Bast Jr, R.C., Beral, V., Berek, J.S., Birrer, M.J., Blagden, S., Bookman, M.A., et al. (2015). Rethinking ovarian cancer II: reducing mortality from high-grade serous ovarian cancer. Nat. Rev. Cancer *15*, 668–679.

Bragt, M.P. van, Hu, X., Xie, Y., and Li, Z. (2014). RUNX1, a transcription factor mutated in breast cancer, controls the fate of ER-positive mammary luminal cells. ELife *3*, e03881.

Brenner, O., Levanon, D., Negreanu, V., Golubkov, O., Fainaru, O., Woolf, E., and Groner, Y. (2004). Loss of Runx3 function in leukocytes is associated with spontaneously developed colitis and gastric mucosal hyperplasia. Proc. Natl. Acad. Sci. U. S. A. *101*, 16016–16021.

Brose, M.S. (2002). Cancer Risk Estimates for BRCA1 Mutation Carriers Identified in a Risk Evaluation Program. CancerSpectrum Knowl. Environ. *94*, 1365–1372.

Browne, G., Taipaleenmäki, H., Bishop, N.M., Madasu, S.C., Shaw, L.M., van Wijnen, A.J., Stein, J.L., Stein, G.S., and Lian, J.B. (2015). Runx1 is associated with breast cancer progression in MMTV-PyMT transgenic mice and its depletion in vitro inhibits migration and invasion. J. Cell. Physiol.

Bruin, A. de, Maiti, B., Jakoi, L., Timmers, C., Buerki, R., and Leone, G. (2003). Identification and Characterization of E2F7, a Novel Mammalian E2F Family Member Capable of Blocking Cellular Proliferation. J. Biol. Chem. *278*, 42041–42049.

Brusgard, J.L., Choe, M., Chumsri, S., Renoud, K., MacKerell, A.D., Sudol, M., and Passaniti, A. (2015). RUNX2 and TAZ-dependent signaling pathways regulate soluble E-Cadherin levels and tumorsphere formation in breast cancer cells. Oncotarget *6*, 28132–28150.

Bryant, H.E., Schultz, N., Thomas, H.D., Parker, K.M., Flower, D., Lopez, E., Kyle, S., Meuth, M., Curtin, N.J., and Helleday, T. (2005). Specific killing of BRCA2-deficient tumours with inhibitors of poly(ADP-ribose) polymerase. Nature *434*, 913–917.

Burgess, A., Chia, K.M., Haupt, S., Thomas, D., Haupt, Y., and Lim, E. (2016). Clinical Overview of MDM2/X-Targeted Therapies. Front. Oncol. *6*.

Cancer Genome Atlas Research Network (2011). Integrated genomic analyses of ovarian carcinoma. Nature *474*, 609–615.

Cannistra, S.A., Matulonis, U.A., Penson, R.T., Hambleton, J., Dupont, J., Mackey, H., Douglas, J., Burger, R.A., Armstrong, D., Wenham, R., et al. (2007). Phase II study of bevacizumab in patients with platinum-resistant ovarian cancer or peritoneal serous cancer. J. Clin. Oncol. Off. J. Am. Soc. Clin. Oncol. *25*, 5180–5186.

Carcangiu, M.L., Peissel, B., Pasini, B., Spatti, G., Radice, P., and Manoukian, S. (2006). Incidental carcinomas in prophylactic specimens in BRCA1 and BRCA2 germ-line mutation carriers, with emphasis on fallopian tube lesions: report of 6 cases and review of the literature. Am. J. Surg. Pathol. *30*, 1222–1230.

Carlton, A.L., Illendula, A., Gao, Y., Llaneza, D.C., Boulton, A., Shah, A., Rajewski, R.A., Landen, C.N., Wotton, D., and Bushweller, J.H. (2018). Small molecule inhibition

of the CBFβ/RUNX interaction decreases ovarian cancer growth and migration through alterations in genes related to epithelial-to-mesenchymal transition. Gynecol. Oncol.

Chang, C.-H., Fan, T.-C., Yu, J.-C., Liao, G.-S., Lin, Y.-C., Shih, A.C.-C., Li, W.-H., and Yu, A.L.-T. (2014). The prognostic significance of RUNX2 and miR-10a/10b and their inter-relationship in breast cancer. J. Transl. Med. *12*.

Chapman, P.B., Hauschild, A., Robert, C., Haanen, J.B., Ascierto, P., Larkin, J., Dummer, R., Garbe, C., Testori, A., Maio, M., et al. (2011). Improved survival with vemurafenib in melanoma with BRAF V600E mutation. N. Engl. J. Med. *364*, 2507–2516.

Chen, S., and Parmigiani, G. (2007). Meta-analysis of BRCA1 and BRCA2 penetrance. J. Clin. Oncol. Off. J. Am. Soc. Clin. Oncol. *25*, 1329–1333.

Chen, E.Y., Tan, C.M., Kou, Y., Duan, Q., Wang, Z., Meirelles, G.V., Clark, N.R., and Ma'ayan, A. (2013). Enrichr: interactive and collaborative HTML5 gene list enrichment analysis tool. BMC Bioinformatics *14*, 128.

Chen, X., Chen, Z., Yu, S., Nie, F., Yan, S., Ma, P., Chen, Q., Wei, C., Fu, H., Xu, T., et al. (2018). Long noncoding RNA LINC01234 functions as a competing endogenous RNA to regulate CBFB expression by sponging miR-204-5p in gastric cancer. Clin. Cancer Res. clincanres.2376.2017.

Chikarmane, S.A., Khurana, B., Krajewski, K.M., Shinagare, A.B., Howard, S., Sodickson, A., Jagannathan, J., and Ramaiya, N. (2012). What the emergency radiologist needs to know about treatment-related complications from conventional chemotherapy and newer molecular targeted agents. Emerg. Radiol. *19*, 535–546.

Chimge, N.-O., Baniwal, S.K., Little, G.H., Chen, Y., Kahn, M., Tripathy, D., Borok, Z., and Frenkel, B. (2011). Regulation of breast cancer metastasis by Runx2 and estrogen signaling: the role of SNAI2. Breast Cancer Res. *13*, R127.

Choi, Ah., Illendula, A., Pulikkan, J.A., Roderick, J.E., Tesell, J., Yu, J., Hermance, N., Zhu, L.J., Castilla, L.H., Bushweller, J.H., et al. (2017). RUNX1 is required for oncogenic Myb and Myc enhancer activity in T-cell acute lymphoblastic leukemia. Blood *130*, 1722–1733.

Chua, C.-W., Chiu, Y.-T., Yuen, H.-F., Chan, K.-W., Man, K., Wang, X., Ling, M.-T., and Wong, Y.-C. (2009). Suppression of androgen-independent prostate cancer cell aggressiveness by FTY720: validating Runx2 as a potential antimetastatic drug screening platform. Clin. Cancer Res. Off. J. Am. Assoc. Cancer Res. *15*, 4322–4335.

Chuang, L.S.H., Ito, K., and Ito, Y. (2013). RUNX family: Regulation and diversification of roles through interacting proteins. Int. J. Cancer J. Int. Cancer *132*, 1260–1271.

Chuang, L.S.H., Ito, K., and Ito, Y. (2017). Roles of RUNX in Solid Tumors. In RUNX Proteins in Development and Cancer, (Springer, Singapore), pp. 299–320.

Ciriello, G., Gatza, M.L., Beck, A.H., Wilkerson, M.D., Rhie, S.K., Pastore, A., Zhang, H., McLellan, M., Yau, C., Kandoth, C., et al. (2015). Comprehensive Molecular Portraits of Invasive Lobular Breast Cancer. Cell *163*, 506–519.

Coleman, R.L., Oza, A.M., Lorusso, D., Aghajanian, C., Oaknin, A., Dean, A., Colombo, N., Weberpals, J.I., Clamp, A., Scambia, G., et al. (2017). Rucaparib maintenance treatment for recurrent ovarian carcinoma after response to platinum therapy (ARIEL3): a randomised, double-blind, placebo-controlled, phase 3 trial. The Lancet *390*, 1949–1961.

Conway, E., Healy, E., and Bracken, A.P. (2015). PRC2 mediated H3K27 methylations in cellular identity and cancer. Curr. Opin. Cell Biol. *37*, 42–48.

Cortez, A.J., Tudrej, P., Kujawa, K.A., and Lisowska, K.M. (2018). Advances in ovarian cancer therapy. Cancer Chemother. Pharmacol. *81*, 17–38.

Crijnen, T.E.M., Janssen-Heijnen, M.L.G., Gelderblom, H., Morreau, J., Nooij, M.A., Kenter, G.G., and Vasen, H.F.A. (2005). Survival of patients with ovarian cancer due to a mismatch repair defect. Fam. Cancer *4*, 301–305.

Cunningham, L., Finckbeiner, S., Hyde, R.K., Southall, N., Marugan, J., Yedavalli, V.R.K., Dehdashti, S.J., Reinhold, W.C., Alemu, L., Zhao, L., et al. (2012). Identification of benzodiazepine Ro5-3335 as an inhibitor of CBF leukemia through quantitative high throughput screen against RUNX1-CBFβ interaction. Proc. Natl. Acad. Sci. U. S. A. *109*, 14592–14597.

Davis, J.N., Rogers, D., Adams, L., Yong, T., Jung, J.S., Cheng, B., Fennell, K., Borazanci, E., Moustafa, Y.W., Sun, A., et al. (2010). Association of core-binding factor β with the malignant phenotype of prostate and ovarian cancer cells. J. Cell. Physiol. *225*, 875–887.

Dean, M., Davis, D.A., and Burdette, J.E. (2017). Activin A stimulates migration of the fallopian tube epithelium, an origin of high-grade serous ovarian cancer, through non-canonical signaling. Cancer Lett. *391*, 114–124.

van der Deen, M., Akech, J., Wang, T., FitzGerald, T.J., Altieri, D.C., Languino, L.R., Lian, J.B., van Wijnen, A.J., Stein, J.L., and Stein, G.S. (2010). The cancer-related Runx2 protein enhances cell growth and responses to androgen and TGFbeta in prostate cancer cells. J. Cell. Biochem. *109*, 828–837.

van der Deen, M., Akech, J., Lapointe, D., Gupta, S., Young, D.W., Montecino, M.A., Galindo, M., Lian, J.B., Stein, J.L., Stein, G.S., et al. (2012). Genomic promoter occupancy of runt-related transcription factor RUNX2 in Osteosarcoma cells identifies genes involved in cell adhesion and motility. J. Biol. Chem. *287*, 4503–4517.

van der Deen, M., Taipaleenmäki, H., Zhang, Y., Teplyuk, N.M., Gupta, A., Cinghu, S., Shogren, K., Maran, A., Yaszemski, M.J., Ling, L., et al. (2013). MicroRNA-34c inversely couples the biological functions of the runt-related transcription factor RUNX2 and the tumor suppressor p53 in osteosarcoma. J. Biol. Chem. *288*, 21307–21319.

Domcke, S., Sinha, R., and Levine, D. (2013). Evaluating cell lines as tumour models by comparison of genomic profiles. Nat. … *4*, 2126–2126.

Ducie, J., Dao, F., Considine, M., Olvera, N., Shaw, P.A., Kurman, R.J., Shih, I.-M., Soslow, R.A., Cope, L., and Levine, D.A. (2017). Molecular analysis of high-grade serous ovarian carcinoma with and without associated serous tubal intra-epithelial carcinoma. Nat. Commun. *8*, 990.

Estécio, M.R.H., Maddipoti, S., Bueso-Ramos, C., DiNardo, C.D., Yang, H., Wei, Y., Kondo, K., Fang, Z., Stevenson, W., Chang, K.-S., et al. (2015). RUNX3 promoter hypermethylation is frequent in leukaemia cell lines and associated with acute myeloid leukaemia inv(16) subtype. Br. J. Haematol. *169*, 344–351.

Falconer, H., Yin, L., Grönberg, H., and Altman, D. (2015). Ovarian cancer risk after salpingectomy: a nationwide population-based study. J. Natl. Cancer Inst. *107*.

Farmer, H., McCabe, N., Lord, C.J., Tutt, A.N.J., Johnson, D.A., Richardson, T.B., Santarosa, M., Dillon, K.J., Hickson, I., Knights, C., et al. (2005). Targeting the DNA repair defect in BRCA mutant cells as a therapeutic strategy. Nature *434*, 917–921.

Ferrari, N., Mohammed, Z.M.A., Nixon, C., Mason, S.M., Mallon, E., McMillan, D.C., Morris, J.S., Cameron, E.R., Edwards, J., and Blyth, K. (2014). Expression of RUNX1 correlates with poor patient prognosis in triple negative breast cancer. PloS One *9*, e100759–e100759.

Fitzgerald, K., White, S., Borodovsky, A., Bettencourt, B.R., Strahs, A., Clausen, V., Wijngaard, P., Horton, J.D., Taubel, J., Brooks, A., et al. (2017). A Highly Durable RNAi Therapeutic Inhibitor of PCSK9. N. Engl. J. Med. *376*, 41–51.

Frank-Kamenetsky, M., Grefhorst, A., Anderson, N.N., Racie, T.S., Bramlage, B., Akinc, A., Butler, D., Charisse, K., Dorkin, R., Fan, Y., et al. (2008). Therapeutic RNAi targeting PCSK9 acutely lowers plasma cholesterol in rodents and LDL cholesterol in nonhuman primates. Proc. Natl. Acad. Sci. U. S. A. *105*, 11915–11920.

Friedlander, M., Hancock, K.C., Rischin, D., Messing, M.J., Stringer, C.A., Matthys, G.M., Ma, B., Hodge, J.P., and Lager, J.J. (2010). A Phase II, open-label study evaluating pazopanib in patients with recurrent ovarian cancer. Gynecol. Oncol. *119*, 32–37.

Galindo, M., Pratap, J., Young, D.W., Hovhannisyan, H., Im, H.-J., Choi, J.-Y., Lian, J.B., Stein, J.L., Stein, G.S., and van Wijnen, A.J. (2005). The bone-specific expression of Runx2 oscillates during the cell cycle to support a G1-related antiproliferative function in osteoblasts. J. Biol. Chem. *280*, 20274–20285.

Gambacorti-Passerini, C., Antolini, L., Mahon, F.-X., Guilhot, F., Deininger, M., Fava, C., Nagler, A., Della Casa, C.M., Morra, E., Abruzzese, E., et al. (2011). Multicenter independent assessment of outcomes in chronic myeloid leukemia patients treated with imatinib. J. Natl. Cancer Inst. *103*, 553–561.

Gao, J., Aksoy, B.A., Dogrusoz, U., Dresdner, G., Gross, B., Sumer, S.O., Sun, Y., Jacobsen, A., Sinha, R., Larsson, E., et al. (2013). Integrative analysis of complex cancer genomics and clinical profiles using the cBioPortal. Sci. Signal. *6*, pl1–pl1.

Gates, M.A., Rosner, B.A., Hecht, J.L., and Tworoger, S.S. (2010). Risk factors for epithelial ovarian cancer by histologic subtype. Am. J. Epidemiol. *171*, 45–53.

Ge, C., Zhao, G., Li, Y., Li, H., Zhao, X., Pannone, G., Bufo, P., Santoro, A., Sanguedolce, F., Tortorella, S., et al. (2015). Role of Runx2 phosphorylation in prostate cancer and association with metastatic disease. Oncogene.

Ge, T., Yin, M., Yang, M., Liu, T., and Lou, G. (2014). MicroRNA-302b Suppresses Human Epithelial Ovarian Cancer Cell Growth by Targeting RUNX1. Cell. Physiol. Biochem. *34*, 2209–2220.

Ghozi, M.C., Bernstein, Y., Negreanu, V., Levanon, D., and Groner, Y. (1996). Expression of the human acute myeloid leukemia gene AML1 is regulated by two promoter regions. Proc. Natl. Acad. Sci. U. S. A. *93*, 1935–1940.

Greer, A.H., Yong, T., Fennell, K., Moustafa, Y.W., Fowler, M., Galiano, F., Ng, S.-W., Berkowitz, R.S., Cardelli, J., Meyers, S., et al. (2013). Knockdown of core binding factorβ alters sphingolipid metabolism. J. Cell. Physiol. *228*, 2350–2364.

Grimwade, D., Hills, R.K., Moorman, A.V., Walker, H., Chatters, S., Goldstone, A.H., Wheatley, K., Harrison, C.J., and Burnett, A.K. (2010). Refinement of cytogenetic classification in acute myeloid leukemia: determination of prognostic significance of rare recurring chromosomal abnormalities among 5876 younger adult patients treated in the United Kingdom Medical Research Council trials. Blood *116*, 354–365.

Gross, S., Rahal, R., Stransky, N., Lengauer, C., and Hoeflich, K.P. (2015). Targeting cancer with kinase inhibitors. J. Clin. Invest. *125*, 1780–1789.

Gu, T.-L., Goetz, T.L., Graves, B.J., and Speck, N.A. (2000). Auto-Inhibition and Partner Proteins, Core-Binding Factor β (CBFβ) and Ets-1, Modulate DNA Binding by CBFα2 (AML1). Mol. Cell. Biol. *20*, 91–103.

Han, S., Zhu, J., and Zhang, Y. (2018). miR-144 Potentially Suppresses Proliferation and Migration of Ovarian Cancer Cells by Targeting RUNX1. Med. Sci. Monit. Basic Res. *24*, 40–46.

Hanahan, D., and Weinberg, R.A. (2011). Hallmarks of Cancer: The Next Generation. Cell *144*, 646–674.

He, Y., Meng, C., Shao, Z., Wang, H., and Yang, S. (2014). MiR-23a Functions as a Tumor Suppressor in Osteosarcoma. Cell. Physiol. Biochem. *34*, 1485–1496.

Hendzel, M.J., Wei, Y., Mancini, M.A., Van Hooser, A., Ranalli, T., Brinkley, B.R., Bazett-Jones, D.P., and Allis, C.D. (1997). Mitosis-specific phosphorylation of histone

H3 initiates primarily within pericentromeric heterochromatin during G2 and spreads in an ordered fashion coincident with mitotic chromosome condensation. Chromosoma *106*, 348–360.

Henrich, K.-O., Schwab, M., and Westermann, F. (2012). 1p36 tumor suppression--a matter of dosage? Cancer Res. *72*, 6079–6088.

Hoi, C.S.L., Lee, S.E., Lu, S.-Y., McDermitt, D.J., Osorio, K.M., Piskun, C.M., Peters, R.M., Paus, R., and Tumbar, T. (2010). Runx1 directly promotes proliferation of hair follicle stem cells and epithelial tumor formation in mouse skin. Mol. Cell. Biol. *30*, 2518–2536.

Hong, D., Messier, T.L., Tye, C.E., Dobson, J.R., Fritz, A.J., Sikora, K.R., Browne, G., Stein, J.L., Lian, J.B., and Stein, G.S. (2017). Runx1 stabilizes the mammary epithelial cell phenotype and prevents epithelial to mesenchymal transition. Oncotarget *8*, 17610–17627.

Illendula, A., Pulikkan, J.A., Zong, H., Grembecka, J., Xue, L., Sen, S., Zhou, Y., Boulton, A., Kuntimaddi, A., Gao, Y., et al. (2015). A small-molecule inhibitor of the aberrant transcription factor CBF -SMMHC delays leukemia in mice. Science *347*, 779–784.

Illendula, A., Gilmour, J., Grembecka, J., Tirumala, V.S.S., Boulton, A., Kuntimaddi, A., Schmidt, C., Wang, L., Pulikkan, J.A., Zong, H., et al. (2016). Small Molecule Inhibitor of CBFβ-RUNX Binding for RUNX Transcription Factor Driven Cancers. EBioMedicine *8*, 117–131.

Imming, P., Sinning, C., and Meyer, A. (2006). Drugs, their targets and the nature and number of drug targets. Nat. Rev. Drug Discov. *5*, 821–834.

Ito, Y., Bae, S.-C., and Chuang, L.S.H. (2015). The RUNX family: developmental regulators in cancer. Nat. Rev. Cancer *15*, 81–95.

Jamil, A., Theil, K.S., Kahwash, S., Ruymann, F.B., and Klopfenstein, K.J. (2000). TEL/AML-1 fusion gene. its frequency and prognostic significance in childhood acute lymphoblastic leukemia. Cancer Genet. Cytogenet. *122*, 73–78.

Jaruga, A., Hordyjewska, E., Kandzierski, G., and Tylzanowski, P. (2016). Cleidocranial dysplasia and RUNX2-clinical phenotype–genotype correlation. Clin. Genet. *90*, 393–402.

Jeselsohn, R., Cornwell, M., Pun, M., Buchwalter, G., Nguyen, M., Bango, C., Huang, Y., Kuang, Y., Paweletz, C., Fu, X., et al. (2017). Embryonic transcription factor SOX9 drives breast cancer endocrine resistance. Proc. Natl. Acad. Sci. U. S. A. *114*, E4482–E4491.

Jiang, Y., Tong, D., Lou, G., Zhang, Y., and Geng, J. (2008). Expression of RUNX3 gene, methylation status and clinicopathological significance in breast cancer and breast cancer cell lines. Pathobiol. J. Immunopathol. Mol. Cell. Biol. *75*, 244–251.

Jiang, Y., Deng, Q., Zhao, H., Xie, M., Chen, L., Yin, F., Qin, X., Zheng, W., Zhao, Y., and Li, Z. (2018). Development of Stabilized Peptide-Based PROTACs against Estrogen Receptor α. ACS Chem. Biol.

Johnson, K., Zhu, S., Tremblay, M.S., Payette, J.N., Wang, J., Bouchez, L.C., Meeusen, S., Althage, A., Cho, C.Y., Wu, X., et al. (2012). A Stem Cell–Based Approach to Cartilage Repair. Science *336*.

Kalli, K.R., Oberg, A.L., Keeney, G.L., Christianson, T.J.H., Low, P.S., Knutson, K.L., and Hartmann, L.C. (2008). Folate receptor alpha as a tumor target in epithelial ovarian cancer. Gynecol. Oncol. *108*, 619–626.

Kamachi, Y., Ogawa, E., Asano, M., Ishida, S., Murakami, Y., Satake, M., Ito, Y., and Shigesada, K. (1990). Purification of a mouse nuclear factor that binds to both the A and B cores of the polyomavirus enhancer. J. Virol. *64*, 4808–4819.

Kandoth, C., McLellan, M.D., Vandin, F., Ye, K., Niu, B., Lu, C., Xie, M., Zhang, Q., McMichael, J.F., Wyczalkowski, M.A., et al. (2013). Mutational landscape and significance across 12 major cancer types. Nature *502*, 333–339.

Keita, M., Bachvarova, M., Morin, C., Plante, M., Gregoire, J., Renaud, M.-C., Sebastianelli, A., Trinh, X.B., and Bachvarov, D. (2013). The RUNX1 transcription factor is expressed in serous epithelial ovarian carcinoma and contributes to cell proliferation, migration and invasion. Cell Cycle Georget. Tex *12*, 972–986.

Kihara, R., Nagata, Y., Kiyoi, H., Kato, T., Yamamoto, E., Suzuki, K., Chen, F., Asou, N., Ohtake, S., Miyawaki, S., et al. (2014). Comprehensive analysis of genetic alterations and their prognostic impacts in adult acute myeloid leukemia patients. Leukemia *28*, 1586–1595.

Kim, D., Langmead, B., and Salzberg, S.L. (2015). HISAT: a fast spliced aligner with low memory requirements. Nat. Methods *12*, 357–360.

Kim, J., Coffey, D.M., Creighton, C.J., Yu, Z., Hawkins, S.M., and Matzuk, M.M. (2012). High-grade serous ovarian cancer arises from fallopian tube in a mouse model. Proc. Natl. Acad. Sci. U. S. A. *109*, 3921–3926.

Kim, M.S., Gernapudi, R., Choi, E.Y., Lapidus, R.G., and Passaniti, A. (2017). Characterization of CADD522, a small molecule that inhibits RUNX2-DNA binding and exhibits antitumor activity. Oncotarget *8*, 70916–70940.

Kim, T.Y., Lee, H.J., Hwang, K.S., Lee, M., Kim, J.W., Bang, Y.-J., and Kang, G.H. (2004). Methylation of RUNX3 in various types of human cancers and premalignant stages of gastric carcinoma. Lab. Investig. J. Tech. Methods Pathol. *84*, 479–484.

Kim, W.-J., Kim, E.-J., Jeong, P., Quan, C., Kim, J., Li, Q.-L., Yang, J.-O., Ito, Y., and Bae, S.-C. (2005). RUNX3 inactivation by point mutations and aberrant DNA methylation in bladder tumors. Cancer Res. *65*, 9347–9354.

Komori, T., Yagi, H., Nomura, S., Yamaguchi, A., Sasaki, K., Deguchi, K., Shimizu, Y., Bronson, R.., Gao, Y.-H., Inada, M., et al. (1997). Targeted Disruption of Cbfa1 Results in a Complete Lack of Bone Formation owing to Maturational Arrest of Osteoblasts. Cell *89*, 755–764.

Kong, D.-H., Kim, M.R., Jang, J.H., Na, H.-J., and Lee, S. (2017). A Review of Anti-Angiogenic Targets for Monoclonal Antibody Cancer Therapy. Int. J. Mol. Sci. *18*, 1786.

Kuang, Y., Lu, F., Guo, J., Xu, H., Wang, Q., Xu, C., Zeng, L., and Yi, S. (2017). Histone demethylase KDM2B upregulates histone methyltransferase EZH2 expression and contributes to the progression of ovarian cancer in vitro and in vivo. OncoTargets Ther. *Volume 10*, 3131–3144.

Kuhn, E., Kurman, R.J., Vang, R., Sehdev, A.S., Han, G., Soslow, R., Wang, T.-L., and Shih, I.-M. (2012). TP53 mutations in serous tubal intraepithelial carcinoma and concurrent pelvic high-grade serous carcinoma--evidence supporting the clonal relationship of the two lesions. J. Pathol. *226*, 421–426.

Kuleshov, M.V., Jones, M.R., Rouillard, A.D., Fernandez, N.F., Duan, Q., Wang, Z., Koplev, S., Jenkins, S.L., Jagodnik, K.M., Lachmann, A., et al. (2016). Enrichr: a comprehensive gene set enrichment analysis web server 2016 update. Nucleic Acids Res. *44*, W90-97.

Kumar, V.A., Abul; Aster, Jon C. (2013). Robbins Basic Pathology (Philadelphia: Elsevier Inc.).

Kuo, K.-T., Mao, T.-L., Jones, S., Veras, E., Ayhan, A., Wang, T.-L., Glas, R., Slamon, D., Velculescu, V.E., Kuman, R.J., et al. (2009). Frequent activating mutations of PIK3CA in ovarian clear cell carcinoma. Am. J. Pathol. *174*, 1597–1601.

Kurman, R.J., and Shih, I.-M. (2010). The origin and pathogenesis of epithelial ovarian cancer: a proposed unifying theory. Am. J. Surg. Pathol. *34*, 433–443.

Kurman, R.J., and Shih, I.-M. (2016). The Dualistic Model of Ovarian Carcinogenesis: Revisited, Revised, and Expanded. Am. J. Pathol. *186*, 733–747.

Kyrgiou, M., Salanti, G., Pavlidis, N., Paraskevaidis, E., and Ioannidis, J.P.A. (2006). Survival benefits with diverse chemotherapy regimens for ovarian cancer: meta-analysis of multiple treatments. J. Natl. Cancer Inst. *98*, 1655–1663.

Lai, A.C., and Crews, C.M. (2017). Induced protein degradation: an emerging drug discovery paradigm. Nat. Rev. Drug Discov. *16*, 101–114.

Lambertini, E., Franceschetti, T., Torreggiani, E., Penolazzi, L., Pastore, A., Pelucchi, S., Gambari, R., and Piva, R. (2010). SLUG: a new target of lymphoid enhancer factor-1 in human osteoblasts. BMC Mol. Biol. *11*, 13.

Lamouille, S., Xu, J., and Derynck, R. (2014). Molecular mechanisms of epithelial-mesenchymal transition. Nat. Rev. Mol. Cell Biol. *15*, 178–196.

Lange, M., Kasper, B., Bohring, A., Rutsch, F., Kluger, G., Hoffjan, S., Spranger, S., Behnecke, A., Ferbert, A., Hahn, A., et al. (2015). 47 patients with FLNA associated periventricular nodular heterotopia. Orphanet J. Rare Dis. *10*, 134.

Lau, Q.C., Raja, E., Salto-Tellez, M., Liu, Q., Ito, K., Inoue, M., Putti, T.C., Loh, M., Ko, T.K., Huang, C., et al. (2006). RUNX3 is frequently inactivated by dual mechanisms of protein mislocalization and promoter hypermethylation in breast cancer. Cancer Res. *66*, 6512–6520.

Ledermann, J.A., Hackshaw, A., Kaye, S., Jayson, G., Gabra, H., McNeish, I., Earl, H., Perren, T., Gore, M., Persic, M., et al. (2011). Randomized phase II placebo-controlled trial of maintenance therapy using the oral triple angiokinase inhibitor BIBF 1120 after chemotherapy for relapsed ovarian cancer. J. Clin. Oncol. Off. J. Am. Soc. Clin. Oncol. *29*, 3798–3804.

Lee, C.W.L., Chuang, L.S.H., Kimura, S., Lai, S.K., Ong, C.W., Yan, B., Salto-Tellez, M., Choolani, M., and Ito, Y. (2011). RUNX3 functions as an oncogene in ovarian cancer. Gynecol. Oncol. *122*, 410–417.

Lee, Y., Miron, A., Drapkin, R., Nucci, M.R., Medeiros, F., Saleemuddin, A., Garber, J., Birch, C., Mou, H., Gordon, R.W., et al. (2007). A candidate precursor to serous carcinoma that originates in the distal fallopian tube. J. Pathol. *211*, 26–35.

Lefebvre, C., Bachelot, T., Filleron, T., Pedrero, M., Campone, M., Soria, J.-C., Massard, C., Lévy, C., Arnedos, M., Lacroix-Triki, M., et al. (2016). Mutational Profile of Metastatic Breast Cancers: A Retrospective Analysis. PLoS Med. *13*, e1002201.

Levanon, D., Bettoun, D., Harris-Cerruti, C., Woolf, E., Negreanu, V., Eilam, R., Bernstein, Y., Goldenberg, D., Xiao, C., Fliegauf, M., et al. (2002). The Runx3 transcription factor regulates development and survival of TrkC dorsal root ganglia neurons. EMBO J. *21*, 3454–3463.

Li, H., Handsaker, B., Wysoker, A., Fennell, T., Ruan, J., Homer, N., Marth, G., Abecasis, G., Durbin, R., and 1000 Genome Project Data Processing Subgroup (2009). The Sequence Alignment/Map format and SAMtools. Bioinforma. Oxf. Engl. *25*, 2078–2079.

Li, H., Cai, Q., Wu, H., Vathipadiekal, V., Dobbin, Z.C., Li, T., Hua, X., Landen, C.N., Birrer, M.J., Sánchez-Beato, M., et al. (2012a). SUZ12 Promotes Human Epithelial Ovarian Cancer by Suppressing Apoptosis via Silencing HRK. Mol. Cancer Res. *10*, 1462–1472.

Li, H., Xu, Y., Qiu, W., Zhao, D., and Zhang, Y. (2015a). Tissue miR-193b as a Novel Biomarker for Patients with Ovarian Cancer. Med. Sci. Monit. Int. Med. J. Exp. Clin. Res. *21*, 3929–3934.

Li, N., Wang, L., Tan, G., Guo, Z., Liu, L., Yang, M., and He, J. (2017). MicroRNA-218 inhibits proliferation and invasion in ovarian cancer by targeting Runx2. Oncotarget *8*, 91530–91541.

Li, W., Xu, S., Lin, S., and Zhao, W. (2012b). Overexpression of runt-related transcription factor-2 is associated with advanced tumor progression and poor prognosis in epithelial ovarian cancer. J. Biomed. Biotechnol. *2012*, 456534.

Li, W., Liu, Z., Chen, L., Zhou, L., and Yao, Y. (2014). MicroRNA-23b is an independent prognostic marker and suppresses ovarian cancer progression by targeting runt-related transcription factor-2. FEBS Lett. *588*, 1608–1615.

Li, X.-Q., Du, X., Li, D.-M., Kong, P.-Z., Sun, Y., Liu, P.-F., Wang, Q.-S., and Feng, Y.-M. (2015b). ITGBL1 is a Runx2 Transcriptional Target and Promotes Breast Cancer Bone Metastasis by Activating the TGF-β Signaling Pathway. Cancer Res. *75*, 3302–3313.

Li, X.-Q., Lu, J.-T., Tan, C.-C., Wang, Q.-S., and Feng, Y.-M. (2016). RUNX2 promotes breast cancer bone metastasis by increasing integrin α5-mediated colonization. Cancer Lett. *380*, 78–86.

Lian, G., Kanaujia, S., Wong, T., and Sheen, V. (2017). FilaminA and Formin2 regulate skeletal, muscular, and intestinal formation through mesenchymal progenitor proliferation. PLOS ONE *12*, e0189285.

Liao, Y., Smyth, G.K., and Shi, W. (2014). featureCounts: an efficient general purpose program for assigning sequence reads to genomic features. Bioinforma. Oxf. Engl. *30*, 923–930.

Little, G.H., Noushmehr, H., Baniwal, S.K., Berman, B.P., Coetzee, G.A., and Frenkel, B. (2012). Genome-wide Runx2 occupancy in prostate cancer cells suggests a role in regulating secretion. Nucleic Acids Res. *40*, 3538–3547.

Little, G.H., Baniwal, S.K., Adisetiyo, H., Groshen, S., Chimge, N.-O., Kim, S.Y., Khalid, O., Hawes, D., Jones, J.O., Pinski, J., et al. (2014). Differential effects of RUNX2 on the androgen receptor in prostate cancer: synergistic stimulation of a gene set exemplified by SNAI2 and subsequent invasiveness. Cancer Res. *74*, 2857–2868.

Lomenick, B., Olsen, R.W., and Huang, J. (2011). Identification of Direct Protein Targets of Small Molecules. ACS Chem. Biol. *6*, 34–46.

Long, G.V., Menzies, A.M., Nagrial, A.M., Haydu, L.E., Hamilton, A.L., Mann, G.J., Hughes, T.M., Thompson, J.F., Scolyer, R.A., and Kefford, R.F. (2011). Prognostic and

clinicopathologic associations of oncogenic BRAF in metastatic melanoma. J. Clin. Oncol. Off. J. Am. Soc. Clin. Oncol. *29*, 1239–1246.

Lopez-Camacho, C., van Wijnen, A.J., Lian, J.B., Stein, J.L., and Stein, G.S. (2014a). Core binding factor β (CBFβ) is retained in the midbody during cytokinesis. J. Cell. Physiol. *229*, 1466–1474.

Lopez-Camacho, C., van Wijnen, A.J., Lian, J.B., Stein, J.L., and Stein, G.S. (2014b). CBFβ and the leukemogenic fusion protein CBFβ-SMMHC associate with mitotic chromosomes to epigenetically regulate ribosomal genes. J. Cell. Biochem. *115*, 2155–2164.

Lu, J., Qian, Y., Altieri, M., Dong, H., Wang, J., Raina, K., Hines, J., Winkler, J.D., Crew, A.P., Coleman, K., et al. (2015). Hijacking the E3 Ubiquitin Ligase Cereblon to Efficiently Target BRD4. Chem. Biol. *22*, 755–763.

Lu, M., Liu, T., Jiao, Q., Ji, J., Tao, M., Liu, Y., You, Q., and Jiang, Z. (2018). Discovery of a Keap1-dependent peptide PROTAC to knockdown Tau by ubiquitination-proteasome degradation pathway. Eur. J. Med. Chem. *146*, 251–259.

Lucero, C.M.J., Vega, O.A., Osorio, M.M., Tapia, J.C., Antonelli, M., Stein, G.S., van Wijnen, A.J., and Galindo, M.A. (2013). The cancer-related transcription factor Runx2 modulates cell proliferation in human osteosarcoma cell lines. J. Cell. Physiol. *228*, 714–723.

Martin, J.W., Chilton-MacNeill, S., Koti, M., Wijnen, A.J. van, Squire, J.A., and Zielenska, M. (2014). Digital Expression Profiling Identifies RUNX2, CDC5L, MDM2, RECQL4, and CDK4 as Potential Predictive Biomarkers for Neo-Adjuvant Chemotherapy Response in Paediatric Osteosarcoma. PLOS ONE *9*, e95843.

Martinez, M., Hinojosa, M., Trombly, D., Morin, V., Stein, J., Stein, G., Javed, A., and Gutierrez, S.E. (2016). Transcriptional Auto-Regulation of RUNX1 P1 Promoter. PLOS ONE *11*, e0149119.

Mayrhofer, M., Kultima, H.G., Birgisson, H., Sundström, M., Mathot, L., Edlund, K., Viklund, B., Sjöblom, T., Botling, J., Micke, P., et al. (2014). 1p36 deletion is a marker for tumour dissemination in microsatellite stable stage II-III colon cancer. BMC Cancer *14*, 872–872.

Mendoza-Villanueva, D., Deng, W., Lopez-Camacho, C., and Shore, P. (2010). The Runx transcriptional co-activator, CBFbeta, is essential for invasion of breast cancer cells. Mol. Cancer *9*, 171–171.

Mendoza-Villanueva, D., Zeef, L., and Shore, P. (2011). Metastatic breast cancer cells inhibit osteoblast differentiation through the Runx2/CBFβ-dependent expression of the Wnt antagonist, sclerostin. Breast Cancer Res. BCR *13*, R106–R106.

Metzeler, K.H., and Bloomfield, C.D. (2017). Clinical Relevance of <Emphasis Type="Italic">RUNX1</Emphasis> and <Emphasis Type="Italic">CBFB</Emphasis> Alterations in Acute Myeloid Leukemia and Other Hematological Disorders. In RUNX Proteins in Development and Cancer, (Springer, Singapore), pp. 175–199.

Michaud, J., Simpson, K.M., Escher, R., Buchet-Poyau, K., Beissbarth, T., Carmichael, C., Ritchie, M.E., Schütz, F., Cannon, P., Liu, M., et al. (2008). Integrative analysis of RUNX1 downstream pathways and target genes. BMC Genomics *9*, 363–363.

Mirza, M.R., Monk, B.J., Herrstedt, J., Oza, A.M., Mahner, S., Redondo, A., Fabbro, M., Ledermann, J.A., Lorusso, D., Vergote, I., et al. (2016). Niraparib Maintenance Therapy in Platinum-Sensitive, Recurrent Ovarian Cancer. N. Engl. J. Med. *375*, 2154–2164.

Mitra, A.K., Chiang, C.Y., Tiwari, P., Tomar, S., Watters, K.M., Peter, M.E., and Lengyel, E. (2015). Microenvironment-induced downregulation of miR-193b drives ovarian cancer metastasis. Oncogene *34*, 5923–5932.

Moellering, R.E., Cornejo, M., Davis, T.N., Bianco, C.D., Aster, J.C., Blacklow, S.C., Kung, A.L., Gilliland, D.G., Verdine, G.L., and Bradner, J.E. (2009). Direct inhibition of the NOTCH transcription factor complex. Nature *462*, 182–188.

Moorman, A.V., Ensor, H.M., Richards, S.M., Chilton, L., Schwab, C., Kinsey, S.E., Vora, A., Mitchell, C.D., and Harrison, C.J. (2010). Prognostic effect of chromosomal abnormalities in childhood B-cell precursor acute lymphoblastic leukaemia: results from the UK Medical Research Council ALL97/99 randomised trial. Lancet Oncol. *11*, 429–438.

Moreira, L., Balaguer, F., Lindor, N., de la Chapelle, A., Hampel, H., Aaltonen, L.A., Hopper, J.L., Le Marchand, L., Gallinger, S., Newcomb, P.A., et al. (2012). Identification of Lynch Syndrome Among Patients With Colorectal Cancer. JAMA J. Am. Med. Assoc. *308*.

Morita, K., Noura, M., Tokushige, C., Maeda, S., Kiyose, H., Kashiwazaki, G., Taniguchi, J., Bando, T., Yoshida, K., Ozaki, T., et al. (2017a). Autonomous feedback loop of RUNX1-p53-CBFB in acute myeloid leukemia cells. Sci. Rep. *7*, 16604.

Morita, K., Suzuki, K., Maeda, S., Matsuo, A., Mitsuda, Y., Tokushige, C., Kashiwazaki, G., Taniguchi, J., Maeda, R., Noura, M., et al. (2017b). Genetic regulation of the RUNX transcription factor family has antitumor effects. J. Clin. Invest. *127*, 2815–2828.

Morita, K., Maeda, S., Suzuki, K., Kiyose, H., Taniguchi, J., Liu, P.P., Sugiyama, H., Adachi, S., and Kamikubo, Y. (2017c). Paradoxical enhancement of leukemogenesis in acute myeloid leukemia with moderately attenuated RUNX1 expressions. Blood Adv. *1*, 1440–1451.

Mullen, A.C., Orlando, D.A., Newman, J.J., Lovén, J., Kumar, R.M., Bilodeau, S., Reddy, J., Guenther, M.G., DeKoter, R., and Young, R.A. (2011). Master Transcription

Factors Determine Cell-Type-Specific Responses to TGF-β Signaling. Cell *147*, 565–576.

Mundlos, S., Otto, F., Mundlos, C., Mulliken, J.., Aylsworth, A.., Albright, S., Lindhout, D., Cole, W.., Henn, W., Knoll, J.H.., et al. (1997). Mutations Involving the Transcription Factor CBFA1 Cause Cleidocranial Dysplasia. Cell *89*, 773–779.

Nakayama, K., Nakayama, N., Kurman, R.J., Cope, L., Pohl, G., Samuels, Y., Velculescu, V.E., Wang, T.-L., and Shih, I.-M. (2006). Sequence mutations and amplification of PIK3CA and AKT2 genes in purified ovarian serous neoplasms. Cancer Biol. Ther. *5*, 779–785.

Neklesa, T.K., Winkler, J.D., and Crews, C.M. (2017). Targeted protein degradation by PROTACs. Pharmacol. Ther. *174*, 138–144.

Network, T.C.G.A.R. (2013). Genomic and Epigenomic Landscapes of Adult De Novo Acute Myeloid Leukemia.

Nevadunsky, N.S., Barbieri, J.S., Kwong, J., Merritt, M.A., Welch, W.R., Berkowitz, R.S., and Mok, S.C. (2009). RUNX3 protein is overexpressed in human epithelial ovarian cancer. Gynecol. Oncol. *112*, 325–330.

Niu, D.-F., Kondo, T., Nakazawa, T., Oishi, N., Kawasaki, T., Mochizuki, K., Yamane, T., and Katoh, R. (2012). Transcription factor Runx2 is a regulator of epithelial-mesenchymal transition and invasion in thyroid carcinomas. Lab. Investig. J. Tech. Methods Pathol. *92*, 1181–1190.

Nomoto, S., Kinoshita, T., Mori, T., Kato, K., Sugimoto, H., Kanazumi, N., Takeda, S., and Nakao, A. (2008). Adverse prognosis of epigenetic inactivation in RUNX3 gene at 1p36 in human pancreatic cancer. Br. J. Cancer *98*, 1690–1695.

Ojesina, A.I., Lichtenstein, L., Freeman, S.S., Pedamallu, C.S., Imaz-Rosshandler, I., Pugh, T.J., Cherniack, A.D., Ambrogio, L., Cibulskis, K., Bertelsen, B., et al. (2014). Landscape of genomic alterations in cervical carcinomas. Nature *506*, 371–375.

Okuda, T., van Deursen, J., Hiebert, S.W., Grosveld, G., and Downing, J.R. (1996). AML1, the Target of Multiple Chromosomal Translocations in Human Leukemia, Is Essential for Normal Fetal Liver Hematopoiesis. Cell *84*, 321–330.

Oo, Z.M., Illendula, A., Grembecka, J., Schmidt, C., Zhou, Y., Esain, V., Kwan, W., Frost, I., North, T.E., Rajewski, R.A., et al. (2017). A tool compound targeting the core binding factor Runt domain to disrupt binding to CBFβ in leukemic cells. Leuk. Lymphoma 1–13.

Oshimo, Y., Oue, N., Mitani, Y., Nakayama, H., Kitadai, Y., Yoshida, K., Ito, Y., Chayama, K., and Yasui, W. (2004). Frequent loss of RUNX3 expression by promoter hypermethylation in gastric carcinoma. Pathobiol. J. Immunopathol. Mol. Cell. Biol. *71*, 137–143.

Ostenfeld, M.S., Bramsen, J.B., Lamy, P., Villadsen, S.B., Fristrup, N., Sørensen, K.D., Ulhøi, B., Borre, M., Kjems, J., Dyrskjøt, L., et al. (2010). miR-145 induces caspase-dependent and -independent cell death in urothelial cancer cell lines with targeting of an expression signature present in Ta bladder tumors. Oncogene *29*, 1073–1084.

Patel, J.P., Gönen, M., Figueroa, M.E., Fernandez, H., Sun, Z., Racevskis, J., Van Vlierberghe, P., Dolgalev, I., Thomas, S., Aminova, O., et al. (2012). Prognostic Relevance of Integrated Genetic Profiling in Acute Myeloid Leukemia. N. Engl. J. Med. *366*, 1079–1089.

Pereira, B., Chin, S.-F., Rueda, O.M., Vollan, H.-K.M., Provenzano, E., Bardwell, H.A., Pugh, M., Jones, L., Russell, R., Sammut, S.-J., et al. (2016). The somatic mutation profiles of 2,433 breast cancers refine their genomic and transcriptomic landscapes. Nat. Commun. *7*, 11479.

Perets, R., Wyant, G.A., Muto, K.W., Bijron, J.G., Poole, B.B., Chin, K.T., Chen, J.Y.H., Ohman, A.W., Stepule, C.D., Kwak, S., et al. (2013). Transformation of the fallopian tube secretory epithelium leads to high-grade serous ovarian cancer in Brca;Tp53;Pten models. Cancer Cell *24*, 751–765.

Perren, T.J., Swart, A.M., Pfisterer, J., Ledermann, J.A., Pujade-Lauraine, E., Kristensen, G., Carey, M.S., Beale, P., Cervantes, A., Kurzeder, C., et al. (2011). A phase 3 trial of bevacizumab in ovarian cancer. N. Engl. J. Med. *365*, 2484–2496.

Philipot, O., Joliot, V., Ait-Mohamed, O., Pellentz, C., Robin, P., Fritsch, L., and Ait-Si-Ali, S. (2010). The core binding factor CBF negatively regulates skeletal muscle terminal differentiation. PloS One *5*, e9425–e9425.

Pipas, J.M. (2009). SV40: Cell transformation and tumorigenesis. Virology *384*, 294–303.

Prahm, K.P., Karlsen, M.A., Høgdall, E., Scheller, N.M., Lundvall, L., Nedergaard, L., Christensen, I.J., and Høgdall, C. (2015). The prognostic value of dividing epithelial ovarian cancer into type I and type II tumors based on pathologic characteristics. Gynecol. Oncol. *136*, 205–211.

Pratap, J., Javed, A., Languino, L.R., van Wijnen, A.J., Stein, J.L., Stein, G.S., and Lian, J.B. (2005). The Runx2 osteogenic transcription factor regulates matrix metalloproteinase 9 in bone metastatic cancer cells and controls cell invasion. Mol. Cell. Biol. *25*, 8581–8591.

Pratap, J., Imbalzano, K.M., Underwood, J.M., Cohet, N., Gokul, K., Akech, J., Wijnen, A.J. van, Stein, J.L., Imbalzano, A.N., Nickerson, J.A., et al. (2009). Ectopic Runx2 Expression in Mammary Epithelial Cells Disrupts Formation of Normal Acini Structure: Implications for Breast Cancer Progression. Cancer Res. *69*, 6807–6814.

Przybycin, C.G., Kurman, R.J., Ronnett, B.M., Shih, I.-M., and Vang, R. (2010). Are all pelvic (nonuterine) serous carcinomas of tubal origin? Am. J. Surg. Pathol. *34*, 1407–1416.

Pujade-Lauraine, E., Hilpert, F., Weber, B., Reuss, A., Poveda, A., Kristensen, G., Sorio, R., Vergote, I., Witteveen, P., Bamias, A., et al. (2014). Bevacizumab Combined With Chemotherapy for Platinum-Resistant Recurrent Ovarian Cancer: The AURELIA Open-Label Randomized Phase III Trial. J. Clin. Oncol. *32*, 1302–1308.

Pujade-Lauraine, E., Ledermann, J.A., Selle, F., Gebski, V., Penson, R.T., Oza, A.M., Korach, J., Huzarski, T., Poveda, A., Pignata, S., et al. (2017). Olaparib tablets as maintenance therapy in patients with platinum-sensitive, relapsed ovarian cancer and a BRCA1/2 mutation (SOLO2/ENGOT-Ov21): a double-blind, randomised, placebo-controlled, phase 3 trial. Lancet Oncol. *18*, 1274–1284.

Qiao, M., Shapiro, P., Fosbrink, M., Rus, H., Kumar, R., and Passaniti, A. (2006). Cell cycle-dependent phosphorylation of the RUNX2 transcription factor by cdc2 regulates endothelial cell proliferation. J. Biol. Chem. *281*, 7118–7128.

Ray, K.K., Landmesser, U., Leiter, L.A., Kallend, D., Dufour, R., Karakas, M., Hall, T., Troquay, R.P.T., Turner, T., Visseren, F.L.J., et al. (2017). Inclisiran in Patients at High Cardiovascular Risk with Elevated LDL Cholesterol. N. Engl. J. Med. *376*, 1430–1440.

Rebbeck, T.R., Kauff, N.D., and Domchek, S.M. (2009). Meta-analysis of risk reduction estimates associated with risk-reducing salpingo-oophorectomy in BRCA1 or BRCA2 mutation carriers. J. Natl. Cancer Inst. *101*, 80–87.

Risch, H.A., McLaughlin, J.R., Cole, D.E., Rosen, B., Bradley, L., Kwan, E., Jack, E., Vesprini, D.J., Kuperstein, G., Abrahamson, J.L., et al. (2001). Prevalence and penetrance of germline BRCA1 and BRCA2 mutations in a population series of 649 women with ovarian cancer. Am. J. Hum. Genet. *68*, 700–710.

Robb, C.M., Contreras, J.I., Kour, S., Taylor, M.A., Abid, M., Sonawane, Y.A., Zahid, M., Murry, D.J., Natarajan, A., and Rana, S. (2017). Chemically induced degradation of CDK9 by a proteolysis targeting chimera (PROTAC). Chem. Commun. Camb. Engl. *53*, 7577–7580.

Robertson, S.P. (2005). Filamin A: phenotypic diversity. Curr. Opin. Genet. Dev. *15*, 301–307.

Rossi, E., Bagalà, C., Inzani, F., Leoncini, E., Brunelli, C., Lanza, P., Basso, M., Mattiucci, G.C., Cassano, A., Rindi, G., et al. (2017). RUNX3 as a Potential Predictor of Metastasis in Human Pancreatic Cancer. In Vivo *31*, 833–840.

Sadikovic, B., Thorner, P., Chilton-Macneill, S., Martin, J.W., Cervigne, N.K., Squire, J., and Zielenska, M. (2010). Expression analysis of genes associated with human osteosarcoma tumors shows correlation of RUNX2 overexpression with poor response to chemotherapy. BMC Cancer *10*, 202–202.

Salani, R., Backes, F.J., Fung, M.F.K., Holschneider, C.H., Parker, L.P., Bristow, R.E., and Goff, B.A. (2011). Posttreatment surveillance and diagnosis of recurrence in women with gynecologic malignancies: Society of Gynecologic Oncologists recommendations. Am. J. Obstet. Gynecol. *204*, 466–478.

San Martin, I.A., Varela, N., Gaete, M., Villegas, K., Osorio, M., Tapia, J.C., Antonelli, M., Mancilla, E.E., Pereira, B.P., Nathan, S.S., et al. (2009). Impaired cell cycle regulation of the osteoblast-related heterodimeric transcription factor Runx2-Cbfbeta in osteosarcoma cells. J. Cell. Physiol. *221*, 560–571.

Santos, R., Ursu, O., Gaulton, A., Bento, A.P., Donadi, R.S., Bologa, C.G., Karlsson, A., Al-Lazikani, B., Hersey, A., Oprea, T.I., et al. (2017). A comprehensive map of molecular drug targets. Nat. Rev. Drug Discov. *16*, 19–34.

Sawicka, M., Kalinowska, M., Skierski, J., and Lewandowski, W. (2004). A review of selected anti-tumour therapeutic agents and reasons for multidrug resistance occurrence. J. Pharm. Pharmacol. *56*, 1067–1081.

Scheitz, C.J.F., Lee, T.S., McDermitt, D.J., and Tumbar, T. (2012). Defining a tissue stem cell-driven Runx1/Stat3 signalling axis in epithelial cancer. EMBO J. *31*, 4124–4139.

Schiedel, M., Herp, D., Hammelmann, S., Swyter, S., Lehotzky, A., Robaa, D., Oláh, J., Ovádi, J., Sippl, W., and Jung, M. (2018). Chemically Induced Degradation of Sirtuin 2 (Sirt2) by a Proteolysis Targeting Chimera (PROTAC) Based on Sirtuin Rearranging Ligands (SirReals). J. Med. Chem. *61*, 482–491.

Schwab, M., Praml, C., and Amler, L.C. (1996). Genomic instability in Ip and human malignancies. Genes. Chromosomes Cancer *16*, 211–229.

Shan, W., and Liu, J. (2009). Epithelial ovarian cancer: Focus on genetics and animal models. Cell Cycle *8*, 731–735.

Shao, Q.-Q., Zhang, T.-P., Zhao, W.-J., Liu, Z.-W., You, L., Zhou, L., Guo, J.-C., and Zhao, Y.-P. (2016). Filamin A: Insights into its Exact Role in Cancers. Pathol. Oncol. Res. *22*, 245–252.

Shen, G.H., Ghazizadeh, M., Kawanami, O., Shimizu, H., Jin, E., Araki, T., and Sugisaki, Y. (2000). Prognostic significance of vascular endothelial growth factor expression in human ovarian carcinoma. Br. J. Cancer *83*, 196–203.

Sherman-Baust, C.A., Kuhn, E., Valle, B.L., Shih, I.-M., Kurman, R.J., Wang, T.-L., Amano, T., Ko, M.S.H., Miyoshi, I., Araki, Y., et al. (2014). A genetically engineered ovarian cancer mouse model based on fallopian tube transformation mimics human high-grade serous carcinoma development. J. Pathol. *233*, 228–237.

Shimizu, K., Yamagata, K., Kurokawa, M., Mizutani, S., Tsunematsu, Y., and Kitabayashi, I. (2013). Roles of AML1/RUNX1 in T-cell malignancy induced by loss of p53. Cancer Sci. *104*, 1033–1038.

Shin, E.J., Kim, H.J., Son, M.W., Ahn, T.S., Lee, H.Y., Lim, D.R., Bae, S.B., Jeon, S., Kim, H., Jeong, D., et al. (2018). Epigenetic inactivation ofRUNX3in colorectal cancer. Ann. Surg. Treat. Res. *94*, 19–25.

Siegel, R.L., Miller, K.D., and Jemal, A. (2017). Cancer Statistics, 2017. CA. Cancer J. Clin. *67*, 7–30.

Singer, G., Oldt, R., Cohen, Y., Wang, B.G., Sidransky, D., Kurman, R.J., and Shih, I.-M. (2003). Mutations in BRAF and KRAS characterize the development of low-grade ovarian serous carcinoma. J. Natl. Cancer Inst. *95*, 484–486.

Singer, G., Stöhr, R., Cope, L., Dehari, R., Hartmann, A., Cao, D.-F., Wang, T.-L., Kurman, R.J., and Shih, I.-M. (2005). Patterns of p53 mutations separate ovarian serous borderline tumors and low- and high-grade carcinomas and provide support for a new model of ovarian carcinogenesis: a mutational analysis with immunohistochemical correlation. Am. J. Surg. Pathol. *29*, 218–224.

Slamon, D.J., Leyland-Jones, B., Shak, S., Fuchs, H., Paton, V., Bajamonde, A., Fleming, T., Eiermann, W., Wolter, J., Pegram, M., et al. (2001). Use of chemotherapy plus a monoclonal antibody against HER2 for metastatic breast cancer that overexpresses HER2. N. Engl. J. Med. *344*, 783–792.

Snyder Sara K., Wessells Jennifer L., Waterhouse Roseann M., Dveksler Gabriela S., Wessner David H., Wahl Larry M., and Zimmermann Wolfgang (2003). Pregnancy-Specific Glycoproteins Function as Immunomodulators by Inducing Secretion of IL-10, IL-6 and TGF-β1 by Human Monocytes. Am. J. Reprod. Immunol. *45*, 205–216.

Spender, L.C., Whiteman, H.J., Karstegl, C.E., and Farrell, P.J. (2005). Transcriptional cross-regulation of RUNX1 by RUNX3 in human B cells. Oncogene *24*, 1873–1881.

Subramanian, A., Tamayo, P., Mootha, V.K., Mukherjee, S., Ebert, B.L., Gillette, M.A., Paulovich, A., Pomeroy, S.L., Golub, T.R., Lander, E.S., et al. (2005). Gene set enrichment analysis: A knowledge-based approach for interpreting genome-wide expression profiles. Proc. Natl. Acad. Sci. *102*, 15545–15550.

Tabernero, J., Shapiro, G.I., LoRusso, P.M., Cervantes, A., Schwartz, G.K., Weiss, G.J., Paz-Ares, L., Cho, D.C., Infante, J.R., Alsina, M., et al. (2013). First-in-humans trial of an RNA interference therapeutic targeting VEGF and KSP in cancer patients with liver involvement. Cancer Discov. *3*, 406–417.

Tahirov, T.H., Inoue-Bungo, T., Morii, H., Fujikawa, A., Sasaki, M., Kimura, K., Shiina, M., Sato, K., Kumasaka, T., Yamamoto, M., et al. (2001). Structural Analyses of DNA Recognition by the AML1/Runx-1 Runt Domain and Its Allosteric Control by CBFβ. Cell *104*, 755–767.

Taipaleenmäki, H., Browne, G., Akech, J., Zustin, J., Wijnen, A.J. van, Stein, J.L., Hesse, E., Stein, G.S., and Lian, J.B. (2015). Targeting of Runx2 by miR-135 and miR-203 Impairs Progression of Breast Cancer and Metastatic Bone Disease. Cancer Res. *75*, 1433–1444.

Takayama, K., Suzuki, T., Tsutsumi, S., Fujimura, T., Urano, T., Takahashi, S., Homma, Y., Aburatani, H., Inoue, S., Takayama, K., et al. (2014). RUNX1, an androgen- and EZH2-regulated gene, has differential roles in AR-dependent and -independent prostate cancer. Oncotarget *6*, 2263–2276.

Tan, C.-C., Li, G.-X., Tan, L.-D., Du, X., Li, X.-Q., He, R., Wang, Q.-S., and Feng, Y.-M. (2016). Breast cancer cells obtain an osteomimetic feature via epithelial-mesenchymal transition that have undergone BMP2/RUNX2 signaling pathway induction. Oncotarget *7*, 79688–79705.

Tanaka, K., Tanaka, T., Kurokawa, M., Imai, Y., Ogawa, S., Mitani, K., Yazaki, Y., and Hirai, H. (1998). The AML1/ETO(MTG8) and AML1/Evi-1 leukemia-associated chimeric oncoproteins accumulate PEBP2beta(CBFbeta) in the nucleus more efficiently than wild-type AML1. Blood *91*, 1688–1699.

Tanaka, Y., Watanabe, T., Chiba, N., Niki, M., Kuroiwa, Y., Nishihira, T., Satomi, S., Ito, Y., and Satake, M. (1997). The protooncogene product, PEBP2beta/CBFbeta, is mainly located in the cytoplasm and has an affinity with cytoskeletal structures. Oncogene *15*, 677–683.

Tandon, M., Chen, Z., and Pratap, J. (2014). Runx2 activates PI3K/Akt signaling via mTORC2 regulation in invasive breast cancer cells. Breast Cancer Res. BCR *16*, R16.

Tang, Y.Y., Shi, J., Zhang, L., Davis, A., Bravo, J., Warren, A.J., Speck, N.A., and Bushweller, J.H. (2000). Energetic and functional contribution of residues in the core binding factor beta (CBFbeta) subunit to heterodimerization with CBFalpha. J. Biol. Chem. *275*, 39579–39588.

Tew, W.P., Colombo, N., Ray-Coquard, I., Del Campo, J.M., Oza, A., Pereira, D., Mammoliti, S., Matei, D., Scambia, G., Tonkin, K., et al. (2014). Intravenous aflibercept in patients with platinum-resistant, advanced ovarian cancer: results of a randomized, double-blind, phase 2, parallel-arm study. Cancer *120*, 335–343.

Tsunematsu, T., Kudo, Y., Iizuka, S., Ogawa, I., Fujita, T., Kurihara, H., Abiko, Y., and Takata, T. (2009). RUNX3 has an oncogenic role in head and neck cancer. PloS One *4*, e5892–e5892.

Tzatsos, A., Pfau, R., Kampranis, S.C., and Tsichlis, P.N. (2009). Ndy1/KDM2B immortalizes mouse embryonic fibroblasts by repressing the Ink4a/Arf locus. Proc. Natl. Acad. Sci. *106*, 2641–2646.

Vasen, H.F.A., Blanco, I., Aktan-Collan, K., Gopie, J.P., Alonso, A., Aretz, S., Bernstein, I., Bertario, L., Burn, J., Capella, G., et al. (2013). Revised guidelines for the clinical

management of Lynch syndrome (HNPCC): recommendations by a group of European experts. Gut *62*, 812–823.

Vassilev, L.T., Vu, B.T., Graves, B., Carvajal, D., Podlaski, F., Filipovic, Z., Kong, N., Kammlott, U., Lukacs, C., Klein, C., et al. (2004). In Vivo Activation of the p53 Pathway by Small-Molecule Antagonists of MDM2. Science *303*, 844–848.

Vergote, I., Tropé, C.G., Amant, F., Kristensen, G.B., Ehlen, T., Johnson, N., Verheijen, R.H.M., van der Burg, M.E.L., Lacave, A.J., Panici, P.B., et al. (2010). Neoadjuvant chemotherapy or primary surgery in stage IIIC or IV ovarian cancer. N. Engl. J. Med. *363*, 943–953.

Vetter, M.H., and Hays, J.L. Use of Targeted Therapeutics in Epithelial Ovarian Cancer: A Review of Current Literature and Future Directions. Clin. Ther.

Vogelstein, B., Papadopoulos, N., Velculescu, V.E., Zhou, S., Diaz, L.A., and Kinzler, K.W. (2013). Cancer Genome Landscapes. Science *339*, 1546–1558.

Voon, D.C.-C., and Thiery, J.P. (2017). The Emerging Roles of RUNX Transcription Factors in Epithelial-Mesenchymal Transition. Adv. Exp. Med. Biol. *962*, 471–489.

Wang, S., and Jia, M. (2016). Antibody Therapies in Cancer. In Progress in Cancer Immunotherapy, (Springer, Dordrecht), pp. 1–67.

Wang, D., Cui, W., Wu, X., Qu, Y., Wang, N., Shi, B., and Hou, P. (2014). RUNX3 site-specific hypermethylation predicts papillary thyroid cancer recurrence. Am. J. Cancer Res. *4*, 725–737.

Wang, L., Brugge, J.S., and Janes, K.A. (2011). Intersection of FOXO- and RUNX1-mediated gene expression programs in single breast epithelial cells during morphogenesis and tumor progression. Proc. Natl. Acad. Sci. U. S. A. *108*, E803-12.

Wang, N., Sui, F., Ma, J., Su, X., Liu, J., Yao, D., Shi, B., Hou, P., and Yang, Q. (2016). Site-specific Hypermethylation of RUNX3 Predicts Poor Prognosis in Gastric Cancer. Arch. Med. Res. *47*, 285–292.

Wang, Q., Stacy, T., Binder, M., Marin-Padilla, M., Sharpe, A.H., and Speck, N.A. (1996a). Disruption of the Cbfa2 gene causes necrosis and hemorrhaging in the central nervous system and blocks definitive hematopoiesis. Proc. Natl. Acad. Sci. U. S. A. *93*, 3444–3449.

Wang, Q., Stacy, T., Miller, J.D., Lewis, A.F., Gu, T.-L., Huang, X., Bushweller, J.H., Bories, J.-C., Alt, F.W., Ryan, G., et al. (1996b). The CBFβ Subunit Is Essential for CBFα2 (AML1) Function In Vivo. Cell *87*, 697–708.

Wang, S., Zhang, Y., Soosairajah, J., and Kraft, A.S. (2007). Regulation of RUNX1/AML1 during the G2/M transition. Leuk. Res. *31*, 839–851.

Wang, Z.-Q., Keita, M., Bachvarova, M., Gobeil, S., Morin, C., Plante, M., Gregoire, J., Renaud, M.-C., Sebastianelli, A., Trinh, X.B., et al. (2013). Inhibition of RUNX2 transcriptional activity blocks the proliferation, migration and invasion of epithelial ovarian carcinoma cells. PloS One *8*, e74384–e74384.

Watson, P., Bützow, R., Lynch, H.T., Mecklin, J.P., Järvinen, H.J., Vasen, H.F., Madlensky, L., Fidalgo, P., and Bernstein, I. (2001). The clinical features of ovarian cancer in hereditary nonpolyposis colorectal cancer. Gynecol. Oncol. *82*, 223–228.

Wen, C., Wen, C., Liu, X., Liu, X., Ma, H., Ma, H., Zhang, W., Zhang, W., Li, H., and Li, H. (2015). miR-338-3p suppresses tumor growth of ovarian epithelial carcinoma by targeting Runx2. Int. J. Oncol. *46*, 2277–2285.

Westendorp, B., Mokry, M., Groot Koerkamp, M.J.A., Holstege, F.C.P., Cuppen, E., and de Bruin, A. (2012). E2F7 represses a network of oscillating cell cycle genes to control S-phase progression. Nucleic Acids Res. *40*, 3511–3523.

Whittle, M.C., Izeradjene, K., Rani, P.G., Feng, L., Carlson, M.A., DelGiorno, K.E., Wood, L.D., Goggins, M., Hruban, R.H., Chang, A.E., et al. (2015). RUNX3 Controls a Metastatic Switch in Pancreatic Ductal Adenocarcinoma. Cell *161*, 1345–1360.

Wiegand, K.C., Shah, S.P., Al-Agha, O.M., Zhao, Y., Tse, K., Zeng, T., Senz, J., McConechy, M.K., Anglesio, M.S., Kalloger, S.E., et al. (2010). ARID1A mutations in endometriosis-associated ovarian carcinomas. N. Engl. J. Med. *363*, 1532–1543.

Winter, G.E., Buckley, D.L., Paulk, J., Roberts, J.M., Souza, A., Dhe-Paganon, S., and Bradner, J.E. (2015). DRUG DEVELOPMENT. Phthalimide conjugation as a strategy for in vivo target protein degradation. Science *348*, 1376–1381.

Wotton, S., Terry, A., Kilbey, A., Jenkins, A., Herzyk, P., Cameron, E., and Neil, J.C. (2008). Gene array analysis reveals a common Runx transcriptional programme controlling cell adhesion and survival. Oncogene *27*, 5856–5866.

Wotton, S.F., Blyth, K., Kilbey, A., Jenkins, A., Terry, A., Bernardin-Fried, F., Friedman, A.D., Baxter, E.W., Neil, J.C., and Cameron, E.R. (2004). RUNX1 transformation of primary embryonic fibroblasts is revealed in the absence of p53. Oncogene *23*, 5476–5486.

Wu, D., Ozaki, T., Yoshihara, Y., Kubo, N., and Nakagawara, A. (2013). Runt-related Transcription Factor 1 (RUNX1) Stimulates Tumor Suppressor p53 Protein in Response to DNA Damage through Complex Formation and Acetylation. J. Biol. Chem. *288*, 1353–1364.

Xiao, Z.S., Thomas, R., Hinson, T.K., and Quarles, L.D. (1998). Genomic structure and isoform expression of the mouse, rat and human Cbfa1/Osf2 transcription factor. Gene *214*, 187–197.

Yamada, C., Ozaki, T., Ando, K., Suenaga, Y., Inoue, K., Ito, Y., Okoshi, R., Kageyama, H., Kimura, H., Miyazaki, M., et al. (2010). RUNX3 Modulates DNA Damage-mediated Phosphorylation of Tumor Suppressor p53 at Ser-15 and Acts as a Co-activator for p53. J. Biol. Chem. *285*, 16693–16703.

Yan, C., Kim, Y.-W., Ha, Y.-S., Kim, I.Y., Kim, Y.-J., Yun, S.-J., Moon, S.-K., Bae, S.-C., and Kim, W.-J. (2012). RUNX3 methylation as a predictor for disease progression in patients with non-muscle-invasive bladder cancer. J. Surg. Oncol. *105*, 425–430.

Yang, J., Zhao, L., Tian, W., Liao, Z., Zheng, H., Wang, G., and Chen, K. (2013). Correlation of WWOX, RUNX2 and VEGFA protein expression in human osteosarcoma. BMC Med. Genomics *6*, 56.

Yang, Y., Ye, Z., Zou, Z., Xiao, G., Luo, G., and Yang, H. (2014). Clinicopathological significance of RUNX3 gene hypermethylation in hepatocellular carcinoma. Tumour Biol. J. Int. Soc. Oncodevelopmental Biol. Med. *35*, 10333–10340.

Yang, Y., Bai, Y., He, Y., Zhao, Y., Chen, J., Ma, L., Pan, Y., Hinten, M., Zhang, J., Karnes, R.J., et al. (2018). PTEN Loss Promotes Intratumoral Androgen Synthesis and Tumor Microenvironment Remodeling via Aberrant Activation of RUNX2 in Castration-Resistant Prostate Cancer. Clin. Cancer Res. *24*, 834–846.

Yap, T.A., Yan, L., Patnaik, A., Tunariu, N., Biondo, A., Fearen, I., Papadopoulos, K.P., Olmos, D., Baird, R., Delgado, L., et al. (2014). Interrogating two schedules of the AKT inhibitor MK-2206 in patients with advanced solid tumors incorporating novel pharmacodynamic and functional imaging biomarkers. Clin. Cancer Res. Off. J. Am. Assoc. Cancer Res. *20*, 5672–5685.

Yoshida, N., Ogata, T., Tanabe, K., Li, S., Nakazato, M., Kohu, K., Takafuta, T., Shapiro, S., Ohta, Y., Satake, M., et al. (2005). Filamin A-bound PEBP2beta/CBFbeta is retained in the cytoplasm and prevented from functioning as a partner of the Runx1 transcription factor. Mol. Cell. Biol. *25*, 1003–1012.

Yuan, L., Li, S., Zhou, Q., Wang, D., Zou, D., Shu, J., and Huang, Y. (2017). MiR-124 inhibits invasion and induces apoptosis of ovarian cancer cells by targeting programmed cell death 6. Oncol. Lett. *14*, 7311–7317.

Yun, S.J., Yoon, H.-Y., Bae, S.-C., Lee, O.-J., Choi, Y.-H., Moon, S.-K., Kim, I.Y., and Kim, W.-J. (2012). Transcriptional repression of RUNX2 is associated with aggressive clinicopathological outcomes, whereas nuclear location of the protein is related to metastasis in prostate cancer. Prostate Cancer Prostatic Dis. *15*, 369–373.

Zehir, A., Benayed, R., Shah, R.H., Syed, A., Middha, S., Kim, H.R., Srinivasan, P., Gao, J., Chakravarty, D., Devlin, S.M., et al. (2017). Mutational landscape of metastatic cancer revealed from prospective clinical sequencing of 10,000 patients. Nat. Med. *23*, 703–713.

Zeng, C., van Wijnen, A.J., Stein, J.L., Meyers, S., Sun, W., Shopland, L., Lawrence, J.B., Penman, S., Lian, J.B., Stein, G.S., et al. (1997). Identification of a nuclear matrix

targeting signal in the leukemia and bone-related AML/CBF-α transcription factors. Proc. Natl. Acad. Sci. U. S. A. *94*, 6746–6751.

Zengerle, M., Chan, K.-H., and Ciulli, A. (2015). Selective Small Molecule Induced Degradation of the BET Bromodomain Protein BRD4. ACS Chem. Biol. *10*, 1770–1777.

Zerlanko, B.J., Bartholin, L., Melhuish, T.A., and Wotton, D. (2012). Premature Senescence and Increased TGFβ Signaling in the Absence of Tgif1. PLoS ONE *7*.

Zhang, C., Long, F., Wan, J., Hu, Y., and He, H. (2016). MicroRNA-205 acts as a tumor suppressor in osteosarcoma via targeting RUNX2. Oncol. Rep. *35*, 3275–3284.

Zhang, H., Wang, Q., Zhao, Q., and Di, W. (2013). MiR-124 inhibits the migration and invasion of ovarian cancer cells by targeting SphK1. J. Ovarian Res. *6*, 84.

Zhang, J., Qin, J., and Su, Y. (2017). miR-193b-3p possesses anti-tumor activity in ovarian carcinoma cells by targeting p21-activated kinase 3. Biomed. Pharmacother. *96*, 1275–1282.

Zhang, L., Lukasik, S.M., Speck, N.A., and Bushweller, J.H. (2003). Structural and functional characterization of Runx1, CBFβ, and CBFβ-SMMHC. Blood Cells. Mol. Dis. *30*, 147–156.

Zhang, Q., Burdette, J.E., and Wang, J.-P. (2014). Integrative network analysis of TCGA data for ovarian cancer. BMC Syst. Biol. *8*, 1338.